Physics – Uspekhi **54** (4) 387 – 427 (2011)

CONFERENCES AND SYMPOSIA

PACS numbers: 01.10.Fv, **01.65.+g**, 05.70.Ce, **07.35.+k**, 07.55.Db, **28.52.–s**, **28.70.+y**, **42.55.–f**, **42.62.–b**, **47.20.–k**, 47.27.wj, **47.40.–x**, **52.57.–z**, 61.05.C–, **64.30.–t**, **74.25.–q**, 84.30.Ng, **84.70.+p**, **85.70.–w**

Celebrating the 65th anniversary of the Russian Federal Nuclear Center — All-Russian Research Institute of Experimental Physics (Scientific session of the Physical Sciences Division of the Russian Academy of Sciences, 6 October 2010)

DOI: 10.3367/UFNe.0181.201104g.0405

A scientific session of the Physical Sciences Division of the Russian Academy of Sciences (RAS) took place on 6 October 2010 in the Conference Hall of the Lebedev Physical Institute, RAS (FIAN) on the occasion of the 65th anniversary of founding of the Russian Federal Nuclear Center — All-Russia Research Institute of Experimental Physics (RFNC – VNIIEF).

The agenda of the session announced on the website www.gpad.ac.ru of the RAS Physical Sciences Division listed the following reports:

(1) **Ilkaev R I** (RFNC–VNIIEF, Sarov, Nizhny Novgorod region). Opening remarks "On the fundamental physics research programs at RFNC–VNIIEF";

(2) **Mikhailov A L** (RFNC–VNIIEF, Sarov, Nizhny Novgorod region) "Hydrodynamic instabilities in various media";

(3) **Trunin R F** (RFNC–VNIIEF, Sarov, Nizhny Novgorod region) "Study of extreme states of metals using shock waves";

(4) **Ivanovskii A V** (RFNC–VNIIEF, Sarov, Nizhny Novgorod region) "Explosive magnetic energy generators and their application in research";

(5) **Podurets A M** (RFNC–VNIIEF, Sarov, Nizhny Novgorod region) "X-ray studies of the structure of matter in shock waves";

(6) **Garanin S G** (RFNC–VNIIEF, Sarov, Nizhny Novgorod region) "High-power lasers in studies of the physics of hot, dense plasma and thermonuclear fusion";

(7) **Selemir V D** (RFNC–VNIIEF, Sarov, Nizhny Novgorod region) "Physics research in ultrahigh magnetic fields";

(8) **Mkhitar'yan L S** (RFNC–VNIIEF, Sarov, Nizhny Novgorod region) "Gasdynamic thermonuclear fusion."

Articles based on reports 1–7 are published below. An extended version of report 3 written as a review paper will be published in a later issue of *Physics–Uspekhi*.

Uspekhi Fizicheskikh Nauk **181** (4) 405 – 447 (2011)
DOI: 10.3367/UFNr.0181.201104g.0405
Translated by V I Kisin, S D Danilov, E N Ragozin, M Sapozhnikov; edited by A Radzig, A M Semikhatov

PACS numbers: **01.65.+g**, **28.52.–s**, **28.70.+y**
DOI: 10.3367/UFNe.0181.201104h.0405

Fundamental physics research at the All-Russian Research Institute of Experimental Physics

R I Ilkaev

1. Introduction

The present article opens a series of publications devoted to the work on the physics of high energy densities at the Russian Federal Nuclear Center — All-Russian Research Institute of Experimental Physics (RFNC–VNIIEF). Historically, the progress in many areas of this science was closely connected with the research aimed at developing nuclear and thermonuclear weapons.

RFNC–VNIIEF was founded on 9 April 1946. The main tasks of the institute were to develop the first Soviet atomic bomb, then the first thermonuclear weapons, and later to design prototypes of nuclear and thermonuclear charges of various types and for various purposes. A number of fundamental physical results were obtained in the course of our activities within this program.

RFNC–VNIIEF is Russia's largest research institute for complex tasks of importance for defense, science, and the economy. The institute has made a decisive contribution to solving problems of the creation of nuclear and thermonuclear weapons in this country and to ending the atomic monopoly of the USA. The activities of the institute allowed achieving nuclear balance during the Cold War and contributed to the balance of powers in the world, thus saving humanity from global military conflicts.

Among those who worked at VNIIEF were eminent scientists I V Kurchatov, Yu B Khariton, Ya B Zel'dovich, A D Sakharov, N N Bogoliubov, M A Lavrent'ev, I E Tamm, G N Flerov, E A Negin, S G Kocharyants, A I Pavlovskii, Yu A Babaev, S B Kormer, and others, who created at the

R I Ilkaev Federal State Unitary Enterprise 'Russian Federal Nuclear Center — All-Russian Research Institute of Experimental Physics,' Sarov, Nizhny Novgorod region, Russian Federation
E-mail: ilkaev@vniief.ru

Uspekhi Fizicheskikh Nauk **181** (4) 405 – 410 (2011)
DOI: 10.3367/UFNr.0181.201104h.0405
Translated by V I Kisin; edited by A M Semikhatov

The first Soviet atomic bomb. The nuclear warhead was tested on 29 August 1949 at the Semipalatinsk test site. The charge power is 22 kilotons of TNT equivalent.

The first hydrogen bomb. The nuclear warhead was tested on 12 August 1953 at the Semipalatinsk test site. The charge power is 400 kilotons of TNT equivalent.

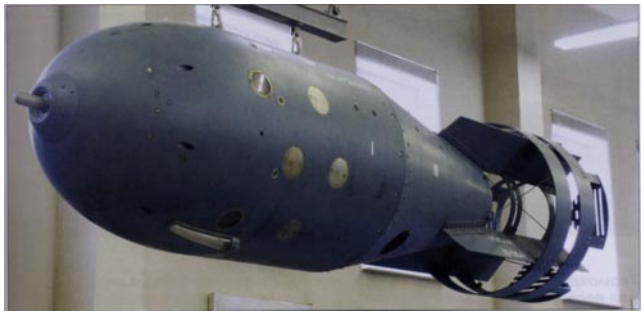

The first serial tactical atomic bomb. Tested in 1953 at the Semipalatinsk test site. The charge power is 30 kilotons of TNT equivalent.

The building of the Institute of Theoretical and Mathematical Physics of RFNC–VNIIEF.

institute much of what constitutes the pride of our science. Large schools of physicists, mathematicians, designers, engineers, and chemists grew up and continue to thrive at the institute.

The main task of the nuclear center today is to ensure and maintain the safety and security of Russia's nuclear weapons.

RFNC–VNIIEF has powerful computational, experimental, testing, technological, and industrial bases, permitting us to rapidly find high-quality solutions to assigned tasks.

RFNC–VNIIEF incorporates several institutes: Theoretical and Mathematical Physics, Experimental Gas Dynamics and the Physics of Explosions, Nuclear and Radiation Physics, Laser Physics Research, and the Center for High Energy Densities, as well as design bureaus and purpose centers under a joint scientific and administrative management.

The high scientific and technological potential allowed RFNC–VNIIEF to broaden the span of research and development, to rapidly join new hi-tech areas, to obtain and successfully develop world-class scientific results, and to carry out unique fundamental and applied research projects. The path to the future of our institute is therefore closely tied to its transformation into the National Security Center of the Russian Federation.

2. Gas dynamics

In the field of applications, the gasdynamic research at RFNC–VNIIEF has always been and continues to be motivated by searching for solutions to various problems of the implosion of fissile materials driven by the explosive energy of chemical high explosives (HEs).

Among the fundamental results in this area, we first of all mention

- determination of the levels of cumulation of explosive energy of HEs under spherically symmetric, axisymmetric, and three-dimensional loading of metals, and conclusions on the sustainability of cumulation;
- implementation of the precision of a shock wave convergence at the center of spherical and axisymmetric systems at the level of $\leqslant 3 \times 10^{-3}$ of the system size;
- achievement of metal compression levels in implosive compression systems by a factor greater than 7 relative to their initial density.

Gasdynamic research is associated with a series of studies aimed at formulating the equations of state for many substances in the range of shock-wave loading, including the pressure range up to ~ 10 TPa.

I must highlight the conclusions about the peculiarities of energy cumulation in highly asymmetric conditions of

dynamic flows that underlie the solutions to the problems of nuclear explosion safety of nuclear weapons.

RFNC–VNIIEF scientists have studied a number of aspects of the physics of detonation processes in detail, including the initiation of detonation, the stability of its propagation, and the transfer of detonation through inert shields. In this area, they formulated a system of process stability criteria and/or criteria of process transformation.

Although the program of gasdynamic research is based first and foremost on physical experiments (the experimental settings and diagnostic tools were also designed in our institute), the scientists at RFNC–VNIIEF have developed precision techniques for physical and mathematical modeling of gas dynamics, including three-dimensional simulation. It can be said that theory and experiment complement and enrich each other in this field.

We are traditionally among the world leaders in gasdynamic studies in this area and feel obliged to maintain this leadership; this requires active support of the science schools created in VNIIEF and systematic upgrade of the experimental facilities.

What fundamental problem still remains unsolved in this area? I would single out gasdynamic fusion.

Work on this issue resulted in a major research field in the mid-1950s, because it was very tempting to try to 'ignite' thermonuclear fuel using the cumulation of explosive energy of HEs. More than a hundred large-scale experiments have been conducted since then, but the problem remains unresolved and, apparently, is still far from resolution. Compression levels of the central metal shells have to exceed 50 and the density of the thermonuclear fuel exceed 10^2 g cm^{-3}. Perhaps we are dealing here with the fundamental development of instabilities and it has been beyond our practical capabilities so far to reduce them.

3. Radiation gas dynamics

This line of basic research is primarily associated with the design of thermonuclear charges. The basic principle here is radiative implosion, which assumes that

- a large fraction of the energy released in the explosion of a nuclear charge (primary module) is in the form of X-ray radiation;
- the energy of X-ray radiation is transported to the thermonuclear module;
- the implosion of the thermonuclear module is accomplished by the energy of the 'transported' X-ray radiation.

The implementation of each of the three components of this principle is based on radiation gas dynamics.

The explosion of a nuclear charge with the major part of the energy released in neutron-initiated reactions in the fissile material is accompanied with the transformation of energy into the energy of X-rays and thermal energy of matter, both at equilibrium, and into the kinetic energy of the medium. The process occurring in matter is that of the transfer of X-ray radiation emitted from the surface of fissile material and continuing to propagate through the outer regions of the primary module.

Obviously, this mechanism depends strongly on the fundamental characteristics, i.e., the free path of X-rays over which their interaction with matter occurs. For substances such as uranium, the processes of decisive importance are photoabsorption and discrete–discrete transitions. This stage of the process was investigated under both the approximation of radiant heat conduction and that of the spectral kinetics. A number of mathematical physics models of radiation gas dynamics were developed at RFNC–VNIIEF, adapted to the computing power available at the time. Currently, we use a three-dimensional model in the approximation of radiant heat conduction and two-dimensional models based on the spectral kinetic equation of radiation transfer, used jointly with the equations of gas dynamics.

For a number of years, our Institute commissioned the calculation of the ranges for radiation propagating through various media at the Institute of Applied Mathematics of the Academy of Sciences. We have created precision software using modern computing capabilities for calculating spectral ranges of radiation for various substances and conditions, and developed algorithms for computing the group and average ranges in accordance with the needs of models of radiation gas dynamics. Research on radiation gas dynamics has allowed implementing control of the transfer of X-rays within the primary unit and dramatically improving the quality of the modules as energy sources for radiation implosion; this was extremely important for practical work.

The second part of the principle of radiation implosion is mainly associated with model-based research on radiation gas dynamics in the processes of reflection and transmission of X-rays through multilayer configurations of various materials, which are often multi-element geometric shapes with complex dynamics. The practical result of this research was the determination of the amount of energy available for radiation implosion of thermonuclear modules. The main requirement at the first stage was to maximize the amount of energy of X-rays emerging from the primary module, but at the second stage, it was replaced with the requirement of minimizing energy losses.

The third part of the radiation implosion principle was associated with studying the transformation of X-ray energy in the pressure field compressing the fusion module. This field, which is the result of a complex process of radiation propagation through various materials, is axisymmetrically structured. To obtain acceptable results in the compression of a thermonuclear module, it is necessary to transform the axisymmetric boundary conditions so as to achieve symmetric implosion. The solution to this problem requires the ability to control the radiation flow and the gasdynamic flows of both high-temperature and low-temperature high-density plasmas, which has been achieved by using two-dimensional models of radiation gas dynamics.

The specific features of 'boundary conditions' are such that implosion of a thermonuclear module may be relatively stable, but may happen to be unstable. Important practical applications exist in which the processes are essentially three-dimensional, and we have therefore developed three-dimensional models of radiation gas dynamics. I emphasize that the level of pressure in radiation implosion that determines the compression of fusion modules reaches several hundred TPa, and compression reached during implosion is so high that the density of materials may be greater than the initial density by a factor of several dozen.

Methods of physical and mathematical simulation play the major role in solving these problems. This is dictated both by the specifics of information obtained in testing thermonuclear charges and by the lack of testing opportunities at present. The determination of 'stability zones' of radiation implosion in thermonuclear modules, as well as the determination of physical factors that push implosion out of these zones, was among the most important experimental results.

I emphasize that the radiation gas dynamics is an outstanding example of a fundamental field of knowledge underpinning the design of structures in which complex physical processes are intertwined and the available experimental information on key parameters was very sparse. Enormous practical achievements obtained on the basis of radiation gas dynamics has undoubtedly made us leaders in this area; the least I can say is that our research results are on a par with those reported in the US.

What are the issues that I consider to be extremely important in this context?

First and foremost, we need to strengthen the experimental basis for laboratory simulation of the specific features of physical processes that have the same nature as their counterparts in radiation implosion. Such facilities are high-power lasers being developed for laser fusion. Two prototypes of such facilities operate at our institute, but their energy is insufficient for implementing the required simulation. We need a laser with the power output of the order of 1 MJ.

Installations of this class have been implemented in the US and in France and are under construction in the UK and in China. Although we submitted a proposal for building a new high-power laser for experimental research into the fundamental parameters of radiation implosion in the 1990s, the implementation has not started yet. We are very concerned about falling behind, although VNIIEF was among the world leaders in this field up to the mid-1990s. Last year, the president of the Russian Federation made a Decision in principle concerning the creation of a megajoule-level laser facility at VNIIEF.

4. Thermonuclear burning

Our institute designed a device (thermonuclear charge RDS-6c) in which the burning of thermonuclear fuel was realized for the first time on 12 August 1953. This device, developed as a model for the high-power 'hydrogen' bomb, is widely known as Andrei Sakharov's 'sloika' (layer cake). A number of fundamental questions were resolved in this project.

The device was a system of alternating layers of fusion material (lithium deuteride-tritide and lithium deuteride) and uranium with various concentrations of the isotope U-235, providing their gasdynamic implosion. I go into some detail here because this device can be regarded as a physical setup for the implementation of a pulsed thermonuclear reaction.

First, the initial heating of the fusion product was effected by the nuclear explosion of the central core of U-235. To ignite the fusion material, it was important to also subject it to implosion. Second, the developing isothermal regime between the fusion material and the surrounding uranium produced additional compression of the thermonuclear material due to pressure equalization (the process known as 'Sakharization'). Third, the burning of thermonuclear material occurred in the thermodynamic equilibrium regime between radiation and matter. Fourth, the fission of uranium by 'thermonuclear' neutrons provided an additional increase in the temperature of the medium and additional intensification of thermonuclear reactions, followed by further fission of uranium and so forth.

In the USA, Edward Teller considered a 'layered' thermonuclear charge in 1946–1947. But such a charge was never created in the United States. One of the factors that influenced this was the limited scalability of the energy release; another was a fundamental factor, the possible development of instabilities in the implosion of a layered system at the initial stage of nuclear burning.

In our design, we attached great importance to ensuring the precision of the gasdynamic implosion; the experiment confirmed the absence of significant effects of gasdynamic instabilities on thermonuclear burning.

The problem of scaling of energy release was solved by choosing radiation implosion as the method. By the time the potentials of this principle had been recognized (1954), we had in fact already designed a prototype fusion module, which was the central part of the RDS-6c. Under these new conditions of implosion that is many times more powerful, the fusion module significantly increased the energy release (lithium deuteride was used as fusion material). This principle was implemented on 22 November 1955 in testing the RDS-37. It is essential that no effect of hydrodynamic instabilities on the thermonuclear burning was found after this new form of implosion was used.

Cases occurred later during full-scale tests of thermonuclear charges of various types in which thermonuclear burning did not comply with design calculations. With time, as the physical and mathematical models were becoming more sophisticated and computing power was increasing, dramatic growth of large-scale hydrodynamic instabilities was detected in a number of cases, which led to the reduced effectiveness of thermonuclear burning.

Nearly perfect prototypes were created as part of the program of construction of thermonuclear charges, and they continue to form the foundation of nuclear deterrent. As regards their quality, they are definitely at least as good as their American counterparts.

What is the problem I would like to highlight here? Not all the results of full-scale field tests of thermonuclear charges were given consistent physical explanations. This means that not all the features of thermonuclear burning in such devices are fully understood, and we are working on further improvements in the physical and mathematical models in this area. I stress that this requires further expansion of computing power.

5. Boosting

The implementation of ignition and steady-state combustion in the tritium–deuterium (TD) mixture of nuclear charges known as boosting was a fundamental achievement of the physics of high energy density. From the practical standpoint, this led to considerable progress in the overall size and mass parameters of nuclear charges and increased their safety and operational stability in certain environments.

This is physically a very complex mode because TD ignition of a mixture occurs at relatively low temperatures created at the initial stage of a nuclear explosion, and by that instant the TD mixture itself constitutes a complex heterogeneous structure integrated with the surrounding fissile material. Gasdynamic studies play an exceptional role in finding the solution to this problem and involve radiographic methods. Radiographic experiments have shown that meeting certain criteria helps convert the potentially unstable regime of implosion in the TD mixture and the surrounding fissile material into a stable final state.

The implementation of boosting is closely linked with the methods of physical and mathematical modeling, and we have developed a number of techniques involving precision calculations in a semiphenomenological formulation. I emphasize that we were able to develop a number of methods

for controlling the boosting based on gasdynamic studies and methods of physical and mathematical modeling. These control capabilities are of exceptional practical value.

Here, I outline a significant problem. The configuration of the 'critical' region that determines the boosting is essentially three-dimensional. To determine it with sufficient accuracy, we need three-dimensional gasdynamics programs, which include a description of the detonation of HEs, and to take the specific properties of burning in this configuration into account, it is necessary to perform three-dimensional calculations of radiation gas dynamics and the nuclear neutron-initiated interaction. Because of the need to take specific characteristics of the 'critical' region into account, we need significantly more powerful computing capabilities than those currently available to us.

6. Initiation of thermonuclear fusion

The fundamental difficulties involved in realizing inertial confinement fusion are well known. This problem was partly solved at RFNC–VNIIEF. To achieve this, in 1962 we subjected a spherical system containing thermonuclear fuel but not containing fissile materials to radiation implosion. As a result, we managed to achieve the ignition of thermonuclear material with low energy release. Again in 1962, we conducted two other successful experiments in which we achieved fusion initiation of lithium deuteride. The fusion-initiation system (FIS) was used to ignite other layers of the thermonuclear fuel.

It was a very important achievement based on fundamental conclusions concerning the key role of the symmetry of compression of the FIS and the feasibility of its practical realization.

The very idea of the FIS in radiation implosion was formulated in 1954 and a series of experiments on its implementation were soon conducted. All of them have been unsuccessful. An analysis of the ignition of the FIS allowed formulating a hypothesis that the level of symmetry acceptable for the implosion of fissile materials is insufficient for the implosion of thermonuclear ignition initiating systems. Success was achieved by implementing the conclusions drawn from this hypothesis.

A large number of different types of FISs were later developed and have found important practical applications. Here, I only mention their fundamental significance for carrying out nuclear explosions for peaceful purposes.

Tests of fusion-initiating systems and the progress in simulation allowed establishing the precise criteria for their ignition taking specific features of their implosion, the materials used, and other factors into account.

7. Neutron-initiated nuclear processes

Fundamental studies of neutron-initiated nuclear processes began at RFNC – VNIIEF with the work on the critical mass of fissile materials in various configurations. This work began simultaneously with the development of the first atomic bomb RDS-1 and continues to this day. This work is based on both experiments performed on critical mass test benches and modern computational methods of simulation. Although the critical masses of important fissile materials have long been known with very high accuracy, new issues arise time and again when special materials are to be used.

Another research avenue is related to the kinetics of chain reaction in various types of systems and under different neutron exposure conditions, which is in turn one of the foundations for solving problems of nuclear explosion safety. The basis for these studies were experiments on fission cross sections, the cross sections of elastic and inelastic scattering, the numbers of secondary neutrons, and the spectra of fission neutrons; these experiments were conducted on a wide scale at our institute in the first half of the 1950s. Special programs in this field were performed for the creation of the first thermonuclear charge RDS-6c. Later, the accuracy of these 'fundamental constants' was regularly improved in new experiments.

The interaction of fusion neutrons with fissile materials under boosting conditions has become a fundamental issue. These same issues are also important for the burning regimes of thermonuclear modules.

The burning of boosted and thermonuclear charges is a very important stage and requires integrated analysis of the processes of radiation gas dynamics, charge burning, and thermonuclear neutron kinetics in multicomponent media. At the current stage, we are using a number of two-dimensional simulation programs for this purpose.

We have developed a number of methods for calculating the neutron transport in complex heterogeneous configurations and compiled high-precision systems of spectral constants and neutron group constants for all isotopes that we encounter in our work.

8. Nonequilibrium processes

Our work is directly related to studying a number of nonequilibrium processes. I cite a few examples.

One of the modes that may be encountered is where the thermodynamic equilibrium does not have enough time to set in, on the one hand, between electrons and ions, and on the other hand, between electrons and radiation. This mode was produced on numerous occasions and recorded in experiments, and we have developed special physical and mathematical models for its description.

There is a certain probability under the conditions of thermonuclear burning that even if the thermodynamic equilibrium sets in, fast particles produced in thermonuclear fusion reactions enter into new thermonuclear reactions before being thermalized. To investigate this process, we conducted a number of dedicated studies, whose results are incorporated into the models and are used in practical work.

A typical situation is that the energy flux density of X-ray radiation is much higher than the equilibrium flux density corresponding to the ambient temperature, while the spectrum of the X-ray flux is essentially non-Planckian. These factors are also included in the programs of radiation gas dynamics.

9. Conclusion

Here, I am unable to provide the most vivid examples of the work mentioned above. At the same time, these studies were accompanied by scientific searches and generated perfectly nonclassified results. Some of them relate directly to solving our main weapon-related problems, but some are only partly related. In the articles published in this issue of *Physics–Uspekhi*, our leading specialists present the results of such nonclassified research. I hope that these articles give a fairly complete picture of a number of the specific characteristics of our work.

Over the span of 65 years, a large number of outstanding specialists and great scientists in our country have taken part in creating and developing new research fields related to the

work at RFNC – VNIIEF. I do not list the names because no sampling would be sufficiently representative. It can be said that we are discussing the science of RFNC – VNIIEF in broad terms.

PACS numbers: **47.20. – k**, 47.27.wj, **47.40. – x**
DOI: 10.3367/UFNe.0181.201104i.0410

Hydrodynamic instabilities

A L Mikhailov, N V Nevmerzhitskii, V A Raevskii

1. Introduction

This article presents results of experimental research on exploring hydrodynamic instabilities and turbulent mixing in liquid, gaseous, and strength media. In particular, it is shown that (1) the development of perturbations and turbulent mixing in gases is sensitive to the Mach number of the shock wave; (2) the speed of propagation of a gas front in liquids does not change as the Reynolds number increases from 5×10^5 to 10^7; (3) the stable and unstable regimes in media with strength depend on the wavelength and amplitude of initial perturbations; (4) hydrodynamic instability may serve as an instrument to explore the strength properties of materials.

One of the most ambitious and important scientific and practical problems is that of controlled nuclear fusion (CNF). The realization of the CNF idea turned out to be principally dependent, among other things, on one 'trifle' — the Rayleigh–Taylor [1], Richtmyer–Meshkov [2, 3], and Kelvin–Helmholtz [4] hydrodynamic instabilities. Arbitrarily small initial perturbations at the interface between different media begin to grow, which, with time, leads to a turbulent mixing of substances. As a result, energy losses occur, leading to limitations on the energy density required for ignition that can be accumulated in targets.

Research on the hydrodynamic instability and turbulent mixing has been carried out at the Russian Federal Nuclear Center — All-Russian Research Institute of Experimental Physics (RFNC–VNIIEF) beginning practically from its foundation date. In particular, the main results found by Taylor (1950) (for the so-called gravitational instability) were independently obtained by S Z Belen'kii and E S Fradkin from the Lebedev Physical Institute (FIAN); they took part in work on the atomic problem at that time, and their results were collected in a series of unpublished VNIIEF reports in the late 1940s and early 1950s. This research also proposed the first semi-empiric model for the evolution of the mixing zone [5]. In 1951, through the initiative of A D Sakharov, Yu F Alekseev, I G Proskurin, and N F Zelentsova carried out the first experimental studies on turbulent mixing on an interface between two liquids, the results of which have not been published even to date.

A L Mikhailov, N V Nevmerzhitskii, V A Raevskii Federal State Unitary Enterprise 'Russian Federal Nuclear Center — All-Russian Research Institute of Experimental Physics,' Sarov, Nizhny Novgorod region, Russian Federation. E-mail: postmaster@ifv.vniief.ru

Uspekhi Fizicheskikh Nauk **181** (4) 410 – 416 (2011)
DOI: 10.3367/UFNr.0181.201104i.0410
Translated by S D Danilov; edited by A M Semikhatov

In the middle of the 1960s, in experiments on a shock tube, E E Meshkov discovered that the interface between two gases is unstable not only when the shock wave (SW) travels from a 'light' gas into a 'heavy' one (according to Richtmyer's results) but also when the SW moves in the opposite direction [3]. Since then, the instability of the interface induced through a SW is referred to as the Richtmyer–Meshkov instability. In the early 1970s, in VNIIEF, V V Nikiforov started developing the first semi-empiric models of turbulence, and the first numerical simulations of turbulent flows saw their implementation at that time (V A Andronov, S M Bakhrakh, A V Pevnitskii, and others).

The first research in the USSR on the Rayleigh–Taylor instability in solids began at VNIIEF in the late 1950s and was associated with the names of A D Sakharov, R M Zaidel', A G Oleinik, and others. The overwhelming majority of their results were not published in the open press, except the series of studies [6].

Over the last decade, hydrodynamic instabilities in different media remained the subject of thorough research, both theoretical, assisted with physical and numerical modeling, and experimental. Experiments, being a source of basic data for verification of physical and numerical models, also serve as the source of information on fundamental laws of process development and properties of substances — their strength, rheology, and phase transitions.

In Sections 2–4, we sketch some directions and results obtained over recent years in classical shock-wave experiments in shock tubes and in explosion gasdynamic systems.

2. Development of turbulent mixing and perturbations at a contact interface between gases

Numerical simulation of flows affected by turbulent mixing requires experimental data to verify and test the models. The information currently available for this purpose (see, e.g., Ref. [7]) is insufficient for the emerging new tasks. To substantiate computational algorithms, in particular, we have carried out a set of experiments in air shock tubes on the evolution of turbulent mixing in three-layer gas systems: air – SF_6 – air, air – He – SF_6, and air – He – air [8]. The contact gas interfaces were arranged perpendicular or at an angle to the direction of the SW, or had breaks. Such location of interfaces resulted in a two-dimensional flow. The gases were initially separated by a thin polymer film (1 μm thick). The Mach number of the SW reached $M \approx 1.3$. The Kelvin–Helmholtz instability, in addition to the Meshkov–Richtmyer instability, was observed at contact interfaces (Fig. 1). A fairly complex flow was formed as a result of the interaction of rarefaction and shock waves with the interfaces, offering ample material to calibrate computational techniques.

When a contact interface between gases is accelerated by a strong shock wave (with the Mach number $M > 5$) or a series of waves passing in sequence through the gases, the gases can be compressed by a factor of several dozen. As a consequence, the contact interface between gases may approach the SW front [9]. In this case, the mixing zone or perturbations appearing at the interface may rest against the front of the SW, which affects the flow character.

To explore such a situation, a laboratory technique enabling research in gases at the SW Mach numbers $M \approx 10$ was proposed in 2002. Obtaining Mach numbers that high in a shock tube was made possible by detonating a gaseous

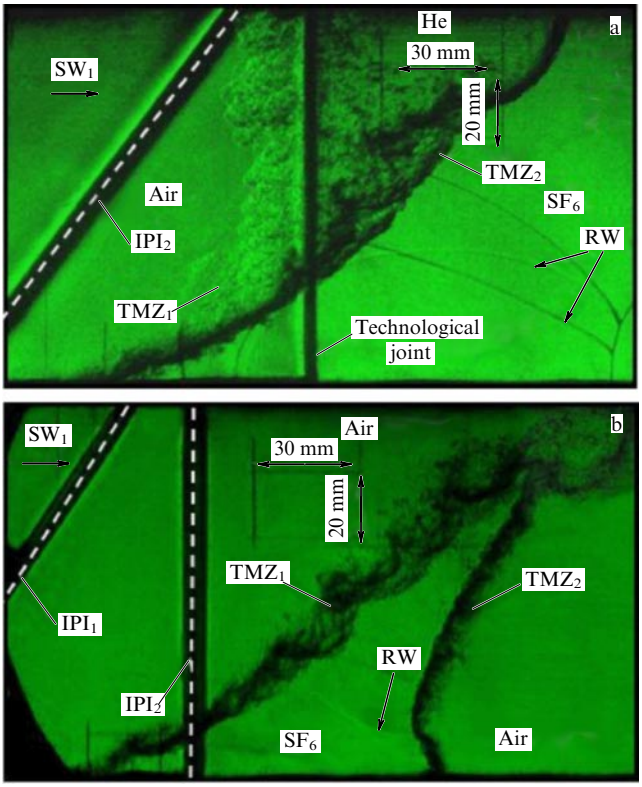

Figure 1. Photos taken in air shock tube experiments exploring the development of turbulent mixing in (a) air–He–SF_6 and (b) air–SF_6–air systems. $IPI_{1(2)}$ is the initial position of the interface, $TMZ_{1(2)}$ is the turbulent mixing zone, and RW is the reflected wave. The size of the reference mesh is 30 × 20 mm.

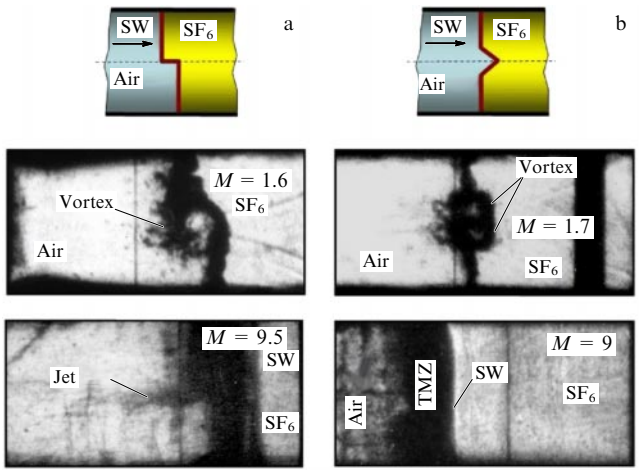

Figure 2. Moving image frames showing the development of two-dimensional local perturbations at the air–SF_6 interface with a contact boundary shaped as a step (a) and a triangular groove (b). M is the Mach number of the SW in SF_6.

explosive mixture ($C_2H_2 + 2.5O_2$) placed into a high-pressure chamber under excessive pressure [9].

Figure 2 displays moving image frames showing the development of two-dimensional localized perturbations at the air–SF_6 interface shaped as a break in the contact boundary (step) and as a triangular groove, which schematically represent possible technological defects of the shell of the nuclear fusion target. Variations in the SW Mach number led to different compression ratios of SF_6.

Experiments show that as the compression of the 'heavy' gas increases with the Mach number being increased, the character of the perturbation evolution changes: the perturbation is retarded by the adjacent shock wave (because of the SW proximity to the contact interface), which leads to its full suppression in the turbulent mixing zone; the mixing zone proper develops more vigorously.

3. Development of turbulent mixing and perturbations at a gas–liquid interface

It is known that for the Rayleigh–Taylor instability at the self-similar stage of turbulent mixing, the penetration depth of a 'heavy' substance into a 'light' one, h_{h-l}, of the light substance into the heavy one, h_{l-h}, and the full mixing zone width H are given by

$$h_{h-l} = \alpha_1 A g t^2, \qquad h_{l-h} = \alpha_2 A g t^2, \qquad H = \alpha A g t^2, \qquad (1)$$

where $A = (\rho_h - \rho_l)/(\rho_h + \rho_l)$ is the Atwood number, ρ_h and ρ_l are the densities of 'heavy' and 'light' substances, g is the acceleration, t is the time, and α_1, α_2, and α are constants characterizing the respective growth rates of h_{h-l}, h_{l-h}, and H. Different sources provide different values of α_1, α_2, and α.

Early experimental study [10] gave $\alpha_2 \approx 0.07$, while calculations in Ref. [11] gave $\alpha_2 \approx 0.05$. Later, Ref. [12] reported $\alpha_2 \approx 0.03$ from computations for ideal liquids, and experiments with mutually soluble liquids gave $\alpha_2 \approx 0.04$ [10]. In experiments on the gas–water interface at $g \approx 10^5 g_0$ (where $g_0 = 9.8$ m s^{-2}), gas temperature $\approx 2000\,^\circ$C, and pressure ≈ 400 atm (i.e., for the supercritical state of the surface liquid layer) and layer displacement $S \leqslant 25$ mm, Ref. [13] reports $\alpha_2 \approx 0.03$. The reasons for scatter in α_2 are still unclear. It was supposed that α_2 decreases with an increase in the Reynolds number of the flow.

To study this question, we constructed a plant enabling flows with Re $\approx 10^7$. In this plant, a liquid layer ≈ 3 kg in mass was accelerated by compressed gas. The acceleration reached $g \approx 10^3 g_0$, the layer displacement was $S = 350$ mm, and the mixing zone width H was equal to 200 mm [14]. The Reynolds number in the experiments was determined as

$$\mathrm{Re} = \frac{H\sqrt{AgH}}{\nu},$$

where $A \approx 1$ and ν is the kinematic viscosity coefficient in water.

It was found in experiments that for Re $\leqslant 10^5$ ($S < 50$ mm), $\alpha_2 \approx 0.11$, and as Re increases to $\approx 5 \times 10^5$ (50 mm $< S <$ 70 mm), α_2 decreases to 0.075. If Re increases further to $\approx 10^7$ ($S > 70$ mm), α_2 does not change. For $S > 70$ mm, the values $\alpha_1 \approx 0.26$ and $\alpha \approx 0.33$ were obtained. The zone asymmetry coefficient is $k = \alpha_1/\alpha_2 \approx 3$.

For the gas–liquid interface (under the conditions of heterogeneous mixing) for $g \approx 10^3 g_0$ and $5 \times 10^5 <$ Re $\leqslant 10^7$, we thus find the value $\alpha_2 \approx 0.07$, which coincides with the results of earlier experiments. Therefore, the reduction in α_2 to 0.03–0.04 cannot be explained solely by an increase in the Reynolds number. The value $\alpha_2 \approx 0.03$ can be related to a special case for particular experiments and computations. Research is needed to find the conditions under which α_2 decreases, because α_2 determines the physical scale of substance mixing.

The development of local perturbations in weakly compressible media can differ substantially from the development of perturbations in compressible media. According to Ref. [15], a hemispheric local perturbation (LP) at an unstable

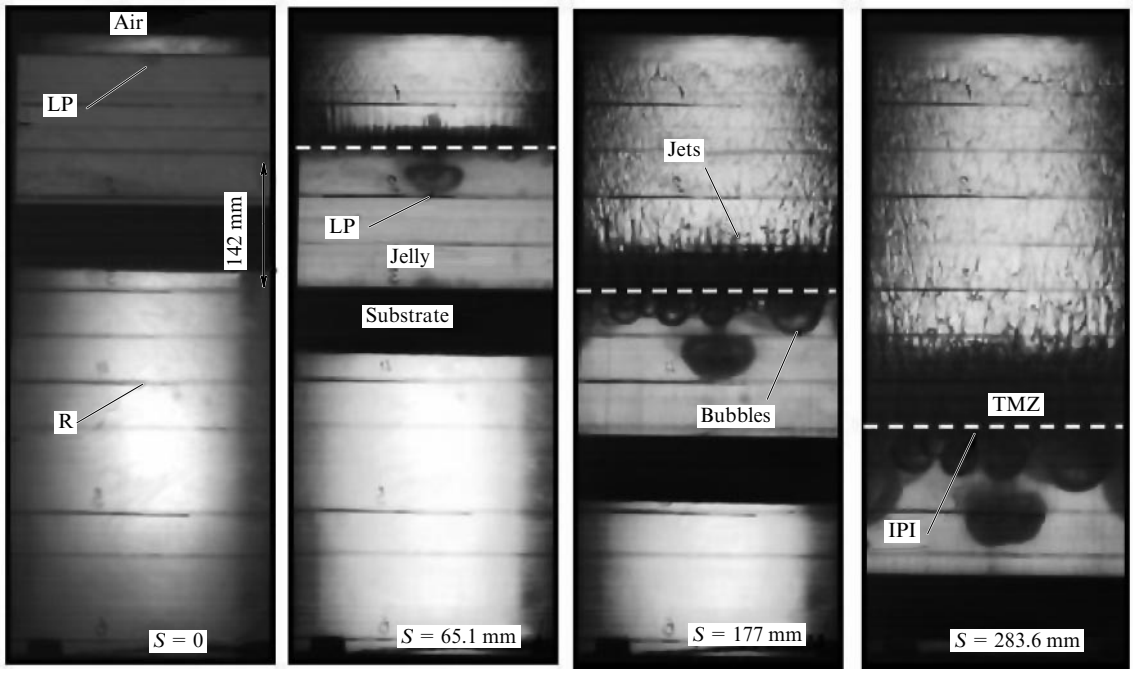

Figure 3. The development of a hemispheric local perturbation (LP) for various displacements of the contact boundary. R is the reference line. A 2.2% (low-strength) jelly of gelatine solution was used as a liquid, similarly to Ref. [16].

interface of an incompressible fluid approaches with time a self-similar regime of evolution. Papers [16, 17] show that as the initial radius of such a perturbation increases from $R \approx 0.5$ mm to $R \approx 3$ mm in the presence of a turbulent mixing zone at a gas–liquid contact interface, the velocity of its penetration in the liquid increases approximately twofold, i.e., self-similarity is absent. Experiments [16] and computations [17] were carried out for fairly small displacements of the contact interface ($S \approx 40$ mm). How does such a perturbation evolve for larger interface displacements? To clarify this question, additional studies were undertaken for layer displacements up to 350 mm.

It was found that a local perturbation initially evolves as in Ref. [16], in the form of a bubble (Fig. 3) ahead of the turbulent mixing front. For the layer displacement $S < 50$ mm, the speed of the perturbation penetrating into the liquid increases as the initial radius of the local perturbation increases, similarly to Refs [16, 17]. For the range of layer displacements $50 \text{ mm} < S < 350$ mm, the rates of perturbation growth become close, i.e., the process of perturbation evolution reaches the self-similar phase. The time it takes the perturbation to reach this mode increases as its initial radius increases. The development of such perturbations in shells of inertial nuclear fusion targets may result in their breakup.

4. Development of perturbations in media with strength

Until some time ago, the presence of strength in solids allowed assuming that they are free of problems with instabilities. But the stabilizing property of strength is lost when stresses exceed it. It is also known that the strength in dynamical nonstationary processes essentially depends on how the material was deformed — on the values of the pressure, temperature, and deformation rate. Additionally, if structural and phase transitions occur in a material under the action of intense dynamical factors, its strength can also change. Hence, it follows that hydrodynamic instabilities, apart from being a subject of research aimed at their eventual suppression, can also serve as a tool for enabling the strength properties and phase state of materials to be explored under extreme conditions.

In their studies of the Richtmyer–Meshkov instability, the authors of Ref. [18] assumed that as the SW intensity approaches values corresponding to SW metal melting, an abrupt reduction in the strength of the layered system is observed, which leads to the turbulization of the flow and the intense mixing of metals. This effect was indeed observed (Fig. 4) and triggered a series of publications and patents on inventions. However, the observed values of SW amplitudes at which the interface between metals becomes unstable correlate, but do not fully agree with computed parameters for the range of SW melting of the more infusible metal. This is most likely related to thermal strength loss in metals as the range of SW melting is approached from below.

As demonstrated in [19], periodic perturbations at the accelerated interface of an elastoplastic layer can increase up to some final magnitude and then perform periodic oscillations, i.e., the interface motion can be stable. But for a certain combination of parameters, an infinite growth in perturbations is possible, i.e., the Rayleigh–Taylor instability occurs. It was found that the boundary between stable and unstable modes in the amplitude (a_0) – wavelength (λ) coordinates obeys the approximate equation [19]

$$a_0^{\mathrm{c}} = \frac{2Y}{\rho g}\left[1 - \frac{4\sqrt{3}-1}{4\sqrt{3}}\exp\left(-\frac{2\pi h}{\sqrt{3}\,\lambda}\right)\right] \times \left\{\left[1 - \exp\left(-\frac{2\pi h}{\sqrt{3}\,\lambda}\right)\right]^2 - \left(\frac{\lambda}{\lambda_\infty}\right)^2\right\}, \qquad (2)$$

where Y is the yield point, ρ is the density, h is the layer thickness, $\lambda_\infty = 4\pi G/(\rho g)$ is the critical wavelength for elastic half-space, and G is the shear modulus.

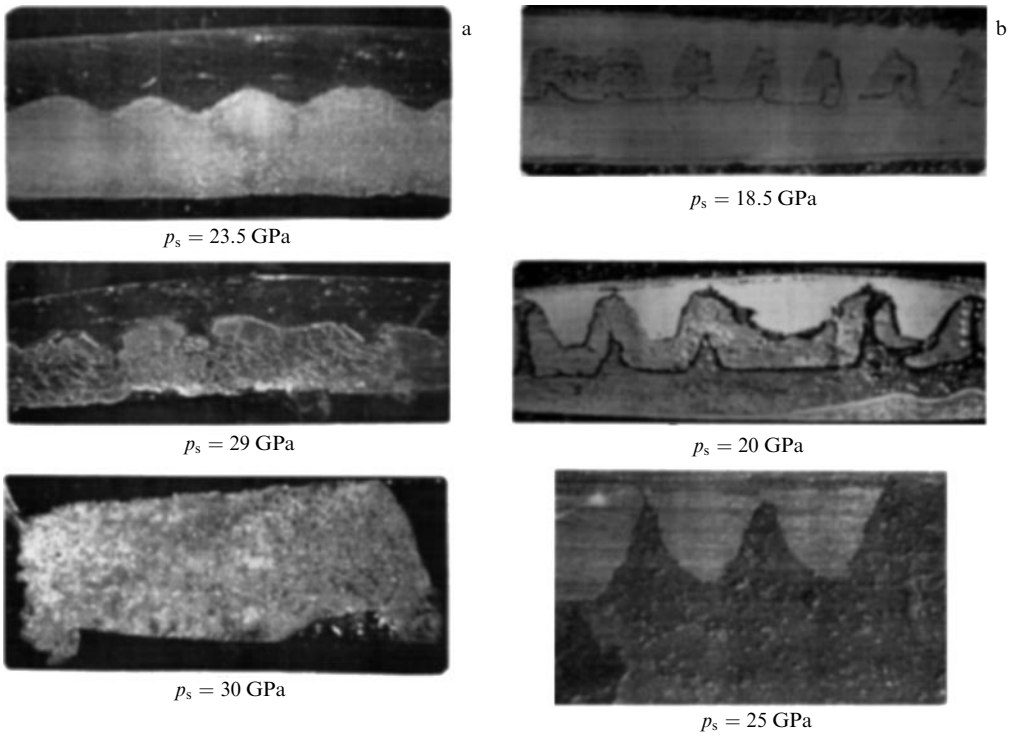

Figure 4. Development of the instability on an Sn–Cd metal interface with $\lambda_0 = 1.1$ mm and $a_0 = 0.2$ mm (a) and Pb–Bi with $\lambda_0 = 1.6$ mm and $a_0 = 0.2$ mm (b) as the SW pressure p_s is increased.

The 'plastic' and 'elastic' instability criteria were respectively proposed in [20, 21]. The Drucker criterion is valid for perturbations with wavelengths much smaller than the critical one ($\lambda \ll \lambda_c$), while the Miles criterion becomes relevant for perturbations with small amplitudes. As follows from Eqn (2), the stability domain in $a_0 - \lambda$ coordinates has a finite area and is realized for fairly small amplitudes and wavelengths. For a wavelength larger than the critical one, $\lambda \geqslant \lambda_c$, the interface is unstable for any perturbation amplitude.

In real SW processes, the layer acceleration has a pulsed character, and the instability domain is smallest at the instant of maximum acceleration. Although a steady boundary of the stability domain does not exist in this case, the growth of the perturbations for a certain combination of the initial amplitude and the wavelength of perturbations appears to be highly sensitive to the initial perturbation size, the value of the occurring stresses, and the real dynamical shear strength of the material.

This is the basis of the method of constructing and testing models of material strength — the dynamic perturbation method. Its essence is as follows. Periodic (or local) perturbations are applied to the surface of a layer of the substance to be explored. The sample is then subjected to pulsed acceleration — in our case, by products of the explosion of a chemical high explosive. The development of the perturbation in the course of liner motion is recorded with the help of the pulsed X-ray or protonographic technique.

A diagram of the method in the case of pulsed liner acceleration by the explosion products is shown in Fig. 5. Shown also are typical protonographic images of the liner obtained in a certain experiment [22].

In choosing a particular model of metal strength, the model parameters are determined by fitting the results of numerical simulations to experimental data on the development of perturbations. The advantage of this method is that by varying the rate and amplitude of the impact and the wavelength and amplitude of perturbations in the case of explosions in planar or cylindrical geometry allows finding the parameters of the constitutive matter equation $Y_d = f(\sigma, T, \varepsilon, \dot{\varepsilon}, \ldots)$ in the pressure range $p \approx 10-300$ GPa, the deformation rate range $\dot{\varepsilon} \approx 10^5 - 10^9$ s^{-1}, and the temperature range from normal to metal melting temperatures.

This method is now used by many laboratories worldwide that deal with extreme states of matter [23, 24] and use not only explosion but also other systems.

One of the principal results obtained with the perturbation method was the discovery of a noticeable excess of the dynamic yield threshold for some metals under quasi-isentropic load ($\dot{\varepsilon} \approx 10^5 - 10^6$ s^{-1}, $p \approx 30-50$ GPa) over that under SW load ($\dot{\varepsilon} \approx 10^8$ s^{-1}). Just behind the SW front, a metal behaves as if it were losing strength over a time interval $\approx 0.1-0.5$ μs and then quickly regained it. The explanation, as currently conceived, consists in the 'instantaneous loss of strength' in narrow ($l \approx 1$ μm) bands of localized shear with the period ≈ 10 μm between them, with a subsequent fast (≈ 1 μs) relaxation of flow. The heterogenous character of the flow behind the SW front is confirmed by independent registration of the metal free surface speed by methods of Doppler diagnostics [25].

Of practical interest is a particular case of the Richtmyer–Meshkov instability when an SW hits a free surface of condensed matter, which is manifested through a microcumulative ejection of the advancing cloud of finely dispersed particles. The main causes of this effect are the initial perturbations of a regular and chaotic character: the roughness of the free surface, structural inhomogeneities of the material, and heterogeneity of the flow behind the SW front mentioned above [26]. Figure 6 presents a moving image frame showing particle ejection from a free surface of a lead

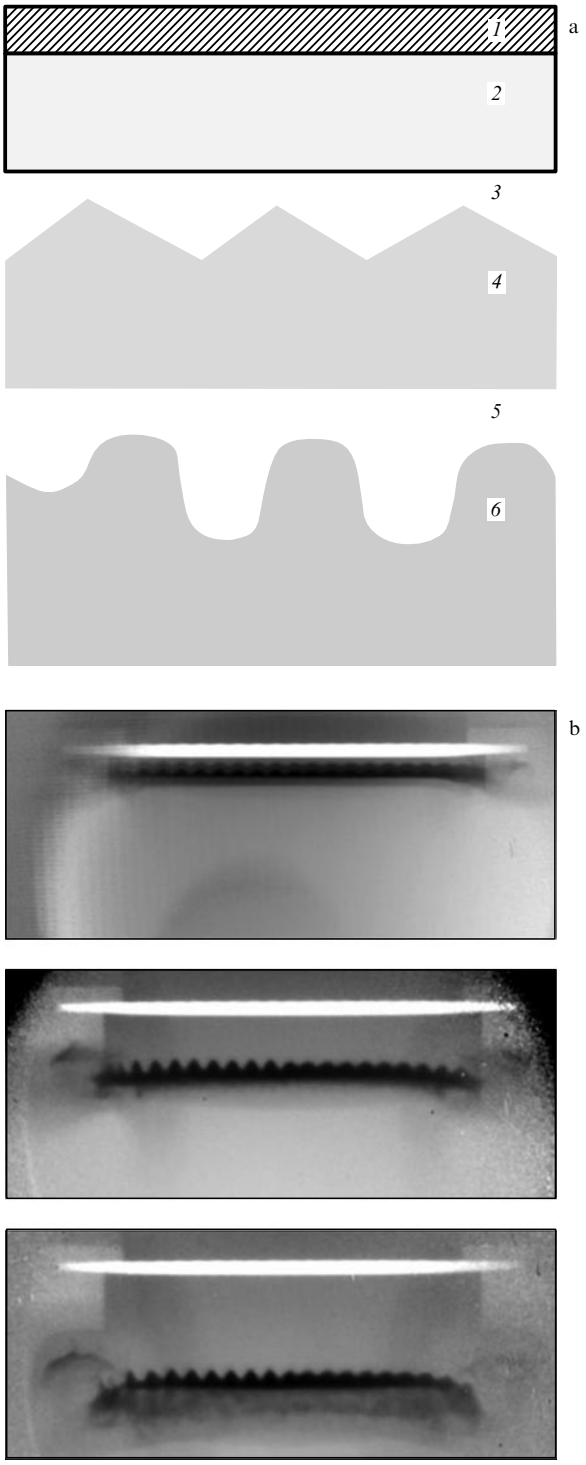

Figure 5. (a) Schematic illustration of the process of pulsed acceleration of a liner: *1* — the generator of a plane detonation wave, *2* — high explosive, *3* — vacuum gap, *4* — the sample in its initial state, *5* — products of explosion, *6* — the sample in motion. (b) Protonographic image of the liner.

sample under the action of an SW with the intensity 15 GPa, obtained by high-speed microscopic electronic-optical recording with pulsed laser illumination [27].

Gravitational instabilities also play a dominant role in the explosive volume expansion, breakup, and dispersion of metals as they melt in an SW and the rarefaction wave that follows [25].

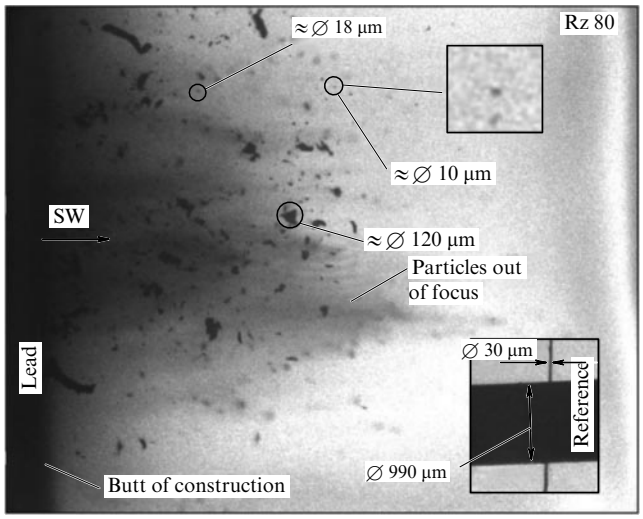

Figure 6. Moving image frame of particle ejection from the free surface of a lead sample under the action of an SW with the intensity 15 GPa. The inset in the right bottom corner shows reference scales that help determine the sizes of ejected particles. Rz 80 is the parameter of surface roughness.

The Kevin–Helmholtz instability in metals in its pure form (free slip) is described in Ref. [28], but much more frequently it is detected in regimes of explosive welding — for the oblique impact of plates with the phase speed of the contact point $U_c < c_0$, where c_0 is the speed of sound in the bulk of the metals to be welded.

The dependence of the amplitude of perturbations of a shear nature, generated under similar conditions of explosive welding, on the Mach number, $a = f(M)$, was obtained for certain metals. It reaches a maximum in the vicinity of $M \approx 1.3-1.5$, at which a flow mode with detached shock waves is overtaken by that with waves attached to the impact point.

The most impressive results of this research are the unexpectedly high and dynamic plasticity of beryllium, fragile under static conditions, and the capability of thin (≈ 10 μm) galvanic coatings to suppress the development of shear instabilities [29].

The authors are indebted to all their colleagues at the Institute of Experimental Gas Dynamics and Physics of Explosions (IPE) at RFNC–VNIIEF, whose efforts and collaboration made the results presented here possible.

References

1. Taylor G *Proc. Roy. Soc. Lond. A* **201** 192 (1950)
2. Richtmyer R D *Commun. Pure Appl. Math.* **13** 297 (1960)
3. Meshkov E E *Izv. Akad. Nauk SSSR Mekh. Zidkosti Gaza* (5) 151 (1969) [*Izv. Acad. Sci. USSR Fluid Dyn.* **4** (5) 101 (1969)]
4. Helmholtz H L F "Über discontinuirlich Flüssigkeits-Bewegungen" *Monatsberichte Königl. Preuß. Akad. Wiss. Berlin* 215 (1868)
5. Belen'kii S Z, Fradkin E S *Tr. Fiz. Inst. Akad. Nauk* **29** 207 (1965)
6. Sakharov A D et al. *Dokl. Akad. Nauk SSSR* **159** 1019 (1964) [*Sov. Phys. Dokl.* **9** 1091 (1965)]
7. Dudin V I et al. "Issledovanie razvitiya vozmushchenii i turbulentnogo peremeshivaniya na granitse gaz–gaz metodom lazernogo nozha" ("Study of the development of perturbations and turbulent mixing using the method of laser knife"), Preprint No. 49-96 (Sarov: RFYaTs–VNIIEF, 1996)
8. Nevmerzhitskii N V et al. *Vopr. At. Nauki Tekh. Teor. Prikl. Fiz.* (3) 44 (2009)

9. Nevmerzhitskii N V et al., in *IX Kharitonovskie Tematicheskie Nauchnye Chteniya* (IX Khariton Topical Scientific Readings) (Sarov: RFYaTs–VNIIEF, 2007) p. 612
10. Read K I *Physica D* **12** 45 (1984)
11. Youngs D L *Physica D* **12** 32 (1984)
12. Youngs D L *Laser Part. Beams* **12** 725 (1994)
13. Nevmerzhitskii N V, Sotskov E A, Drennov A O, in *V Kharitonovskie Tematicheskie Nauchnye Chteniya* (V Khariton Topical Scientific Readings) (Sarov: RFYaTs–VNIIEF, 2003) p. 357
14. Nevmerzhitskii N V et al., in *XI Kharitonovskie Tematicheskie Nauchnye Chteniya* (XI Khariton Topical Scientific Readings) (Sarov: RFYaTs–VNIIEF, 2009) p. 583
15. Garanin S F *Vopr. At. Nauki Tekh. Teor. Prikl. Fiz.* (3/1) 12 (1994/1995)
16. Sotskov E A et al., in *V Kharitonovskie Tematicheskie Nauchnye Chteniya* (V Khariton Topical Scientific Readings) (Sarov: RFYaTs–VNIIEF, 2003) p. 362
17. Raevskii V A, Sinitsyna S N, Yanilkin Yu V, in *V Kharitonovskie Tematicheskie Nauchnye Chteniya* (V Khariton Topical Scientific Readings) (Sarov: RFYaTs–VNIIEF, 2003) p. 366
18. Mikhailov A L et al., in *Proc. of the Conf. of Am. Phys. Soc., SCCM-1995, Seattle, Washington, 1995*, p. 985
19. Lebedev A I et al., in *4th Intern. Workshop on the Physics of Compressible Turbulent Mixing, Cambridge, 1993*, p. 81
20. Drucker D C "'Taylor instability' of the surface of an elastic-plastic plate" *Mech. Today* **5** 37 (1980) [Translated into Russian, in *Mekhanika Deformiruemykh Tverdykh Tel. Napravleniya Razvitiya* (Moscow: Mir, 1983) p. 151]
21. Miles J W, General Atomics Report, GAMD-7335 (1960)
22. Antipov Yu M et al. *Prib. Tekh. Eksp.* (3) 5 (2010) [*Instrum. Exp. Tech.* **53** 319 (2010)]
23. Kaul M Ann et al., in *IV Kharitonovskie Tematicheskie Nauchnye Chteniya* (V Khariton Topical Scientific Readings) (Sarov: RFYaTs–VNIIEF, 2003) p. 327
24. Covallo M R, in *Dynamic Strength Experiments, Joint US-Russia Conf. on Advance in Material Science, 2009*
25. Mikhailov A L *Fiz. Mezomekh.* **10** (5) 53 (2007)
26. Ogorodnikov V A et al. *Fiz. Goreniya Vzryva* **34** (6) 103 (1998) [*Combustion Explosion Shock Waves* **34** 696 (1998)]
27. Nevmerzhitskii N V et al., in *Mezhd. Seminar po Fizike Turbulentnogo Peremeshivaniya Szhimaemykh Sred, Rossiya, Moskva, 2010* (Intern. Seminar on Turbulent Mixing in Compressible Media, Russia, Moscow, 2010)
28. Mikhailov A L *Fiz. Goreniya Vzryva* **15** (2) 158 (1979)
29. Drennov O B et al., in *Proc. of the APS Conf. SCCM-2001, Atlanta, USA, 2001*, p. 595

PACS numbers: 05.70.Ce, **07.35.+k**, **47.40.–x**
DOI: 10.3367/UFNe.0181.201104j.0416

Extreme states of metals: investigation using shock wave techniques

R F Trunin

1. Introduction

The beginning of the research reviewed here dates back to 1947, when the gasdynamics scientists of KB-11 [presently the Russian Federal Nuclear Center — All-Russian Research Institute of Experimental Physics (RFNC–VNIIEF)] were given the task of investigating the shock wave properties of the substances used in the design of the atomic bomb developed in the USSR. These properties were required to select its design on the basis of calculations, because the properties-based equation of state, i.e., the relation between pressure, density, and energy, closed the system of equations of motion and thereby allowed estimating the parameters of compression of the active and other substances.

Our pioneers of experimental investigations in this area were L V Al'tshuler, K K Krupnikov, V A Tsukerman, B N Ledenev, V I Zhuchikhin, S B Kormer, and their collaborators. Scientists of the theoretical divisions, Ya B Zel'dovich, E I Zababakhin, G M Gandel'man, N A Dmitriev, V P Kopyshev, and others, actively participated in the development of research methods and the interpretation of the data obtained. The contribution of Yu B Khariton was inestimable as regards the scientific organizational aspects.

The techniques proposed for determining the parameters of shock-compressed substances enabled making the first measurements of their characteristics already in 1947.

The first substance whose properties had to be known to ensure the success of a bomb test was the explosive that was part of the bomb. Many are familiar with the epic work to obtain the detonation parameters of this explosive (see, e.g., Ref. [1]), and I do not therefore enlarge on this issue. I merely mention that only owing to Zel'dovich was it possible to eliminate the existing discrepancies between detonation parameters and thereby resolve the burning problem of the bomb test.

Uranium became the first metal investigated in 1947; its compression was studied at pressures up to 500 kbar.

The measurements were initially made using the spall technique; owing to its low precision, it soon gave way to the absolute method of 'deceleration' [2] and the method of 'reflection' [3] based on its principles.

The majority of measurements whose results are partially outlined in Sections 3–5 were carried out using the last two techniques. According to them, two kinematic parameters are determined from experiments: the shock velocity D in a sample and the velocity of motion of the substance behind the front, the so-called particle velocity U.

The shock velocity is easily determined in both techniques: all that has to be done is, in the path of wave propagation, to place sensors of an arbitrary type that react to the high pressures of the front and to record the time of wave passage between them.

Special methods were introduced for determining the particle velocity, permitting indirect determination of this parameter. The reader can become familiarized with them using source materials [2, 3]. Here, I only recall that according to the deceleration method proposed by Al'tshuler, the velocity W of a striker (liner) approaching a target is precisely equal to the doubled value of the particle velocity U in the target (when the liner and the target consist of the same material). Applications of the reflection method (Al'tshuler, Krupnikov, and Gandel'man) require the knowledge of the equation of state of the material of the screen that covers the samples on the side of the approaching shock wave and the parameters of this wave in the screen. The particle velocity U in the substance under investigation is found by considering the decay of an arbitrary discontinuity in the pressure–particle velocity diagram.

R F Trunin Federal State Unitary Enterprise 'Russian Federal Nuclear Center — All-Russian Research Institute of Experimental Physics,' Sarov, Nizhny Novgorod region, Russian Federation
E-mail: root@gdd.vniief.ru

Uspekhi Fizicheskikh Nauk **181** (4) 416–422 (2011)
DOI: 10.3367/UFNr.0181.201104j.0416
Translated by E N Ragozin; edited by A M Semikhatov

The thermodynamic parameters of the compressed substance — the pressure, density, and energy of shock compression — are determined via these kinematic quantities from the conservation laws for momentum $P - P_0 = DU/V_0$, mass $V/V_0 = (D - U)/D$, and energy $E - E_0 = 0.5(P + P_0)(V_0 - V)$. Here, P, V, and E are the pressure, the specific volume, and the internal energy; the subscript '0' pertains to the initial values of these quantities. The temperature of shock-compressed substances is not measured directly but obtained from the equation of state (EoS) constructed on the basis of these parameters.

The conservation equations underlie the so-called Hugoniot adiabat — the adiabat $P_H = P_H(V, P_0, V_0)$ of the material under investigation, which is the continuum of thermodynamic states resulting from the shock compression of the material that was initially in the state with P_0 and V_0.

The Hugoniot adiabat is the main source of experimental information that underlies the determination of other matter equations of state. Other shock wave characteristics of material — sound velocities behind the shock front, expansion and twofold compression adiabats, shock compression temperatures, and so on — are directly related to the shock adiabat and are largely determined by it. This is the reason why emphasis is placed on the investigation of shock adiabats in the determination of matter equations of state.

A remarkable property of shock adiabats is that they are approximated by linear or nearly linear dependences in the $D-U$ coordinates in a wide range of these parameters. This rule — the linearity of $D(U)$ — was experimentally shown over a wide range of D and U in several hundred cases of investigation of different materials, from gaseous to initially solid. Of course, this representation is some approximation to reality, because real 'perturbations' exist on the linear $D(U)$ representations arising from physical processes that occur under shock compression: melting, evaporation, dissociation, and so on. This gives rise to deviations from linearity; however, they are not large enough to invalidate the general tendency rule, the linearity of adiabats in the $D-U$ diagrams.

Another property of shock adiabats demonstrated in experiments must also be mentioned. For high shock parameters ($D > 10-15$ km s^{-1}), the shock adiabats exhibit a universal slope $D'_U \approx 1.2$, which is characteristic both of different substances and of materials with different initial densities.

To determine the kinematic parameters D and U, two types of measuring devices are primarily used at VNIIEF: 'planar' devices [4], which produce a plane stationary shock wave in the samples under investigation, and spherical (to be more precise, hemispherical) [5], which form a spherical shock wave converging to the center of the system.

Almost until the end of the past century, a third source of shock waves also existed, which was far superior to the first two. The case in point is the high-power shock waves in rock induced by underground nuclear explosions, which could be used as an instrument for solving research problems [6].

This brings up the question: why should we aspire to increase the pressure at all? The pressure 0.5 Mbar in uranium was achieved back in 1947! Can we stay with that figure? But in the operation of a nuclear charge, the compression of its constituent materials proceeds at different pressures, including those that far exceed the value specified above. That is why these states had to be studied. This was the subject of active research in our laboratory during the subsequent period.

2. Measuring devices

The hemispherical measuring charge proposed by Al'tshuler, Zababakhin, Zel'dovich, and Krupnikov in 1948 is a universal measuring device for determining the shock compression of materials. Its structure has been repeatedly conceptualized in many papers (see, e.g., Refs [5, 7, 8]), and is therefore not reproduced here. I only recall that the charge is a hemisphere of a high-power explosive, which is simultaneously initiated over its entire outer surface. Inserted into the inner (also hemispherical) cavity of the charge is a steel hemisphere — the striker — which is accelerated to the center of the system by the explosion products of a converging detonation wave and strikes the target samples at the radius selected for the investigation and imparts the converging shock wave to them. The first measuring devices of this kind had several disadvantages (insufficiently high symmetry of the converging shock wave, ambiguity in the inclusion of the wave nonstationarity, the density nonuniformity of the explosive, and so on). The devices were improved [5, 7, 8] in the 1960s so as to minimize these and some other disadvantages: higher-power explosives with a higher density stability were used and the focusing system was replaced with a higher-performance one. This resulted in a significant improvement in wave symmetry, which in turn permitted decreasing the thickness of the samples and made the inclusion of nonstationarity less ambiguous. An air gap was introduced between the striker and the explosive, which softened the pressure of the first wave arriving at the striker. These and some other alterations served to stabilize the initial discharge parameters. The shell velocity measured at different radii in its motion ranges from 7 km s^{-1} at 'high' radii to 23 km s^{-1} at 'deep' radii.

The modern theory of the charge was elaborated by L V Al'tshuler, A A Bakanova, N V Panov, and the author.

3. Growth dynamics of the pressures investigated

I next consider the dynamics of pressure growth in the compressive investigation of one of the main structural materials, iron (a similar picture is also observed for uranium and other substances). The corresponding diagram is given in Fig. 1. Of course, our attention is drawn to the rapid progress as regards the increase in pressures attained. Even in 1951, we obtained pressures above 10 Mbar in iron. These measurements were made by Al'tshuler, Krupnikov, Ledenev, and M I Brazhnik. The dashed vertical segments in Fig. 1 signify that at that time, the authors of these data had some slight doubts about the accuracy of the high points achieved. More recently, the position of these points was confirmed using modern measuring devices with improved characteristics. Therefore, these doubts were removed. It is pertinent to note that similar values for the parameters in iron were obtained in the USA more than 30 years later.

The highest parameters that we obtained in the investigation of the compressibility of iron in laboratory facilities are equal to 18 Mbar; even higher values (25 Mbar) were recorded in the investigation of tantalum [8–10].

Is it possible to obtain even higher pressures with spherical systems? Yes, it is. But these systems would be so expensive that the pros and cons should be weighed when considering the expediency of their implementation. Furthermore, even the values already attained permit us to accurately select the theoretical model suitable for calculating our structures, including those for significantly higher pressures than the experimentally attained ones.

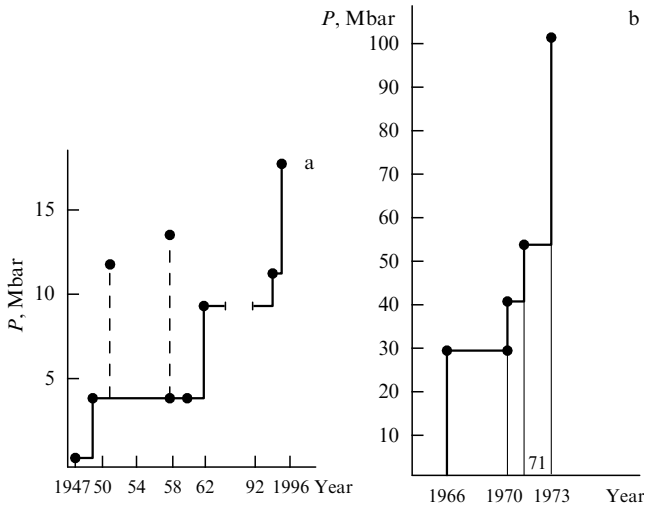

Figure 1. Temporal diagrams of pressure growth in the investigation of shock wave compression of iron: (a) laboratory research, (b) investigations involving underground nuclear explosions.

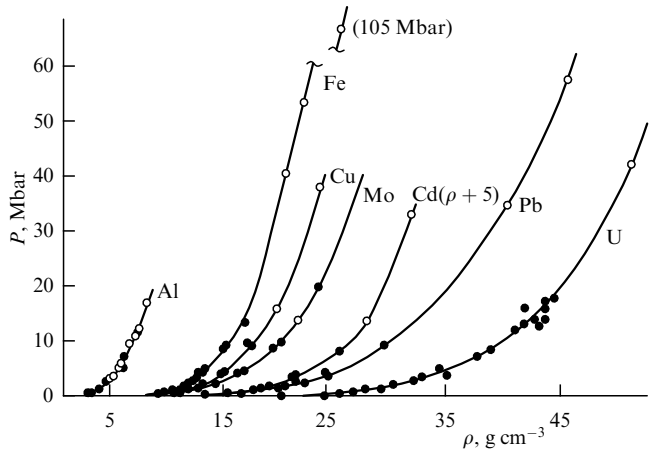

Figure 2. Shock adiabats of metals investigated in laboratory conditions (dark circles) and in underground nuclear explosions (empty circles). The inscription 'Cd $(\rho + 5)$' signifies that all density values for the corresponding adiabat are shifted along the horizontal axis by 5 g cm^{-3} for convenience of representation.

Figure 1b shows the growth in pressures (also for iron) under conditions of nuclear test explosions.

I briefly recall the setup of these experiments [6]. In a tunnel, near the nuclear charge to be tested, a technological site was made directly in the rock, the center of the site area being perpendicular to the direction to the charge center. The site accommodated a measuring device, which comprised a steel striker-plate and a steel target located at the optimal distance from the plate (optimal from the standpoint of attaining a constant plate flight velocity). The design of the measuring device ensured a lowering of the shock wave load on the striker and the suppression of perturbations propagating in front of the striker toward the recording system.

Because iron plays an important role in the method of reflections as the reference material, several measurements of iron compression were performed by the absolute method of deceleration [2], whereby measurements were simultaneously made of the velocity of the impinging steel striker-plate and the velocity of the shock wave in the target (steel-3).

These measurements turned out to be effective in three experiments. Their data have been widely discussed in the scientific literature, at conferences, and so on (see, e.g., Refs [6, 11, 12]), and I therefore only mention the main results.

The following parameters were obtained:

— the pressures 41.3, 54.2, and 105.0 Mbar in three iron specimens;

— the respective compressed sample densities 21.7, 23.00, and 26.5 g cm^{-3};

— the respective impinging striker velocities 36.5, 42.7, and 60.8 km s^{-1}.

Under similar conditions and much later, our colleagues in the USA attained a pressure of only 20 Mbar (with molybdenum).

The resultant data points defined the position of the shock adiabat of iron throughout the range of pressure investigated, up to 105 Mbar, thereby opening the way to the pursuance of material compression measurements both in laboratory conditions and in conditions of underground nuclear tests under ultrahigh pressures (reflection method, iron screen).

The same data provided the answer to the question about the selection of the material behavior model in the ultrahigh pressure domain that was most adequate for the experiment.

Figure 2 shows our metal compression curves obtained both in laboratory investigations and with underground nuclear explosions. Attention is drawn to the fact that underground nuclear test and laboratory pressure data for Mo and especially for Al overlap and are mutually consistent. Similar agreement is supposedly observed for other elements. This is supported by the agreement of similar data for complex compounds like plexiglass and rock salt [13, 14]. Furthermore, a reasonable interpolation of the data pertaining to different pressures suggests that laboratory and nuclear test data are mutually consistent for other metals as well.

I now consider how the resultant experimental data correspond to the theoretical dependence in our use. For example, Fig. 3 shows the data on iron and lead. The dashed line is the adiabat calculated by the Thomas–Fermi model with the inclusion of nuclear interaction (TFCK, an acronym for 'the Thomas–Fermi model + corrections due to Kalitkin and Kopyshev'). At pressures of the order of 100 Mbar, the calculated and experimental adiabats are virtually coincident, as are their derivatives.

Much the same picture also occurs for other metals [6, 7]. Also noteworthy is the fact that other theoretical models are in a much poorer agreement with experiment [6].

The experimental verification of the TFCK model opened the door to an extension of research into the compressibility of different materials to the ultrahigh-pressure domain. And these opportunities were rather amply used.

To summarize, the shock compression of more than 250 substances was studied in our laboratory. These include virtually all metals of the periodic system, including hydrogen isotopes and several transuranium elements, metal alloys, oxides, metal hydrides and nitrides, the majority of representatives of organic compounds, and liquids. To this may be added more than a hundred shock adiabats of surface rocks [15].

4. Compression of porous metals

I next consider the investigation of the shock compression of porous metals, i.e., metals with an artificially lowered initial

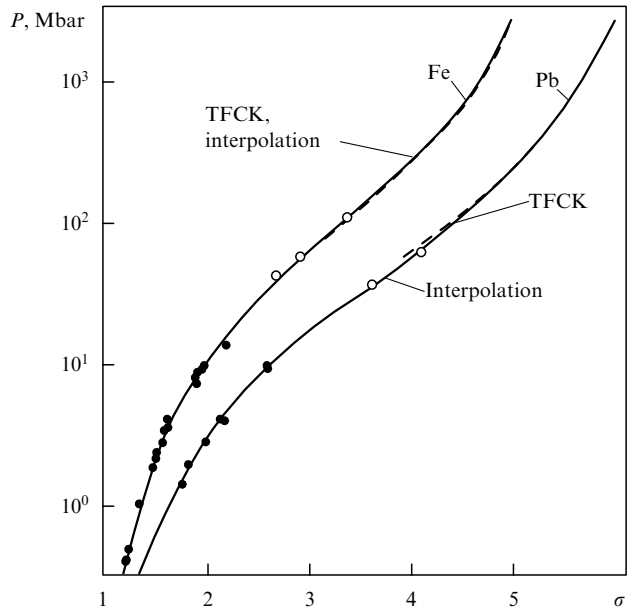

Figure 3. Interpolative shock adiabats of iron and lead: ● — laboratory measurements, ○ — underground nuclear explosion measurements, dashed curves — TFCK model calculations, solid curves — interpolation.

density, when the average sample density is $\rho_{00} = \rho_0/m$ (m is the degree of porosity). The necessity of investigating these systems was first emphasized by Zel'dovich in the late 1940s. The interest in these systems is primarily due to their significance in selecting and substantiating the models of matter equations of state, in particular, the thermal constituents of these equations [16]. Indeed, in the $P(\rho)$ diagram, the shock adiabats of porous materials occupy the main part of the area to the left of the adiabat with the initial crystal density ρ_0. Furthermore, they are characterized by substantially higher sample-heating temperatures in comparison with the temperature on the adiabat of a material with the initial density ρ_0. That is why investigations of porous materials yield a broad field of different states for testing model parameters.

The first compressibility measurements of porous iron samples date back to the late 1940s [3].

In the investigation of tungsten, a paradoxical effect was first discovered in [17]: for initial densities below some critical density ρ_{00}, applying pressures of even several megabars to the sample did not compress it to the initial density of crystalline tungsten.

Measurements on four metals (iron, lead, aluminum, and copper) were performed in [18]. The pressure ceiling was substantially increased to 9 Mbar. In Ref. [18], an interpolative equation of state was first proposed, based of the data of investigations of the shock adiabats of porous and continuous metals.

The general properties of the compression of porous metals and different compounds (for a wide variety of initial densities) were investigated in considerably greater detail in Refs [19–25]. For instance, 13 (!) 'porous' adiabats were obtained for nickel alone.

All these investigations used the 'reflection' method.

In the acquisition of experimental data, much attention was devoted to methodical issues arising from the specific character of sintered samples and its effect on the resultant data.

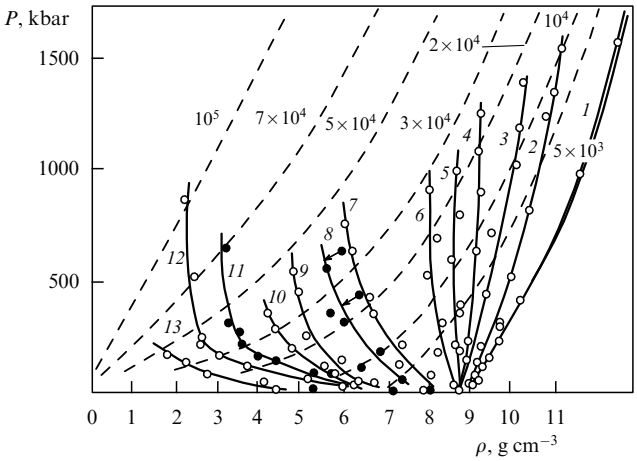

Figure 4. A $P-\rho$ diagram of nickel. Laboratory measurements. The numbers by the adiabats (*1–13*) correspond to the degree of porosity $m = \rho_0/\rho_{00} = 1.1, 1.41, 1.72, 2.0, 2.3, 2.7, 4.55, 5.5, 7.2, 10, 15, 20, 28$. The dashed curves are the isotherms calculated based on Refs [28, 29], the figures by the isotherms indicate temperature values.

The effects of the particle size, of the air, and of humidity of the samples on the parameters of shock waves were studied. The corresponding measurements were made both in laboratory experiments and in underground tests [26, 27]. These investigations allowed the following general conclusion: for a reasonable variation of the parameters involved, they exert no effect on the characteristics of the shock waves. Of course, this conclusion holds for the presently existing technical recording capabilities and experimental uncertainties. At the same time, this conclusion permitted treating the shock wave regimes in the compression of porous specimens as being close to equilibrium, which reduced the formulation of experiments to the conventional one and substantially simplified the interpretation of resultant data.

The compressibility of 16 metals in total was investigated in [15]. Apart from nickel, these were copper (9 adiabats) and molybdenum (8); magnesium was studied less than other metals (one 'porous' adiabat). From 8 to 12 experimental points were obtained for each adiabat. For example, the data on the compressibility of nickel are given in Fig. 4. The shock adiabats of other metals exhibit the same behavior.

We see that porous shock adiabats occupy almost the whole $P-\rho$ plane on the left of the adiabat with $m = 1$. The highest porosity (the lowest initial density) corresponds to the leftmost adiabat. Its initial density is 0.32 g cm^{-3}.

The adiabats exhibit the following characteristic features.

(1) Each adiabat contains two parts with different slopes. The first, mildly sloping part, 'creeps' along the abscissa and terminates at a density close to the normal metal density. The pressures in the adiabats of this part almost coincide with one another (on the scale of the drawing) and are close to the abscissa. They are not shown in Fig. 4.

The second part begins with an abrupt change (with a change of sign in the derivative $dP/d\rho$) in the slope in the adiabat. The pressure at which it occurs ranges from several kilobars to several tens of kilobars. This is the so-called 'packing pressure' — the minimal experimental value that results in the density of compressed material closest to the normal density. Each porosity corresponds to its own 'packing pressure.'

(2) The second parts are steep, 'poorly compressible' branches, characterized by different slopes: for $m < 2$, the

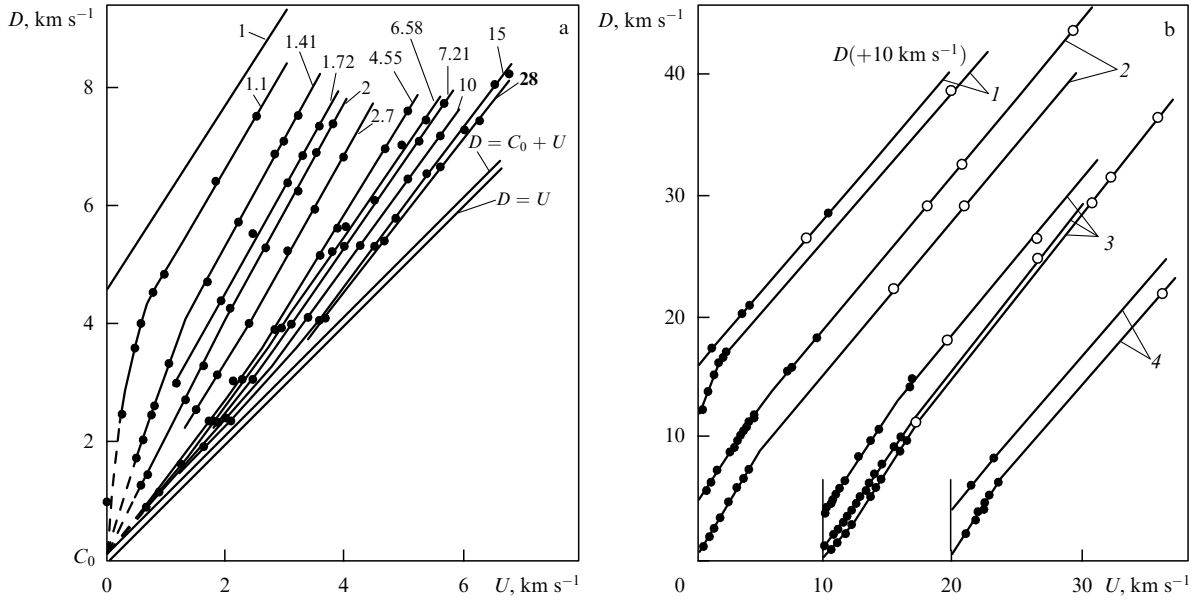

Figure 5. (a) A $D-U$ diagram of nickel. Laboratory measurements. The figures by the adiabats indicate the corresponding values of porosity. (b) $D-U$ diagrams of 'continuous' and 'porous' metals: *1* — molybdenum ($m = 1.0$, 1.23), *2* — iron ($m = 1.0$, 3.3), *3* — copper ($m = 1.0$, 3.1, 4.0), *4* — tungsten ($m = 1.0$, 3.1); ● — laboratory data, ○ — measurements for underground explosions. (For clarity, all velocities in the shock adiabat of Mo (adiabat *1*) are shifted upwards by 10 km s^{-1} along the ordinate axis.)

slope $\mathrm{d}P/\mathrm{d}\rho > 0$; in the interval $2 < m < 3$, $\mathrm{d}P/\mathrm{d}\rho \sim \infty$; and lastly, for $m > 3$, the slope $\mathrm{d}P/\mathrm{d}\rho < 0$.

The highest temperature calculated from the EoS [28, 29] corresponds to the porous nickel adiabat with the initial density 0.45 g cm^{-3} and is equal to 110,000 degrees for the pressure 0.9 Mbar. For comparison, on the 'continuous' adiabat, the same temperature is attained for the pressure about 16 Mbar.

Finally, we must consider at least a couple of shock adiabats plotted in the primary coordinates, i.e., those in which our experimental data are acquired.

Figure 5a gives the same data on nickel. We see that the adiabats of porous samples occupy the domain between the adiabat of the 'continuum' material ($m = 1$) and the straight line $D = C_0 + U$, which is shifted relative to the bisecting line $D = U$ by a value C_0 ($C_0 \geqslant 0.1$ km s^{-1} is the minimal value of D of all the values obtained in the extrapolation of porous shock adiabats to the ordinate axis).

Investigation of kinematic parameters is restricted to the region in the $D-U$ plane located to the left of this straight line: conservation laws forbid going beyond this curve to the right of it. A natural restriction on the low-m side is the position of the adiabat with $m = 1$. Similar situations also occur for other metals.

It is evident from Fig. 5 that we have closely approached the limiting straight line and that there is little point in a further increase in porosity, i.e., the acquisition of adiabats for initial densities even lower than 0.32 g cm^{-3}. Worth noting is the characteristic form of porous adiabats, which originate from the neighborhood of the common initial point and adjust to the run of the normal-density adiabat.

Lastly, in the same coordinates, Fig. 5b shows the data acquired in the laboratory and in underground nuclear tests. What is noteworthy in this case? For some velocities, the shock adiabats corresponding to different m turn into straight lines that are approximately parallel to each other and have about the same slope $\mathrm{d}D/\mathrm{d}U \approx 1.2$. This testifies to equalization of their dynamic properties. Under these conditions, incidentally, the adiabats themselves and their slope correspond to the parameters calculated by the TFCK model.

5. Compression of hydrogen isotopes

To conclude, we give our recent data on shock compression of the hydrogen isotopes protium and deuterium. One of the objectives of this research was to verify the results obtained by American researchers from the Lawrence Livermore National Laboratory: at pressures above 400 kbar, with the use of the Nova laser facility, they discovered an anomalous increase in compression of liquid deuterium, its density increasing from 0.6 g cm^{-3} to ≈ 0.9 g cm^{-3} [30, 31]. By its character, the adiabat at these pressures resembled a dependence corresponding to a first-order phase transition with a large density step (Fig. 6).

These data were doubted both in our country and abroad. That is why we set ourselves the task of verifying the American data at the explosion facilities of our institute in a comparable density domain. For greater rigor, our measurements were carried out not only on deuterium (initially in the liquid and solid phases), but also on protium (solid phase). Simultaneously, researchers of the Sandia National Laboratory verified the results of their colleagues (with liquid deuterium) [32, 33].

Of course, the aim of our investigations was not only to verify the American data but also, and most importantly, to obtain the test data required to determine the parameters of the equations of state for hydrogen isotopes.

The resultant data are plotted in $P-\rho$ coordinates in Fig. 6. It follows that the data obtained at the Nova facility in Livermore are at variance with our data, as well as with the data of the Sandia Laboratory. The mutual uncertainties of the approximating curves arising from the aggregate inaccuracy of our data and those of the Sandia Laboratory do not overlap with the data obtained at the Nova facility.

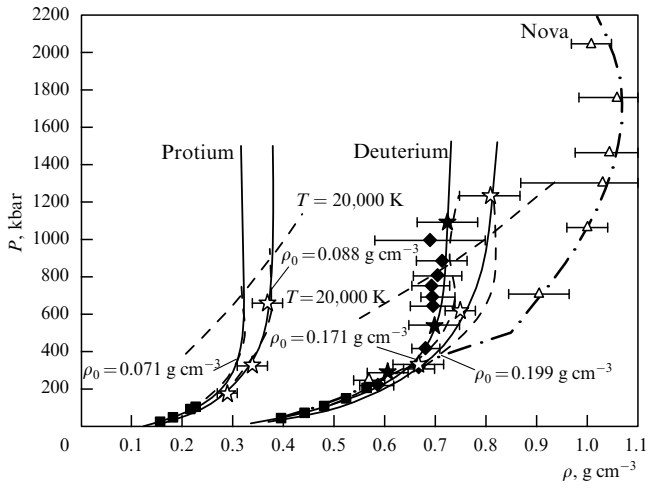

Figure 6. Shock adiabats of hydrogen isotopes: ■ — measurements at low pressures (American data), ◆ — the data in Refs [32, 33], △ — the data in Refs [30, 31], ★, ☆ — VNIIEF measurements (liquid and solid initial states, respectively).

This formally demonstrates the fallaciousness of the Nova results. In essence, the internal consistency of the data in Refs [34–36], which were obtained with a technique repeatedly borne out in several hundred independent experiments (with gas guns and explosion systems involving high explosives) is by itself an indication that the Nova results are fallacious.

Apart from elucidation of the issue about the stepwise change of the liquid deuterium density, we obtained data on the shock compression of initially solid phases of deuterium and protium. There are no publications on this issue in the literature.

It is worthy of mention that V E Fortov has proposed to verify the data of the Livermore researchers and that the work itself was actively supported by R I Il'kaev.

6. Conclusions

In this brief report, I have not touched upon the results of measurements of other material properties: isentropic and double compression, sound velocities, phase transformations, and so on. The reader is referred to the reports on these investigations that have appeared in numerous publications in scientific journals.

I add several words about equations of state. Efforts have been repeatedly mounted, both in our country and abroad, to obtain the equations of metal state in a wide range of thermodynamic parameters without recourse to experimental data in the relevant domain of states of matter. These attempts are being made even nowadays. Incidentally, one of the first endeavors was made precisely at VNIIEF (Gandel'man). But none of these attempts has met with success from the standpoint of the requirements that we impose on these equations. It is valid to say that as regards the applied problems facing VNIIEF (and not only it), preference was given to semiempirical models rather than a priori ones.

There are several semiempirical models. The widest acceptance has been gained by versions of the so-called equations with thermal lattice and electronic terms. These equations typically rely on solid-state notions, although some of the versions include the properties of liquids as well. One of the disadvantages of these models is that they do not take the evaporation of liquids into account.

This disadvantage is not inherent in another type of equation, the modified van der Waals model, whose applicability extends to the domain of higher fluid compression. The model takes the difference between the solid and fluid properties into account, as well as the evaporation of the fluid and ionization. The modified van der Waals model equation offers several advantages over other model equations as regards breadth in describing metals in different states of the phase diagram.

Generally, the equations of state are of course a major subject on their own, which invites special consideration. In this connection, I have the pleasure to refer the reader to the recently published book by Kopyshev [37].

And, finally, I cannot help recalling the pathfinders and those who provided crucial services to the formation and development of high energy density physics. These are, first and foremost, L V Al'tshuler, E I Zababakhin, Ya B Zel'dovich, S B Kormer, K K Krupnikov, and Yu B Khariton — the organizers and supervisors of the research carried out on this subject at the Nuclear Center of the Soviet Union. Their closest colleagues and supervisors of research in separate areas at VNIIEF are A A Bakanova, M I Brazhnik, F V Grigor'ev, N A Dmitriev, M V Zhernokletov, V N Zubarev, A G Ivanov, V P Kopyshev, B N Ledenev, A B Medvedev, V N Mineev, S A Novikov, M N Pavlovskii, M A Podurets, A M Podurets, G V Simakov, M V Sinitsin, V D Urlin, A I Funtikov, K B Yushko, and many others.

This brief report deals with only a small fraction of the results obtained in our laboratory at VNIIEF. At the same time, many interesting and important investigations have been carried out at the second Russian Nuclear Center — Zababakhin All-Russian Scientific Research Institute of Technical Physics (E N Avrorin), Moscow institutes (V E Fortov), the Siberian Branch of the RAS (V M Titov), and several other organizations.

However, it is we, not they, who are 65 today.

References

1. Al'tshuler L V *Usp. Fiz. Nauk* **85** 197 (1965) [*Sov. Phys. Usp.* **8** 52 (1965)]
2. Al'tshuler L V, Krupnikov K K, Brazhnik M I *Zh. Eksp. Teor. Fiz.* **34** 886 (1958) [*Sov. Phys. JETP* **7** 614 (1958)]
3. Al'tshuler L V et al. *ЖЭТФ* **34** 874 (1958) [*Sov. Phys. JETP* **7** 606 (1958)]
4. Al'tshuler L V et al. *Fiz. Tverd. Tela* **5** 279 (1963)
5. Al'tshuler L V et al. *УФН* **166** 575 (1996) [*Phys. Usp.* **39** 539 (1996)]
6. Trunin R F *Usp. Fiz. Nauk* **164** 1215 (1994) [*Phys. Usp.* **37** 1123 (1994)]
7. Trunin R F, in *Udarnye Volny i Ekstremal'nye Sostoyaniya Veshchestva* (Shock Waves and Extreme States of Matter) (Eds V E Fortov et al.) (Moscow: Nauka, 2000) p. 76
8. Trunin R F *Usp. Fiz. Nauk* **171** 387 (2001) [*Phys. Usp.* **44** 371 (2001)]
9. Trunin R F, Panov N V, Medvedev A B *Khim. Fiz.* **14** (2–3) 97 (1995)
10. Trunin R F, Panov N V, Medvedev A B *Pis'ma Zh. Eksp. Teor. Fiz.* **62** 572 (1995) [*JETP Lett.* **62** 591 (1995)]
11. Trunin R F et al. *Zh. Eksp. Teor. Fiz.* **102** 1433 (1992) [*JETP* **75** 777 (1992)]
12. Trunin R F et al. *Zh. Eksp. Teor. Fiz.* **103** 2189 (1993) [*JETP* **76** 1095 (1993)]
13. Trunin R F et al. *Zh. Eksp. Teor. Fiz.* **108** 851 (1995) [*JETP* **81** 464 (1995)]
14. Trunin R F *Teplofiz. Vys. Temp.* **35** 901 (1997) [*High Temp.* **35** 888 (1997)]
15. Trunin R F et al., in *Eksperimental'nye Dannye po Udarno-Volnovomu Szhatiyu i Adiabaticheskomu Rasshireniyu Kondensiro-*

vannykh Veshchestv (Experimental Data on Shock-Wave Compression and Adiabatic Expansion of Condensed Substances) (Ed. R F Trunin) (Sarov: RFYaTs–VNIIEF, 2001)
16. Zel'dovich Ya B *Zh. Eksp. Teor. Fiz.* **32** 1577 (1957) [*Sov. Phys. JETP* **5** 1287 (1957)]
17. Krupnikov K K, Brazhnik M I, Krupnikova V P *Zh. Eksp. Teor. Fiz.* **42** 675 (1962) [*Sov. Phys. JETP* **15** 470 (1962)]
18. Kormer S B et al. *Zh. Eksp. Teor. Fiz.* **42** 686 (1962) [*Sov. Phys. JETP* **15** 477 (1962)]
19. Trunin R F, Simakov G V *Zh. Eksp. Teor. Fiz.* **103** 2180 (1993) [*JETP* **76** 1090 (1993)]
20. Trunin R F et al. *Zh. Eksp. Teor. Fiz.* **96** 1024 (1989) [*JETP* **69** 580 (1989)]
21. Trunin R F, Simakov G V, Panov N V *Teplofiz. Vys. Temp.* **39** 430 (2001) [*High Temp.* **39** 401 (2001)]
22. Simakov G V, Trunin R F *Izv. Akad. Nauk SSSR Ser. Fiz. Zemli* (11) 72 (1991)
23. Trunin R F et al. *Teplofiz. Vys. Temp.* **37** 732 (1999) [*High Temp.* **37** 702 (1999)]
24. Trunin R F, Panov N V *Teplofiz. Vys. Temp.* **38** 754 (2000) [*High Temp.* **38** 728 (2000)]
25. Trunin R F, Simakov G V, in *Trudy RFYaTs–VNIIEF* (Proc. RFYaTs–VNIIEF) (Ed. R I Il'kaev) (Sarov: RFYaTs–VNIIEF, 2003) p. 234
26. Zubarev V N et al., in *Dokl. 1-go Vsesoyuz. Simposiuma po Impul'snym Davleniyam* (Reports to the First All-Union Symposium on Pulsed Pressures) Vol. 1 (Moscow: VNIIFTRI, 1974) p. 61
27. Trunin R F et al. *Zh. Eksp. Teor. Fiz.* **95** 631 (1989) [*Sov. Phys. JETP* **68** 356 (1989)]
28. Medvedev A B *Vopr. At. Nauki Tekh. Teor. Prikl. Fiz.* (1) 23 (1990)
29. Medvedev A B *Vopr. At. Nauki Tekh. Teor. Prikl. Fiz.* (1) 12 (1992)
30. Da Silva L B et al. *Phys. Rev. Lett.* **78** 483 (1997)
31. Collins G W et al. *Phys. Plasmas* **5** 1864 (1998)
32. Knudson M D et al. *Phys. Rev. Lett.* **87** 225501 (2001)
33. Knudson M D et al. *Phys. Rev. B* **69** 144209 (2004)
34. Boriskov G V et al. *Phys. Rev. B* **71** 092104 (2005)
35. Trunin R F et al. *Zh. Tekh. Fiz.* **76** (7) 90 (2006) [*Tech. Phys.* **51** 907 (2006)]
36. Trunin R F, Urlin V D, Medvedev A B *Usp. Fiz. Nauk* **180** 605 (2010) [*Phys. Usp.* **53** 577 (2010)]
37. Kopyshev V P *Teoriya Uravnenii Sostoyaniya* (Theory of Equations of State) (Sarov: FGUP "RFYaTs–VNIIEF", 2009)

PACS numbers: 84.30.Ng, **84.70.+p**, **85.70.–w**
DOI: 10.3367/UFNe.0181.201104k.0422

Explosive magnetic generators and their application in scientific experiments

B E Grinevich, V A Demidov,
A V Ivanovsky, V D Selemir

1. Introduction

The quest for energy sources that approach high explosives (HEs) in energy reserves inevitably brings up the idea of using electric or magnetic fields. But the store of specific energy in dielectrics $(\varepsilon_0\varepsilon E^2/2)$ and magnets $(\mu_0\mu H^2/2)$ is ordinarily moderate, of the order of 100 J l^{-1}.

B E Grinevich, V A Demidov, A V Ivanovsky, V D Selemir Federal State Unitary Enterprise 'Russian Federal Nuclear Center — All-Russian Research Institute of Experimental Physics,' Sarov, Nizhny Novgorod region, Russian Federation
E-mail: ivanovsky@elph.vniief.ru

Uspekhi Fizicheskikh Nauk **181** (4) 422–427 (2011)
DOI: 10.3367/UFNr.0181.201104k.0422
Translated by E N Ragozin; edited by A M Semikhatov

As a consequence, it turns out that making capacitor banks capable of storing energy in the range of several dozen megajoules is a highly intricate and expensive task. For HEs, the specific energy is $\rho D^2/16 \approx 10$ MJ l^{-1} (where ρ is the HE density and D is the speed of the detonation wave). An endeavor can be made to convert this energy into the energy of a magnetic field and simultaneously increase the energy density. This idea was first expressed by Andrei Sakharov [1] in 1951. As he pointed out, by rapidly decreasing the inductance of the current-carrying circuit with the magnetic flux conserved and drawing the conductors carrying oppositely directed currents closer with the aid of an explosion, the HE energy can be converted into the magnetic field energy. The greater the field energy is in comparison with the Joule heat, the higher the conversion efficiency.

Sakharov proposed two types of generators implementing magnetic cumulation: field generators and energy generators [2]. There are two main limitations imposed on the rate of magnetic flux compression. First, the compression should be fast enough so as to satisfy the condition $\mathrm{d}L/\mathrm{d}t \gg R$ and prevent load damage by the action of ponderomotive forces. Second, because a fast variation of the flux Φ gives rise to a high electric voltage $U = -L\,\mathrm{d}I/\mathrm{d}t$, it is necessary to provide sufficiently strong electric insulation to guard against electric breakdowns. For efficient generator operation, the voltage should be kept constant at the maximum permissible level. In the absence of flux losses, this may be achieved for an exponential law of the inductance reduction.

2. Operating principle and main characteristics of a disk explosive magnetic generator

Figure 1 is a schematic representation of a disk explosive magnetic generator (DEMG). When the magnetic flux in the generator attains the desired magnitude, the generator circuit closes, thereby trapping the introduced magnetic flux. At the same instant, with the aid of an initiation system, the HE charges along the axis are exploded in a synchronous mode. As the current-carrying plates draw closer together under the action of explosion products, they compress the magnetic flux simultaneously in all cavities and force it out of the compression cavities to the load via a transmission line. The shape of the current-carrying plates is selected such that the compression obeys the exponential law.

We outline the test results in [3] for one of the first DEMGs, 400 mm in diameter, which was made according to the diagram in Fig. 1. The device consisted of a two-stage

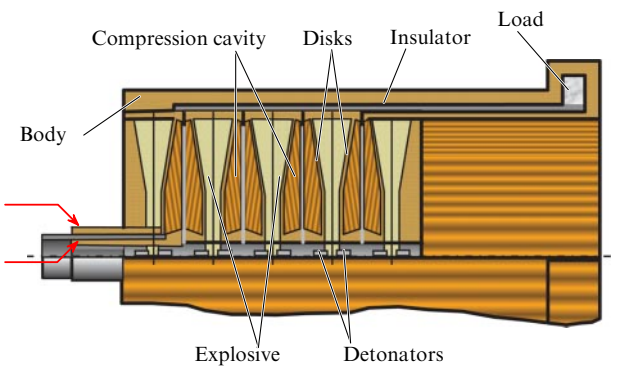

Figure 1. Disk explosive magnetic generator.

Table 1. Results of experiments with DEMGs.

HE charge diameter, mm	Number of elements	HE mass in one element, kg	Powering current, MA	Load inductance, nH	In-load current, MA	In-load magnetic energy, MJ	Characteristic in-load rise time, μs	Reference
240	3	2	5.2	1.5	60	2.7	≈ 3.5	[12]
250	3	0.9	6.1	1.14	62.6	2.25	4.4	[13]
400	10	6.7	6.1	4.7	102	24.7	≈ 5	[14]
480	5	16	8.1	6.8	90	28	≈ 6.5	[15]
1000	5	38	10	4	225	90	≈ 10	[14]
	5	54	14.6	5.8	265	205	12	[9]

explosive magnetic generator (EMG) and an inductive load L_{load}.

In the experiment, for the initial magnetic flux ≈ 1 Wb introduced into the circuit of the device with the help of a capacitor bank, a preamplifier formed an initial current pulse with the amplitude 6.5 MA, which was then amplified by a DEMG up to 90 MA. A high coefficient of magnetic flux retention was obtained: $\eta \approx 0.6$. The energy ≈ 10 MJ was stored in the DEMG.

The feasibility of increasing the energy in a useful load by increasing the number of DEMG elements was verified in an experiment with a ten-module DEMG 400 mm in diameter. For the final DEMG inductance 4.7 nH, the energy of the magnetic field was equal to 25 MJ, with 15 MJ of that in the load.

Recently, a family of DEMGs was made with HE charges ranging from 240 mm to 1000 mm in diameter (see Table 1). The following parameters were attained in experiments with DEMGs [4–15]: the energy gain coefficient 10–30, characteristic time 3–10 μs, specific energy 600 J cm^{-3}, output energy 200 MJ, the velocity 50 km s^{-1} for a liner of mass 1 g [16], and the velocity 15 km s^{-1} for a liner of mass 0.25 kg [17]. Furthermore, the feasibility of the quasispherical implosion of a liner under the action of an axially symmetric magnetic field was experimentally confirmed [11].

Russia [All-Russian Scientific Research Institute of Experimental Physics (VNIIEF)] has a monopoly on DEMGs: the attempts to develop a DEMG that have been repeatedly undertaken abroad have not met with success.

3. Helical explosive magnetic generators

Helical explosive magnetic generators (HEMGs), which have a substantially higher inductance and rate of its reduction than those in other types of explosive magnetic generators, can efficiently operate on loads over a wide range of inductances and resistances (Fig. 2). The key HEMG elements are a cylindrical solenoid and a metal tube with an HE charge, which are coaxially arranged and connected via a load. The magnetic flux produced in the generator bulk by an external energy source is compressed by the central armature. When the HE charge is initiated at the end face opposite the load, under the action of detonation products, this tube expands in the form of a cone that travels with the detonation velocity along the device axis [1, 2]. The central armature is made of soft copper or soft aluminum alloys.

The efficiency of an HEMG depends heavily on the distribution of coils over the solenoid length. Generators with a coil spacing that increases toward the load provide an essentially higher current and a higher energy gain than HEMGs with a constant spacing between the coils. The

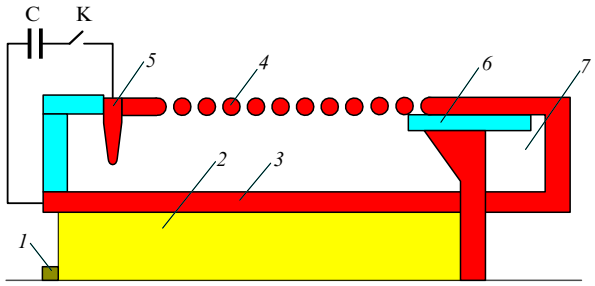

Figure 2. Spiral explosive magnetic generator: *1* — electric detonator, *2* — HE charge, *3* — liner, *4* — solenoid (stator), *5* — crowbar, *6* — insulator, *7* — load, C — capacitor, K — gap.

distribution of coils along the stator axis should provide the constancy of the peak voltage in the generator [18]. The dielectric strength of the insulation of the coils should be no less than 100 kV mm^{-1} [19].

The magnetic energy in an HEMG is generated due to the work done by the expanding central armature against the magnetic field pressure. In the general case, the expression for the HEMG power is

$$P = \frac{\mu_0}{2} \int_S H^2(t)\, V_\perp(t)\, \mathrm{d}S\,,$$

where H is the magnetic field strength on the tube surface, S is the tube surface area, and $V_\perp$ is the radial velocity of the tube wall. Hence, it is clear that increasing the HEMG power requires maximizing the values of H, $V_\perp$, and S at the end of its operation. In real generators, the magnetic field is limited to a value about 1 MG. The velocity $V_\perp$ of radial tube expansion is related to the HE energy properties. The area of the portion of deformation of the central armature depends on the initial tube geometry and the HE charge in the final section of the generator, as well as on the way the charge is initiated in this section.

For a rational use of the HE, a tube conically widening toward the load was proposed in [20]. In Refs [21, 22], to increase the HEMG power, the wall thickness of the conical part of the central armature was uniformly decreased in the direction of tube widening.

The most important factor that limits the energy and power of an HEMG is the magnetic-field-induced axial shift of the coils that are extreme on the load side. This results in insulation disruption and bridging of the coils, which is responsible for major losses in the magnetic flux. This effect is to be taken into consideration in HEMG design [22].

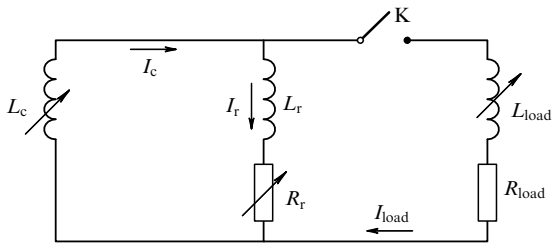

Figure 3. Electric circuit with a current interrupter: L_c, L_r, and L_{load} are the inductances of the final EMG circuit, the release circuit, and the load; R_r and R_{load} are the resistances of the release and the load; K is the key (interrupter); I_c, I_r, and I_{load} are the currents in the circuit to be broken, the release, and the load.

One of the highest-power HEMGs developed at VNIIEF is a generator with the internal diameter of coils equal to 240 mm [23]. For the initial energy ≈ 40 kJ, in 50–120 nH loads it provides the current up to 15 MA and the magnetic energy ≈ 8 MJ. The characteristics of the generator outperform the world level by a factor of 2–3 in specific energy, by a factor of 10–20 in the energy gain coefficient, and by about a factor of 2 in specific speed.

4. Problems with the current pulse formation

The period of energy accumulation in an EMG is relatively long (several tens of microseconds), which, in particular, impedes their use in experiments in high-temperature plasma heating by means of plasma compression with thin liners. This is due to the development of instabilities. To shorten the current flow time to the microsecond level, a commutation scheme is used, whereby the EMG storage circuit and the load are connected in parallel via a current interrupter (Fig. 3). This way of current pulse formation allows substantially shortening the rise time of the pulse in the load.

Several kinds of current interrupters have been developed at VNIIEF: explosive, which use HEs [24, 25], electric explosive [26–28], and liner interrupters [29].

The operating principle of an explosive current interrupter (ECI) relies on the mechanical destruction of a foil with the aid of an HE charge. The use of ten ECIs connected in parallel has allowed obtaining a current pulse with the amplitude ≈ 50 MA and the derivative $\approx 4 \times 10^{13}$ A s^{-1} in a load with the inductance ≈ 1.5 nH. In this case, the magnitude of the interrupted current was about 85 MA [30]. With the use of an ECI, in a load with the inductance 10–15 nH, it was possible to form a current pulse with the amplitude 20 MA and the pulse rise time ≈ 2 μs [31]. In Ref. [12], an HEMG equipped with an ECI produced a 6.6 MA current pulse with the rise time 0.4 μs in a 20 nH load. The feasibility of employing an ECI for sharpening the current pulse of a DEMG was demonstrated in Ref. [32].

The operating principle of an electrically exploded current interrupter (EECI) is based on a many-fold increase in the resistance of a metal foil or wire under an electric explosion. This type of interrupter is widely used in various electrophysical facilities. A cylindrically shaped copper-foil-based interrupter of this type was used at VNIIEF in experiments with a DEMG for currents 60–90 MA and power up to ≈ 10 TW [27].

A liner interrupter transferred more than 2 MJ of energy to the load in about 1 μs for the current ≈ 70 MA in an experiment with a DEMG [29].

The following parameters were highest attained in experiments with interrupters: the linear current density ≈ 0.9 MA cm^{-1} (a liner interrupter); the energy ≈ 10 MJ and power ≈ 10 TW transferred to the load (EECI), and the total current ≈ 85 MA (10 explosive interrupters); the shortest rise time for the in-load current pulse formed by an ECI was 0.3 μs [12].

5. Application of explosive magnetic generators

Among the applications of HEMGs is the powering of disk generators. In this case, it is highly significant that the spiral generator has a high speed, i.e., has a short characteristic rise time in order to minimize the thermal and mechanical action of the current on the DEMG elements [33].

We consider other fields of application of HEMGs. Two HEMGs are required for the operation of the MAGO ('MAGnitnoe Obzhatie,' which is the Russian for magnetic compression) chamber, which comprises two compartments connected with a Laval nozzle and filled with a deuterium–tritium mixture. The first HEMG fulfils preliminary powering of the chamber; on its completion, a fast powering source is turned on, which consists of an HEMG and a current pulse peaker. In the first chamber compartment, a gas discharge emerges, with the result that the magnetic field becomes frozen into the plasma. Under the action of a magnetic field, the resultant plasma flows from the first compartment into the second one through the nozzle. For a fast build-up of the magnetic field, the plasma flow at the exit from the nozzle is supersonic, and in the second compartment, a shock wave forms, in which the plasma decelerates and heats up [34, 35]. The MAGO chamber operation is diagrammed in Fig. 4. The chamber yielded 5×10^{13} neutrons per pulse. The authors of Refs [36, 37] proposed an HEMG that combined the functions of preliminary and fast powering of the MAGO chamber.

An explosive magnetic pulsed neutron source (EMPNS) was made on the basis of a high-inductance HEMG with a stator 80 mm in diameter [38]. For the current ≈ 1 MA, the EMPNS generated about 10^{12} neutrons per pulse with high temporal and amplitude stability.

A spiral EMG 200 mm in diameter with an ECI, which produced a current higher than 5 MA with the rise time 400 ns, was used for powering a Z-pinch. Recorded in this case was the generation of a soft X-ray (SXR) pulse with the energy ≈ 180 kJ and half-amplitude duration 20 ns [39]. At VNIIEF,

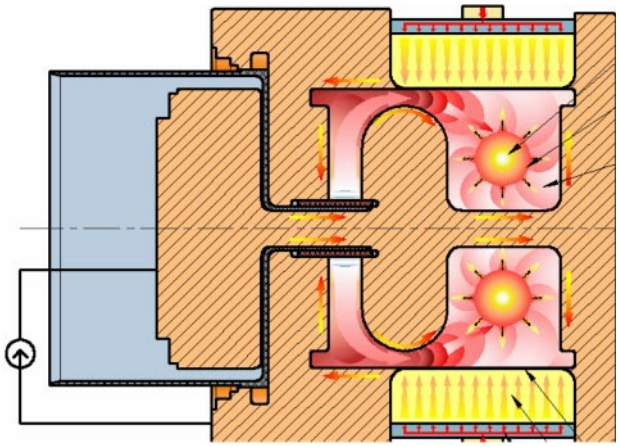

Figure 4. Operating diagram of the MAGO chamber.

spiral EMGs were first used for powering microwave generators [40].

HEMGs found use in accelerating solid liners to high velocities. Best known is the series of seven experiments *R-Damage* executed jointly by VNIIEF and the Los Alamos National Laboratory (LANL) to study dynamic fracture in convergent geometry using an explosive magnetic device as the driver of a cylindrical aluminum liner, which produced an axially symmetric impact action on the target [41]. The experiments were intended to investigate the features of initiation and development of spall fracture, as well as of damage compacting in extruded Alcan aluminum.

The *R-Damage* experiment series demonstrated the feasibility of using EMG-based pulsed power sources for producing pulsed loads with controllable amplitude and duration in engineering structural materials. In particular, the simplicity of realization of the regime with two sequential transient shock waves in a target opens broad possibilities for investigating the features of spall fracture and compacting in a real damaged medium.

The outcome of the *R-Damage* series involved the first-ever information about compacting and verification of the compacting model.

The advantages of the above technique over HE-aided loading are as follows: the liner not backed up by explosion products; the inertialess character of the magnetic field; the possibility of producing the requisite current pulse (amplitude, rise times, and duration); the high symmetry of loading; the possibility of preserving the targets under investigation.

In the powering of high-impedance loads with a current, the issues of high energy generation in the final EMG circuit and energy transfer to the load with a step-up transformer are brought to the forefront. One of the tasks solved with the aid of EMGs in this scheme was the pumping of neodymium and photodissociation lasers [42, 43]. The energy of laser radiation was about 100 kJ.

A spiral-coaxial EMG 160 mm in diameter with a cable-type transformer provides the energy up to 2 MJ in a 12–15 μH load. The highest output voltage ranged up to ≈ 200 kV.

The possibility of making fully independent HEMGs permits their use for testing the lightning proof level of important industrial objects. In experiments involving the reproduction of a lightning current pulse in a protective grounding, for the first time it was possible to record the production and development of high-power spark channels up to 30 m in length along the surface of the ground. In these experiments, for the current ≈ 70 kA, the active resistance of the earth electrode decreased by more than an order of magnitude [44].

A medium-class DEMG (with the HE charge diameter 400 mm) was validly used in a series of joint VNIIEF–LANL experiments called Russian High Strain Rate (RHSR) [45] and involving investigations of the dynamic material strength by the deformation growth technique for deformation rates $d\varepsilon/dt = 10^5 - 10^6$ s^{-1} in the shock-free loading mode. The three-layer liner consisted of current-carrying aluminum, polyethylene or water, and the material under investigation (copper) (Al – H_2O (polyethylene)–Cu). Axially symmetric sinusoidal perturbations with wavelengths $\lambda = 2$ and 4 mm were excited on two sequential segments of the outer surface of the copper.

The series of RHSR experiments yielded data on the dynamic strength of polyethylene (2–3 kbar, greater than the static one by a factor ≈ 20) and confirmed the data on the dynamic strength of copper. The stable operation of the DEMG-based pulsed power system underlay the success of this series of experiments: the inaccuracy of current pulse reproduction was $\leqslant 3\%$.

One of the lines of the inertial confinement fusion (ICF) research involves the production of high-power SXR pulses with the energy up to ≈ 10 MJ in the time ≈ 10 ns and compression of the thermonuclear fusion target by this radiation [46–48]. To generate SXR radiation in the Emir Project [48], one- and two-stage liners of tungsten wires ≈ 0.01 mm in diameter powered by an EMG were used. At the initial stage of the research, spiral EMGs 100 and 200 mm in diameter with ECIs were employed. In these experiments, the current pulses had the amplitude 2.5–5.5 MA and the pulse rise time 300–400 ns. An SRX yield up to ≈ 180 kJ was recorded; the duration of SXR radiation was ≈ 20 ns and its temperature was ≈ 50 eV [49]. With the use of a 10-element DEMG with HE charges 240 mm in diameter and an EECI, it was possible to obtain currents in liners at the level of 14 MA with the characteristic rise time 1.1 μs. The energy of the SXR radiation was ≈ 0.8 MJ [39]. This is the highest-power SXR radiation source in Russia. Envisaged for the future is the use of DEMGs with HE charges 480 mm in diameter, 5 to 15 elements, and ECIs. Currents in the liner are expected to range up to ≈ 50 MA and have the rise time ≈ 0.5 μs. According to calculations, the SXR energy will exceed 10 MJ for these current parameters.

Among the interrupters basically capable of forming current pulses of several tens of megaamperes in about 100 ns, we note electric explosive, plasma, and plasma-stream varieties. Electric explosive interrupters are the best-studied and simplest ones. It is likely that the faster and cheaper answer to the question of ignition feasibility can be given by using a DEMG 1000 mm in diameter able to produce a current pulse with the amplitude ≈ 150 MA and the rise time 1–2 μs in a ≈ 10 nH load with the aid of an electrically exploded foil current interrupter in the form of a serpentine. The working capacity of the electric explosive interrupter of this type was tested in an experiment with a 10-element DEMG 250 mm in diameter [50].

To study the feasibility of peaking the current to ~ 100 ns, calculations were made of the in-load current. It was shown that the EECI and the load should be 'decoupled' at the stage of electric explosion. This may be realized with the aid of a gap. Calculations of the operations of an HEMG with the gap showed that the voltage across the EECI amounts to ~ 400 kV and the in-load current to 5 MA in 130 ns. Higher currents may be obtained in the operation of the EECI with a DEMG. Vacuum low-inductance gaps, which commute current pulses at megavolt voltages in a time < 10 ns, were developed in the framework of the Baikal project [51].

Therefore, the state-of-the-art of explosive pulsed power technology and current pulse commutation systems permits delivering energy up to 100 MJ to a Z-pinch and achieving the conditions for thermonuclear ignition.

A comparison of the characteristics of explosive magnetic generators and stationary pulsed power sources is given in Fig. 5. The EMGs offer advantages in several key parameters.

Figure 5. (a) Atlas facility (Nevada, USA), which produces current with the amplitude up to 30 MA in ≈ 5 μs; rate of fire: one experiment in two weeks (capital expenditure: 43 million US dollars). (b) HEMG with an ECI: 20 MA current in 1–2 μs (fabrication cost: about 150 thousand US dollars). (c) DEMG of the Potok familiy: 400 mm diameter, 100 MA current in 6 μs (fabrication cost: about 250 thousand US dollars). (d) DEMG of the Potok familiy: 1000 mm diameter, 300 MA current in 10 μs.

6. Conclusions

The history of magnetic cumulation runs nearly 60 years. During this period, the problem of diffusion of strong magnetic fields into metals has been adequately studied. Many different designs of explosive generators of electromagnetic energy pulses have been made and tested. Multielement disk EMGs with energies above 100 MJ and high-inductance high-speed spiral EMGs with the energy gain coefficient up to ≈ 1000 were made; different interrupters for peaking the current pulse of an EMG to shorter than 1 μs were developed. Special step-up transformers were developed for powering high-inductance loads (lasers, protective groundings, and so on).

In recent years, the interest in explosive pulsed power systems has been rekindled in connection with the problem of thermonuclear ignition in the regime of inertial confinement. EMGs provide an opportunity to test the efficiency of many attractive ignition schemes without capital expenditures on the construction of high-power electrophysical facilities. The EMGs are unique sources of current pulses; there is no alternative to them in the execution of many physical experiments.

References

1. Sakharov A D et al. *Dokl. Akad. Nauk SSSR* **165** 65 (1965) [*Sov. Phys. Dokl.* **10** 1045 (1966)]
2. Sakharov A D *Usp. Fiz. Nauk* **88** 725 (1966) [*Sov. Phys. Usp.* **9** 294 (1966)]
3. Protasov M S et al., in *Sverkhsil'nye Magnitnye Polya. Fizika. Tekhnika. Primenenie* (Superhigh Magnetic Fields. Physics. Technology. Applications) (Eds V M Titov, G A Shvetsov) (Moscow: Nauka, 1984) p. 26
4. Chernyshev V K et al., in *Sverkhsil'nye Magnitnye Polya. Fizika. Tekhnika. Primenenie* (Superhigh Magnetic Fields. Physics. Technology. Applications) (Eds V M Titov, G A Shvetsov) (Moscow: Nauka, 1984) p. 23
5. Pavlovskii A I et al., in *Megagauss Field and Pulsed Power Systems* (Eds V M Titov, G A Shvetsov) (New York: Nova Sci. Publ., 1990) p. 331
6. Chernyshev V K et al., in *Megagauss Field and Pulsed Power Systems* (Eds V M Titov, G A Shvetsov) (New York: Nova Sci. Publ., 1990) p. 347
7. Fowler C M et al., in *Megagauss Field and Pulsed Power Systems* (Eds V M Titov, G A Shvetsov) (New York: Nova Sci. Publ., 1990) p. 337
8. Pavlovskii A I et al., in *Sverkhsil'nye Magnitnye Polya. Fizika. Tekhnika. Primenenie* (Superhigh Magnetic Fields. Physics. Technology. Applications) (Eds V M Titov, G A Shvetsov) (Moscow: Nauka, 1984) p. 347
9. Shevtsov V A et al., in *Megagaussnaya i Megaampernaya Impul'snaya Tekhnologiya i Primenenie* (Megagauss and Megaampere Pulsed Technology and Applications) (Eds V K Chernyshev, V D Selemir, L N Plyashkevich) (Sarov: RFYaTs – VNIIEF, 1997) p. 282
10. Demidov V A et al., in *Megagauss Field and Pulsed Power Systems* (Eds V M Titov, G A Shvetsov) (New York: Nova Sci. Publ., 1990) p. 351
11. Mokhov V N et al. *Dokl. Akad. Nauk SSSR* **247** (1) 83 (1979) [*Sov. Phys. Dokl.* **24** 557 (1979)]
12. Demidov V A et al., in *Megagauss Magnetic Fields and High Energy Liner Technology* (Eds G F Kiuttu, R E Reinovsky, P J Turchi) (Piscataway, NJ: IEEE, 2007) p. 245
13. Aryutkin M Yu et al., in *The 13th Intern. Conf. on Megagauss Magnetic Field Generation and Related Topics, Suzhou, China, 2010* (to be published)
14. Chernyshev V K et al. *Vopr. At. Nauki Tekh. Mat. Model. Fiz. Protsessov* **4** 33 (1992)
15. Selemir V D et al. *IEEE Trans. Plasma Sci.* **38** 1762 (2010)
16. Buyko A M et al., in *Megagauss Field and Pulsed Power Systems* (Eds V M Titov, G A Shvetsov) (New York: Nova Sci. Publ., 1990) p. 743
17. Grinevich B E et al., in *Megagaussnaya i Megaampernaya Impul'snaya Tekhnologiya i Primenenie* (Megagauss and Megaampere Pulsed Technology and Applications) (Eds V K Chernyshev, V D Selemir, L N Plyashkevich) (Sarov: RFYaTs – VNIIEF, 1997) p. 677
18. Demidov V A et al. *Zh. Prikl. Mekh. Tekh. Fiz.* (6) 106 (1981) [*J. Appl. Mech. Tech. Phys.* **22** 829 (1981)]

19. Demidov V A *IEEE Trans. Plasma Sci.* **38** 1773 (2010)
20. Pavlovskii A I et al., Invention Certificate No. 243103. MKI H02N 11/00. Priority of 28.22.67; *Byull. Izobret.* (33) (1969)
21. Veselov V N et al., Invention Certificate No. 1409087. MKI H02N 11/00. Priority of 09.10.85; *Byull. Izobret.* (13) (2000)
22. Demidov V A *IEEE Trans. Plasma Sci.* **38** 1780 (2010)
23. Selemir V D et al., in *Megagaussnaya i Megaampernaya Impul'snaya Tekhnologiya i Primenenie* (Megagauss and Megaampere Pulsed Technology and Applications) (Eds V K Chernyshev, V D Selemir, L N Plyashkevich) (Sarov: RFYaTs – VNIIEF, 1997) p. 248
24. Chernyshev V K, Volkov G I, Vakhrushev V V, in *Megagauss Physics and Technology* (Ed. P J Turchi) (New York: Plenum Press, 1980) p. 663
25. Pavlovskii A I, Vasyukov V A, Russkov A S *Pis'ma Zh. Tekh. Fiz.* **3** 789 (1977)
26. Petrukhin A A et al., in *Sverkhsil'nye Magnitnye Polya. Fizika. Tekhnika. Primenenie* (Superhigh Magnetic Fields. Physics. Technology. Applications) (Eds V M Titov, G A Shvetsov) (Moscow: Nauka, 1984) p. 384
27. Chernyshev V K et al., in *Megagauss Field and Pulsed Power Systems* (Eds V M Titov, G A Shvetsov) (New York: Nova Sci. Publ., 1990) p. 465
28. Demidov V A, Skokov V I, in *Megagaussnaya i Megaampernaya Impul'snaya Tekhnologiya i Primenenie* (Megagauss and Megaampere Pulsed Technology and Applications) (Eds V K Chernyshev, V D Selemir, L N Plyashkevich) (Sarov: RFYaTs – VNIIEF, 1997) p. 385
29. Petrukhin A A et al., in *Sverkhsil'nye Magnitnye Polya. Fizika. Tekhnika. Primenenie* (Superhigh Magnetic Fields. Physics. Technology. Applications) (Eds V M Titov, G A Shvetsov) (Moscow: Nauka, 1984) p. 406
30. Chernyshev V K et al., in *Megagauss Field and Pulsed Power Systems* (Eds V M Titov, G A Shvetsov) (New York: Nova Sci. Publ., 1990) p. 533
31. Chernyshev V K et al., in *Megagauss Magnetic Field Generation and Pulsed Power Applications* (Eds V Cowan, R B Spielman) (New York: Nova Sci. Publ., 1994) p. 731
32. Demidov V A et al. *IEEE Trans. Plasma Sci.* **38** 1768 (2010)
33. Chernyshev V K et al., in *Megagauss Magnetic Field Generation and Pulsed Power Applications* (Eds V Cowan, R B Spielman) (New York: Nova Sci. Publ., 1994) p. 519
34. Buiko A M et al. *Vopr. At. Nauki Tekh. Metod. Prog. Chisl. Resh. Zadach Mat. Fiz.* (3(14)) 30 (1983)
35. Buiko A M et al. *Dokl. Akad. Nauk SSSR* **344** 323 (1992)
36. Veselov V N et al., Invention Certificate No. 1616386. MKI H02N 11/00. Priority of 14.03.88; *Byull. Izobret.* (22) (1995)
37. Demidov V A et al., Invention Certificate No. 1526480. MKI H02N 11/00. Priority of 14.03.88; *Byull. Izobret.* (6) (1996)
38. Demidov V A, Kazakov S A *IEEE Trans. Plasma Sci.* **38** 1758 (2010)
39. Selemir V D, Demidov V A, Repin P B *IEEE Trans. Plasma Sci.* **38** 1754 (2010)
40. Brodskii A Ya et al. *Dokl. Akad. Nauk SSSR* **314** 846 (1990) [*Sov. Phys. Dokl.* **35** 876 (1990)]
41. Vasyukov V A et al., in *Proc. of the 13th Intern. Conf. on Megagauss Magnetic Field Generation and Related Topics, 2010* (to be published)
42. Pavlovskii A I et al., in *Megagauss Magnetic Field Generation and Pulsed Power Applications* (Eds V Cowan, R B Spielman) (New York: Nova Sci. Publ., 1994) p. 969
43. Pavlovskii A I et al., in *Megagauss Magnetic Field Generation and Pulsed Power Applications* (Eds V Cowan, R B Spielman) (New York: Nova Sci. Publ., 1994) p. 977
44. Selemir V D et al., in *Proc. of the 15th IEEE Intern. Pulsed Power Conf., Monterey, Calif., 2005* (Eds J Maenchen, E Schamiloglu) p. 541
45. Arinin V A et al., in *Megagauss Magnetic Field Generation and Related Topics, Berlin, Germany, 2005* (Ed. M Von Ortenberg) p. 348
46. Spielman R B et al., in *Proc. of the 10th IEEE Intern. Pulsed Power Conf., Albuquerque, NM, USA, 1995* (Eds W Baker, G Cooperstein) p. 396
47. Dyabilin K S et al. *Teplofiz. Vys. Temp.* **34** 479 (1996) [*High Temp.* **34** 473 (1996)]
48. Selemir V D et al. *Fiz. Plazmy* **25** 1085 (1999) [*Plasma Phys. Rep.* **25** 1000 (1999)]
49. Selemir V D et al. *Fiz. Plazmy* **33** 424 (2007) [*Plasma Phys. Rep.* **33** 381 (2007)]
50. Ivanovsky A V et al., in *VIII Kharitonovskie Chteniya po Problemam Fiziki Vysokikh Plotnostei Energii* (VIIIth Khariton Readings on the Problems of High Energy Density Physics) (Sarov: RFYaTs – VNIIEF, 2006) p. 563
51. Dolgachev G I et al. *Prib. Tekh. Eksp.* (2) 1 (2007)

PACS numbers: **07.35.+k**, **47.40.–x**, 61.05.C–
DOI: 10.3367/UFNe.0181.201104l.0427

Pulsed X-ray diffraction structure study of shocked materials

A M Podurets

Shock wave investigations are performed, as a rule, by measuring physical quantities which provide only indirect information on the structure of matter behind the shock wave (SW) front. Thus, the structure of high-pressure phases is mainly obtained from experiments on the static compression or laboratory studies of samples preserved after shock loading. At the same time, it is obvious that no direct correspondence between structures in static and dynamic experiments can exist because of the difference in the time scales of processes proceeding in these experiments. Therefore, the problem of obtaining structural information directly in shock wave experiments becomes very important. In addition, the equations of state are studied, as a rule, by interpreting the SW data based on the assumption of the complete relaxation of materials (the hydrodynamic approximation); however, this assumption should also be verified. The only direct method for studying the structure of materials immediately behind the SW front is pulsed X-ray diffraction (PXRD) analysis. This method attracts great interest because it provides X-ray patterns of a substance recorded during its compression by a SW, i.e. for no more that a few hundred nanoseconds.

The aim of this paper is to review the results of PXRD studies obtained for more than 40 years of applying this method. The review is based on work performed at the Russian Federal Nuclear Center — All-Russian Research Institute of Experimental Physics (ARIEP or VNIIEF in *Russ. abbr.*).

In the second half of the 1960s, L V Al'tshuler, L A Egorov and their coauthors developed and demonstrated a technique for photographing structural X-ray patterns during times on the order of 1 μs [1, 2]. Soon, the problem of recording pulsed X-ray patterns at the moment of action of shock waves on a sample was also solved [3].

The X-ray diffraction analysis is based on the linkage between the X-ray scattering angle θ and the spacing d of

A M Podurets Federal State Unitary Enterprise 'Russian Federal Nuclear Center — All-Russian Research Institute of Experimental Physics', Sarov, Nizhny Novgorod region, Russian Federation
E-mail: am.podurets@gmail.com

Uspekhi Fizicheskikh Nauk **181** (4) 427 – 434 (2011)
DOI: 10.3367/UFNr.0181.201104l.0427
Translated by M Sapozhnikov; edited by A Radzig

crystal lattice planes described by the Bragg relation

$$2d\sin\theta = \lambda\,,$$

where λ is the radiation wavelength (the method is used in the range where λ and d are of the same order of magnitude). Thus, a change in the crystal structure (d) is determined by a change in the angular position of a diffraction line (by its 'shift').

The two basic problems to be solved by researchers using this method were:

(1) How is a crystal lattice deformed behind the SW front?

(2) What is a material structure in the case of its phase transformation in the SW? (This is especially interesting if the high-pressure phase is not recovered after unloading to the normal pressure, thereby becoming inaccessible for structural studies by standard materials science methods.)

The first PXRD studies were published at the early 1970s by Soviet [3] and American [4–6] researchers. Soon, similar studies were also performed in France [7], Japan [8–11], and Germany [12].

The arrangement of PXRD experiments involve a number of difficulties. The first of them is the proper selection of samples for analysis. The required exposure times are short, and therefore only samples with a high reflectivity can be used. This imposes restrictions on both the sample material and its structure. In most papers, the single crystals of LiF, NaCl, KCl, SiO_2, Si, Bi, and some other materials were investigated. This is explained by the fact that single crystals, being in a proper reflecting position, give considerably more intense reflections in X-ray patterns than polycrystalline materials (a single crystal as a whole reflects radiation in one direction, whereas in a polycrystal only a part of the grains with a certain orientation are involved in radiation reflection). However, the photography of polycrystals (when possible) offers some advantages; in particular, it is possible to obtain at once several reflections in one X-ray pattern by using monochromatic radiation. Sometimes it is possible to record a rather intense X-ray pattern by utilizing polycrystals with a pronounced texture.

The method was further developed and X-ray pattern photography schemes were proposed to obtain simultaneously two reflections from the two planes of a single crystal in one experiment [13]. This method, which is called multiple X-ray diffraction [14, 15], allows one to investigate the compressibility of crystals in two mutually perpendicular directions under the same loading conditions and even in one experiment.

The intensity of a diffraction line (neglecting the crystal structure type) is defined as

$$I \sim \frac{1}{\mu\rho}\,,$$

where μ is the mass radiation absorption coefficient of a sample material, and ρ is the density. Therefore, samples consisting of elements with small atomic numbers are, as a rule, preferable for studies because the X-ray absorption coefficient μ increases with increasing atomic number and, hence, the amount of material involved in the formation of reflections decreases.

Another important problem in experiments is the synchronization of a radiation source with a device generating SWs in the sample. The lifetimes of the states in SW-loaded samples rarely exceed a few fractions of a microsecond. Correspondingly, the PXRD exposure times are from about 0.1–1 ns (upon excitation of an X-ray pulse by a laser beam) [16, 17] up to approximately 100–200 ns when pulsed X-ray tubes are used [3, 8].

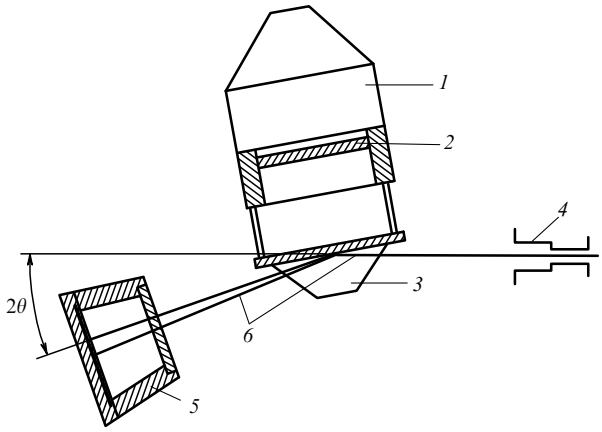

Figure 1. Schematic of the experimental setup [3]: (*1*) explosive charge; (*2*) accelerated striker; (*3*) lithium layer; (*4*) X-ray collimator; (*5*) X-ray film holder, and (*6*) incident and reflected beams.

Upon excitation of SWs in a sample, the equipment (the detection system and radiation source) can be damaged by explosion fragments or products. Therefore, it is necessary to protect the equipment, including detectors, during experiments from the possible action of an SW generator. Below, we will consider some options for organizing experiments and their peculiarities.

Figure 1 displays the layout of related experiments performed at VNIIEF [3, 18, 19]. A generally similar scheme was also employed in the work of other researchers. The mutual geometrical arrangement of a pulsed X-ray source, a sample, and a radiation detector corresponds to the focusing of X-rays (it can be different in various experimental setups).

The general focusing condition in experiments with flat samples is expressed by the Kurdyumov relation [20]

$$\tan\psi = \frac{\sin 2\theta}{\cos 2\theta + L/l}\,,$$

where ψ is the angle between the incident beam and a sample, θ is the diffraction angle, and L and l are the distances from the sample to the radiation source and detector, respectively. The relation between L and l is chosen to avoid damage to the detector and source, providing the required X-ray pattern intensity.

The sample is loaded with a plane SW produced by a striker which is accelerated by the explosion of a chemical explosive. This method was used in most work performed at VNIIEF and in the work of Q Johnson and coauthors [5, 6]. Shock waves can also be produced by using an electric explosion [12, 21, 22] or a solid propellant [7, 23] or gas [8, 9, 24, 25] gun. In Refs [16, 17, 26], SWs were generated in silicon samples by a laser pulse. The range of pressures achieved in experiments depends on the method of generating sample-loading SWs. Thus, pressures achieved in samples (up to a few GPa) by using an electric explosion or a powder accelerator are lower than those obtained in experiments with explosives or gas guns (up to a few dozen GPa). The diagnostics of the gas-dynamic characteristics in laser-loading experiments was

poorly developed and therefore the pressures achieved in these experiments could be estimated only approximately or obtained from calculations. Another significant advantage of explosives and guns is the possibility of keeping a sample under pressure for some time (in the presence of a stationary loading wave).

X-ray patterns are usually photographed through a supporting layer of a light inert material preventing the sample from unloading during measurements. This layer, which is simultaneously transparent to X-rays, can be made of lithium, carbon, beryllium, or Plexiglas. By photographing without the supporting layer, it is possible to detect the state existing in the sample immediately after its unloading. In this way, information on the stability of the high-pressure phase in a rarefaction wave can be obtained [27].

We used in our experiments pulsed X-ray tubes of various designs with a copper or a molybdenum anode. The diffracted radiation was detected with an X-ray film or photosensitive equipment.

To interpret X-ray diffraction patterns obtained in experiments, it is necessary to relate the observed reflections to the absolute scale of diffraction angles. The simplest solution to this problem reduces to X-ray photographing a sample in the same geometry before and during the SW action. In this case, the angular position of lines in the explosion X-ray pattern is determined by their displacement with respect to the lines of the unloaded sample in a preliminary photograph. Sometimes it is possible to obtain simultaneously the photographs of the uncompressed and compressed structure on the same film. In this regard, synchronization is performed so that a part of the exposure falls at the uncompressed state before the SW arrival, while another part falls at the already compressed state [9]. A similar effect can also be achieved by photographing a thin compressed layer, when the yet uncompressed crystal layer lying under the former is also simultaneously 'seen' [17]. Photographing samples by utilizing standard samples is also applied. As a standard, a material can be used whose type of compression in SWs is already known. For example, different samples were studied by placing molybdenum or aluminium standards nearby, which were subjected to the action of SWs along with the samples of interest (the so-called loaded standard). This method is convenient because the position of the sample lines is determined in this case relative to the lines of the standard substance recorded in the same X-ray pattern [19, 27, 28]. In experiments performed in Refs [22, 29], the standard was not subjected to SW action, but its lines were also recorded on the same film with the sample lines (the unloaded standard).

Most of the PXRD papers are devoted to the study of single crystals. A *lithium fluoride* (LiF) crystal has been investigated most thoroughly. This cubic NaCl type crystal without high-pressure phase transitions is used in pulsed X-ray diffraction studies more often than other crystals because its compressibility in SWs has been investigated in detail by other methods. Nevertheless, to date the behavior of LiF is not completely clear.

At pressures of 6.6 and 13.5 GPa, L A Egorov and coauthors observed reflections corresponding to the isotropic compression of the lattice of LiF single crystals with the (100), (110), and (111) crystallographic planes oriented perpendicular to the SW direction [22]. At the same time, the X-ray patterns exhibited diffraction lines coinciding with the lines of the uncompressed crystal. The authors assigned them to the compressed crystal regions, but turned and compressed along the $\langle 111 \rangle$ direction. In this case, the volume compressibility $\sigma = V_0/V$ of crystal regions compressed isotropically and crystal regions compressed along the $\langle 111 \rangle$ direction was the same, equal to the compressibility calculated from the shock adiabat:

$$\sigma = \frac{D}{D-u}\,,$$

where D and u are the shock wave and particle velocities, respectively. This interpretation of unshifted lines in X-ray patterns seems controversial at present; however, such lines were also observed in studies of other substances [22, 29].

At pressures up to 5 GPa, a different compressibility was observed for LIF single crystals with various orientations. Crystals with the (100) orientation were compressed both in the SW propagation direction and perpendicular to it, whereas crystals with the (111) orientation did not show the transverse compressibility [15].

At pressures of 22 and 24 GPa, K Kondo and coauthors also found the absence of the isotropic compression of the LiF crystal lattice. In this case, the lattice compressibility in the $\langle 100 \rangle$ direction was greater than the compressibility that would be observed in the case of isotropic deformation, while the compressibility in the $\langle 111 \rangle$ direction was smaller. The anisotropic compression was also revealed in the studies of an LiF polycrystal at $P = 18$ GPa [9, 11]. At higher pressures of 30 GPa [5], 38.5 GPa [30], and 40–110 GPa [24], only the isotropic compression of the crystal lattice was observed.

The deformation pattern for *sodium chloride* (NaCl) crystals is different. The one-dimensional deformation of the lattice was observed in the [100] direction at pressures of 0.3–1 GPa [7], 1.75 GPa [13], and 30 GPa [12]. Due to a short exposure time (4 ns), the authors of Ref. [12] managed to record the SW structure (elastic and plastic waves) by taking photographs at different moments after the arrival of the SW on the sample surface.

In a *potassium chloride* (KCl) single crystal, the isotropic compression of the lattice in the $\langle 100 \rangle$ direction was observed at pressures lower than the phase transition pressure of 1.4–2 GPa.

In polycrystalline *aluminium* at low pressures (1.92, 2.97, and 3.91 GPa), the lattice compression close to uniaxial was observed from the (111) and (200) diffraction lines. At higher pressures of 11.8 and 23.1 GPa, the (111) and (200) diffraction lines were also obtained in work [18], but changes in the Al lattice parameter calculated from these lines proved to be different. While the compressibility calculated from the shift of the (200) line, assuming that the lattice symmetry is preserved, proved to be equal within the scatter of the measurement to the bulk compressibility (obtained from the shock adiabat), the compressibility calculated from the shift of the (111) line proved to be 1.03–1.04 times greater than the bulk compressibility. This suggests that the deformation of the cubic Al crystal lattice is anisotropic along crystallographic axes. Photographs of the Al single crystal oriented in the $\langle 111 \rangle$ direction at a pressure of 32 GPa demonstrated isotropic compression [6].

The behavior of *beryllium* was studied in Ref. [22]. At a pressure of 22.8 GPa, an X-ray pattern with the (100) and (101) lines was obtained. It was concluded from the X-ray diffraction data that the hexagonal Be lattice is compressed along the crystallographic c-axis.

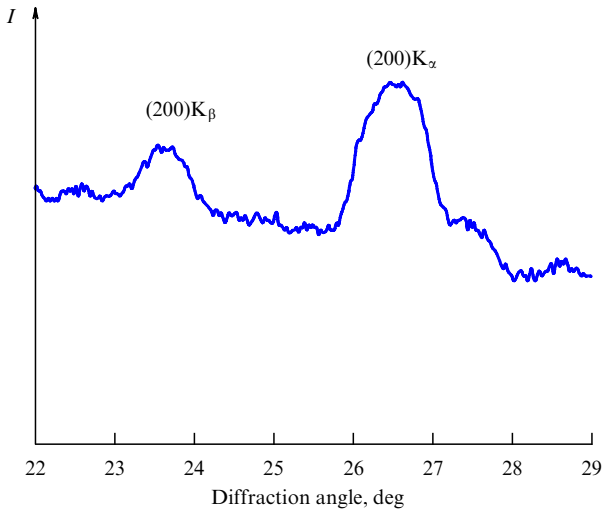

Figure 2. X-ray pattern of molybdenum in an SW at $P = 15$ GPa.

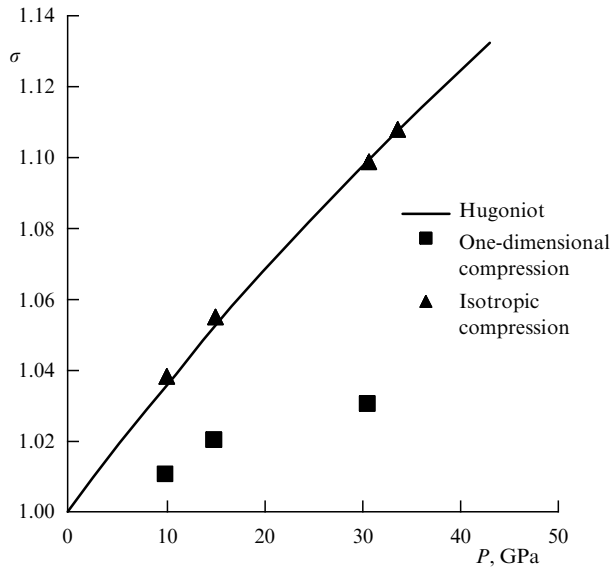

Figure 3. Shock compressibility of molybdenum. The Hugoniot [32] compared with compression calculated from X-ray diffraction data, assuming the isotropic and uniaxial deformations of the polycrystal lattice.

Another example of studying the type of compression of a material undergoing no phase transformations is the investigation of polycrystalline textured *molybdenum* [19]. Experiments were performed at pressures of 10, 15, 30.5, and 33.5 GPa. Figure 2 shows the X-ray pattern for Mo at $P = 15$ GPa. Two diffraction (200) lines from the K_α and K_β lines of a molybdenum anode were recorded. The spacing d of lattice planes was determined from the angular distance between the K_α and K_β lines. The accuracy of measuring d by this method is low because the compressibility of Mo in this pressure range is small, and therefore an increase in the angular distance between the lines is insignificant. According to estimates, the accuracy of measuring d reaches 0.001 nm, and of σ 2–3%. The results are displayed in Fig. 3, where the values of σ calculated assuming that compression is isotropic and uniaxial (in the SW propagation direction) are presented. These data suggest that within the accuracy achieved isotropic compression is observed behind the SW front in molybdenum for 200–300-ns X-ray pulses in the pressure interval studied.

All the studies of *silicon* single crystals performed by different researchers demonstrated uniaxial compression at pressures below the phase transition pressure [14, 33, 34] (the transition onset in an SW was revealed in the region of 12–13 GPa). This behavior of Si was explained by the low velocity and density of dislocations [14]; in this case, deformation has no time to relax plastically during photographic process and the lattice compression remains uniaxial.

The data obtained upon the compression of a *copper* single crystal along the ⟨100⟩ direction at $P = 18$ GPa are assigned either to isotropic hydrostatic compression [14] or to a deviation from hydrostatics [35]. According to the estimates of the authors, the dislocation structure in the case of copper, unlike that in Si, allows plastic deformation to proceed for times shorter than a microsecond.

Finally, the uniaxial compression of an *iron* lattice in the ⟨100⟩ direction at a pressure of 5.4 GPa was observed in Ref. [36].

Thus, we considered the results of structural studies of materials without phase transitions in SWs (or in the states below these transitions if the latter are present in these materials). The aim of these studies was to elucidate the type of compressibility at the crystal lattice level. In this regard, we paid attention mainly to final conclusions, by omitting the details of experiments, although some of them are quite significant, for example, the X-ray exposure time, the lifetime of the state under study, and the relation between these two times. Materials that have been studied differ in their crystal lattices (cubic or hexagonal) and chemical bonds (metals, halides, etc.), and they all can have their own kinetic parameters of the structural relaxation and deformation mechanisms requiring further investigations. Obviously, it is promising to use the concepts of the dislocation structure and microscopic mechanisms of the plastic flow to analyze the X-ray diffraction data.

Below, we consider the results of studies concerning the changes in the structure of materials during SW-driven phase transitions.

The first such study was reported in Ref. [5], where the X-ray patterns of shock-compressed pyrolytic *boron nitride* (BN) were obtained. Single-crystal samples oriented by the (001) plane parallel to the shock front were utilized. The diffraction (001) line was also recorded in X-ray patterns. At pressures of 14.5 and 20.5 GPa, the decrease in the lattice parameter c was observed. At $P = 24.5$ GPa, a line with $d = 0.220$ nm appeared in the X-ray pattern This line was interpreted by the authors as the (100) reflection of the wurtzite-like phase.

Graphite was studied in Ref. [4]. The change in the lattice parameter, $c/c_0 = 0.82$, was measured from the shift of the (002) line during SW loading (pressure was not indicated). By assuming that $a/a_0 = 0.99$, the authors obtained $\sigma = 1.25$, in accordance with the value obtained from the Hugoniot in the hydrostatic approximation.

To confirm the assumption about the difference in the compressibilities along the ⟨100⟩ and ⟨001⟩ directions, it was necessary to measure the pressure dependences of both the parameters of the hexagonal graphite lattice. This was done in Ref. [28] for natural graphite samples. The compressibility along the basic c-axis was determined from the angular shift of the (002) line, and along the a-axis from the shift of the

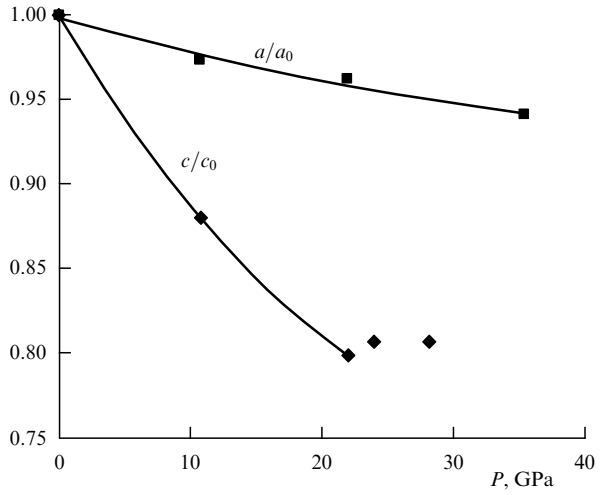

Figure 4. Pressure dependences of the relative change in the parameters of a graphite lattice in an SW (c/c_0 — rhombs, and a/a_0 — squares).

(110) line. Because X-ray patterns should have the required intensity, different lines were obtained from samples with various textures and differing initial densities [the (002) and (100) lines were obtained from samples with $\rho_0 = 2.15$ and 1.93 g cm^{-3}, respectively]. The estimates made by the authors showed that this did not introduce a large error into the interpretation of the results. Experiments were performed at pressures of 11, 22, 24, 28, and 35.5 GPa. The results are presented in Fig. 4. The analysis of these results leads to the following conclusions:

(1) The shock compressibility of graphite along the $\langle 001 \rangle$ c-axis is greater than that along the $\langle 100 \rangle$ a-axis.

(2) The values of the volume compressibility calculated from X-ray diffraction data at pressures of up to 22 GPa are in good agreement with those obtained from the Hugoniot in the hydrodynamic approximation.

(3) The break in the plot of c/c_0 at $P \approx 22$ GPa indicates the phase transformation. It is impossible to calculate compressibility from X-ray diffraction data at pressures above this value because, along with graphite, a new high-pressure phase is already present behind the SW front.

The high-pressure phase was detected in the X-ray pattern of graphite at a pressure of 35.5 GPa, when, during the photographing of the (002) line, a line with $d = 0.218$ nm was recorded, which was interpreted as the (100) line of hexagonal diamond — lonsdaleite.

Potassium chloride (KCl) single crystals were investigated at pressures exceeding the phase transition pressure in the range from 2 to 6 GPa [22, 31, 37]. In all cases, the authors observed reflections from the high-pressure phase. The transition of KCl from the NaCl type structure to the CsCl structure, which is known from static experiments, occurs at a pressure of ~ 2 GPa. The phase transition onset in dynamics was revealed at the same pressure [38]. The authors of all three papers observed, along with lines belonging to the CsCl type structure, diffraction lines that could not be interpreted within the framework of the two known phases, and were assigned to intermediate states accompanying the phase transformation process. However, the intermediate structures were interpreted by the authors differently. A whole package of rhombohedral structures was described in Ref. [22], which were produced depending on the loading pressure on a sample and its orientation with

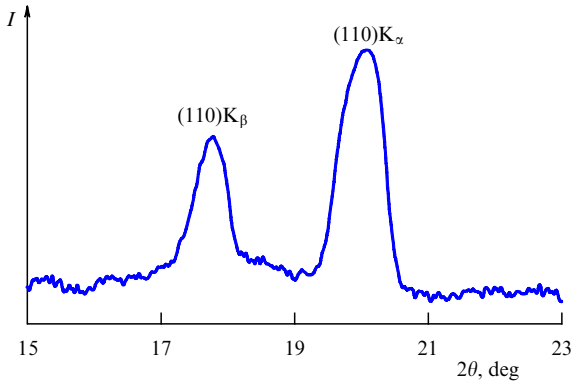

Figure 5. X-ray pattern of siliceous iron in an SW at $P = 10$ GPa.

respect to crystallographic axes. In paper [37], the intermediate structure at $P = 3$ GPa was identified as a simple cubic structure.

The X-ray patterns of the high-pressure ε-phase of *iron* were obtained by applying PXRD analysis in Ref. [19]. The intensity of pulsed X-ray patterns was increased by employing the textured samples of Fe + 3% Si transformer steel with a density of 7.68 g cm^{-3} and the $\langle 100 \rangle \{110\}$ texture increasing the (100) diffraction line intensity in X-ray patterns. It is known that a Fe–Si alloy, like pure iron, undergoes the $\alpha \rightarrow \varepsilon$ phase transition in SWs (the transition onset is at 12–15 GPa) [39]. The X-ray patterns of siliceous Fe were obtained at pressures of 10, 15, and 29 GPa. Figure 5 displays the X-ray pattern photographed at $P = 10$ GPa.

As would be expected, only the (110) K_α and K_β lines of the α-phase are observed in the preliminary and explosion X-ray patterns at pressures below the phase transition pressure. At pressures of 15 and 20 GPa, the pattern changes (Fig. 6): the diffraction lines in X-ray patterns correspond to the ε-phase.[1] The crystallographic data for this phase are given in Table 1.

Table 1. Crystallographic data for the ε-phase of Fe.

Parameter	$P = 15$ GPa	$P = 29$ GPa
d (100), nm	0.220	0.215
d (002), nm	0.204	0.201
d (101), nm	0.191	0.188
a, nm	0.252	0.247
c, nm	0.408	0.401
a/c	1.62	1.62

An attempt was made to study the phase transformation in *zirconium* [27]. As the static pressure is increased, Zr undergoes a transition from the hexagonal closely packed modification (the α-phase) to the hexagonal ω-phase. The

[1] The statement of the authors of papers [36] and [40] that they were the first to obtain *in situ* X-ray patterns of SW compressed iron is not correct. The X-ray patterns of Fe in SWs were first obtained by A M Podurets, A I Barenboim, V V Pul, and R F Trunin at VNIIEF in 1986–1987. The first results were published in "Proceedings of the IV-th All-Union Conference on Detonation" [41] in 1988, and in a Russian academic journal in 1989 [19]. The results of Fe studies were also published in English in "Proceedings of the International Conference on Condensed Matter under High Pressures" in Bombay in 1996 [42].

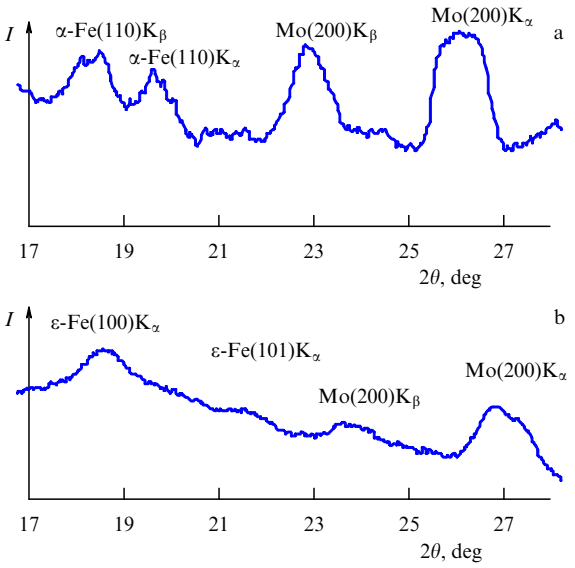

Figure 6. X-ray pattern of siliceous iron with a molybdenum standard in an SW (a) at $P = 0$ (preliminary photograph), and (b) at $P = 15$ GPa.

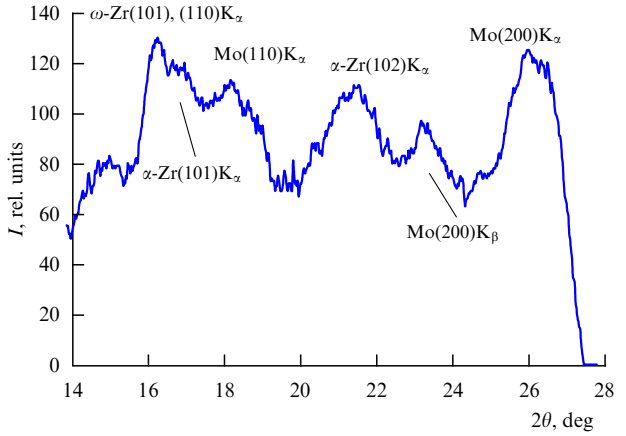

Figure 7. X-ray pattern of zirconium with a molybdenum standard unloaded after compression in an SW of up to $P = 12$ GPa.

phase transformation in Zr also occurs upon shock loading. The break in the Hugoniot was revealed at $P = 26$ GPa [43]. It is not clear so far to which transformation this break corresponds because, as a rule, pressures at which transitions occur at static and dynamic loadings are close. In contrast, phase transformations in Zr in shock waves occur at pressures considerably exceeding the equilibrium pressure. However, despite numerous experimental data, the crystallographic nature of the phase transformation (or transformations) in Zr remains unclear.

The X-ray patterns of Zr samples loaded with shock waves were photographed at pressures of 5, 9.5, 15, and 25 GPa. At pressures of 5 and 9.5 GPa, the structure of the initial α-phase was observed. At higher pressures, the picture changed. At $P = 15$ GPa, the two Zr lines corresponding to the interplanar spacings of 0.227 and 0.211 nm were detected in X-ray patterns. The line with $d = 0.211$ nm was also observed at $P = 29$ GPa. It is impossible to relate unambiguously these interplanar spacings to the structure of an isotropically compressed ω-phase (or the β-phase of Zr). We can only assume that either one of these highly deformed phases exists behind the SW front or some different Zr phase is produced. Because both these unidentified lines can belong to different phases with various degrees of deformation, it is impossible to assign them unambiguously.

It is known from experiments with the recovery of shock-loaded samples that the ω-phase in the pressure interval 9–24 GPa is recovered after unloading [44]. To 'match' the data obtained by the method of pulsed X-ray photography at the moment of loading with the data obtained for recovered samples, experiments were performed in which the X-ray pattern of the free surface of a Zr sample was captured after an SW at a pressure of 12 GPa arrived at this surface and the unloading started.

The X-ray pattern obtained (Fig. 7) shows that within 1 μs after the SW emergence on the sample surface, the sample consisted of a mixture of the α- and ω-phases, which confirms the data obtained in the study of recovered samples. The X-ray patterns did not contain the lines of an unknown nature.

A complex sequence of structural transformations in an SW was detected in *bismuth*. At the lowest pressure of 6.7 GPa, the Bi-V structure revealed itself [27], which is known from static measurements. A pressure of 6.7 GPa lies near the stability region of this phase. The phase VI region, which has the body-centered cubic (bcc) structure lies at higher pressures.

At pressures of 8.5 and 13.7 GPa, the X-ray pattern was the same and contained a diffraction line corresponding to the interplanar spacing of 0.222–0.225 nm. Such spacings could belong to the (111) line of the cubic structure; however, a line with such indices is forbidden in a bcc lattice due to extinction effect (caused by the structure symmetry). If we assume that the bcc-phase structure behind the SW front in Bi differs from ideally symmetric, then no extinction of this line will occur. The Bi structure at pressures of 8.5 and 13.7 GPa was interpreted as the distorted bcc structure, which was not observed under static conditions. This conclusion is confirmed by the presence of lines with $d = 0.185-0.202$ nm in some X-ray patterns, which can correspond to the (200) line of the bcc phase; at $P = 9$ GPa, the value of d for this phase under static conditions was 0.1900 nm [45].

At a pressure of 22 GPa, a broad diffuse halo revealed itself in X-ray patterns in the region of angles θ corresponding to the interplanar spacings from 0.25 to 0.3 nm (Fig. 8). The diffuse halo in the absence of distinct diffraction peaks suggests that the long-range order in the crystal is violated, and the structure becomes closer to the structure of liquids or amorphous matter.

At a pressure of 27 GPa, no diffraction lines were detected in any explosion X-ray patterns. This can be explained by the melting of Bi in the SW. The pressure in these experiments is rather close to the melting threshold of Bi, equal to 33 GPa, which was obtained by another experimental technique [46].

Thus, the sequence of structural changes in Bi in the SW at the pressures considered above demonstrates considerable differences between the SW picture and the static picture. Amorphization observed at $P = 22$ GPa suggests that a further increase in pressure will lead to melting, i.e., structure disturbance preceding the complete loss of the long-range order.

We have analyzed the main results obtained by the pulsed X-ray diffraction method, not considering thoroughly the technical details. However, it is the technical aspects of the

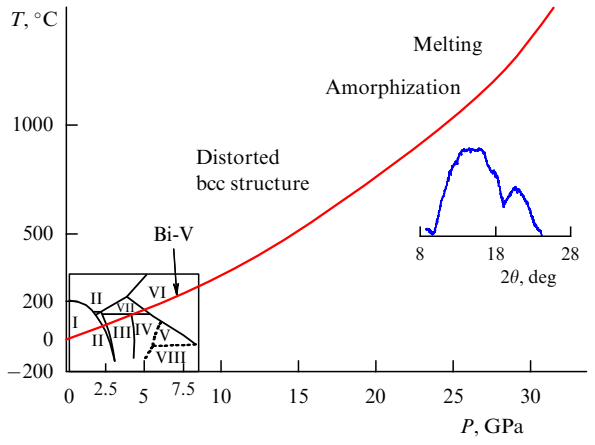

Figure 8. Sequence of structural changes in bismuth in an SW. The solid curve depicts a Hugoniot. The inset to the figure at the left corner shows the static phase diagram of Bi [38]; the inset at the right displays the X-ray pattern of amorphous Bi.

method that play a key role in its further development. The examples considered in the paper show that the PXRD analysis can be very informative and useful for the understanding of processes proceeding upon the action of SWs on a material. Therefore, this method will be undoubtedly further used and developed. Notably, to obtain more reliable data, it is necessary to employ more stable loading systems and radiation sources. However, difficulties encountered in the use of the PXRD analysis do not concern the experimental equipment alone. The experimental data accumulated at present demonstrate the complexity of processes accompanying the shock loading of crystals. It is necessary to develop the microstructure concepts of the shock compression, mechanism, and kinetics of phase SW transformations. Therefore, PXRD experiments should not only demonstrate the phenomenon (today the illustrative type of experiment is often due to their comparatively low accuracy, which is not discussed here), but also facilitate the understanding of the physical mechanism of the phenomenon. In particular, PXRD analysis can be useful in studying melting in SWs, which was demonstrated for bismuth.

The author is grateful to R F Trunin for many helpful discussions and scientific editing of the paper and his attention for many years to PXRD method at RFNC–VNIIEF.

References

1. Al'tshuler L V et al. in *Devyatoe Nauchno-Tekhnicheskoe Soveshchanie po Primeneniyu Rentgenovskikh Luchei k Issledovaniyu Materialov, 18–24 Dekabrya 1967 g., Leningrad, Tezisy Dokladov* (9th Scientific and Technical Meeting on X-Ray Applications for Studying Materials, 18–24 December 1967, Leningrad, Abstracts of Papers) (Leningrad, 1967) p. 37
2. Egorov L A et al. *Prib. Tekh. Eksp.* (2) 200 (1968)
3. Egorov L A, Nitochkina E V, Orekin Yu K *Pis'ma Zh. Eksp. Teor. Fiz.* **16** 8 (1972) [*Sov. Phys. JETP* **16** 4 (1972)]
4. Johnson Q et al. *Phys. Rev. Lett.* **25** 1099 (1970)
5. Johnson Q, Mitchell A C *Phys. Rev. Lett.* **29** 1369 (1972)
6. Johnson Q, Mitchell A C, Evans L *Appl. Phys. Lett.* **21** 29 (1972)
7. Jamet F, in *High Pressure Science and Technology, Proc. VII AIRAPT Conf., Le Creusot, 1978*, p. 974
8. Kondo K, Sawaoka A, Saito S, in *Proc. of the 4th Intern. Conf. on High Pressure, Kyoto, 1974*, p. 845
9. Kondo K, Sawaoka A, Saito S, in *High Velocity Deformation of Solids, Tokyo, 1978*, Vol. B, p. 176
10. Kondo K et al., in *High Pressure Science and Technology, New York, 1979*, Vol. 2, p. 883
11. Kondo K, Sawaoka A, Saito S, in *High Pressure Science and Technology, New York, 1979*, Vol. 2, p. 905
12. Muller F, Schulte E *Z. Naturforsch. A* **33** 918 (1978)
13. Zaretsky E, in *Shock Compression of Condensed Matter — 1997, Woodbury, 1998*, p. 883
14. Loveridge-Smith A et al. *Phys. Rev. Lett.* **86** 2349 (2001)
15. Rigg P A, Gupta Y M *Phys. Rev. B* **63** 094112 (2001)
16. Wark J S et al. *Phys. Rev. B* **35** 9391 (1987)
17. Wark J S et al. *J. Appl. Phys.* **68** 4531 (1990)
18. Al'tshuler L V et al. *Zh. Eksp. Teor. Fiz.* **81** 672 (1981) [*Sov. Phys. JETP* **54** 359 (1981)]
19. Podurets A M et al. *Izv. Akad. Nauk SSSR Fiz. Zemli* (6) 26 (1989)
20. Umanskii Ya S *Rentgenografiya Metallov i Poluprovodnikov* (X-radiography of Metals and Semiconductors) (Moscow: Metallurgiya, 1969) p. 209
21. Barenboim A I et al. *Prib. Tekh. Eksp.* (1) 189 (1992)
22. Egorov L A et al. *Zh. Eksp. Teor. Fiz.* **103** 135 (1993) [*JETP* **76** 73 (1993)]
23. Zaretskii E B et al. *Teplofiz. Vys. Temp.* **29** 1002 (1991)
24. Johnson Q, Mitchell A C, in *High Pressure Science and Technology. Proc. VII AIRAPT Conf., Le Creusot, 1978*, p. 977
25. Zaretsky E *J. Phys. IV France* **7** (C3) 329 (1997)
26. Woolsey N C et al., in *Shock Compression of Condensed Matter — 1995, Woodbury* Pt. 2 (New York: AIP Press, 1996) p. 997
27. Podurets A M, Dorokhin V V, Trunin R F *Teplofiz. Vys. Temp.* **41** 254 (2003) [*High Temp.* **41** 216 (2003)]
28. Podurets A M et al. *Izv. Akad. Nauk SSSR Fiz. Zemli* (1) 107 (1991)
29. Egorov L A et al. *Khim. Fiz.* **14** (2–3) 100 (1995)
30. Barenboim A I, Dorokhin V V, Egorov L A, in *1 Vsesoyuz. Simp. po Makroskopicheskoi Kinetike i Khimicheskoi Gazodinamike, Alma-Ata, Tezisy Dokladov* (1st All-Union Symp. on Macroscopic Kinetics and Chemical Hydrodynamics, Alma-Ata, Abstract of Papers) Vol. 2, Pt. 2 (Chernogolovka, 1984) p. 51
31. d'Almeida T, Gupta Y M *Phys. Rev. Lett.* **85** 330 (2000)
32. Trunin R F (Ed.) *Eksperimental'nye Dannye po Udarno-Volnovomu Szhatiyu i Adiabaticheskomu Rasshireniyu Kondensirovannykh Veshchestv* (Experimental Data on the Shock Compression and Adiabatic Expansion of Condensed Matter) (Sarov: RFYaTs–VNIIEF, 2006)
33. Podurets A M, Mokhova V V, in *8 Intern. Conf. on High Pressure Semiconductor Physics, August 9–13, 1998, Thessaloniki*
34. Kishimura H et al. *Phys. Rev. B* **74** 224301 (2006)
35. Meyers M A et al. *Acta Mater.* **51** 1211 (2003)
36. Kalantar D H et al. *Phys. Rev. Lett.* **95** 075502 (2005)
37. Zaretskii E B et al. *Dokl. Akad. Nauk SSSR* **316** 111 (1991) [*Sov. Phys. Dokl.* **36** 76 (1991)]
38. Tonkov E Yu *Fazovye Diagrammy Soedinenii pri Vysokom Davlenii* (Phase Diagrams of Compounds at High Pressure) (Moscow: Nauka, 1983)
39. Graham R A *J. Appl. Phys.* **39** 437 (1968)
40. Hawreliak J et al. *Phys. Rev. B* **74** 184107 (2006)
41. Podurets A M et al., in *IV Vsesoyuz. Konf. po Detonatsii, Telavi, 1988* (IVth All-Union Conference on Detonation, Telavi, 1988) Vol. 1, p. 162
42. Podurets A M, Barenboim A I, Trunin R F, in *Intern. Conf. on Condensed Matter Under High Pressures, Bombay, 1996, Proc.: Advances in High Pressure Research in Condensed Matter* (Eds S K Sikka, S C Gupta, B K Godwal) (New Delhi, 1997) p. 285
43. McQueen R G et al., in *High-Velocity Impact Phenomena* (Ed. R Kinslow) (New York: Academic Press, 1970) p. 293 [Translated into Russian (Moscow: Mir, 1973) p. 299]
44. Kutsar A R, Lyasotski I V, Podurets A M, Sanches-Bolinches A F *High Pressure Research* **4** 475 (1990)
45. Schaufelberger Ph, Merx H, Contre M *High Temp. High Pressures* **4** 111 (1972)
46. Trunin R F et al. *Teplofiz. Vys. Temp.* **33** 222 (1995)

PACS numbers: **42.55.–f, 42.62.–b, 52.57.–z**
DOI: 10.3367/UFNe.0181.201104m.0434

High-power lasers and their applications in high-energy-density physics studies

S G Garanin

1. Introduction

Work on the development of high-power lasers was initiated at the All-Russian Research Institute of Experimental Physics (ARIEP or VNIIEF in *Russ. abbr.*) in 1963 by the scientific supervisor Yu B Khariton. These studies were headed by S B Kormer and G A Kirillov. Active experimental investigations in this field were started in the mid-1960s. In 1965, N G Basov proposed to Yu B Khariton that collaborative studies be carried out on the possibility of the development of lasers emitting the maximum achievable output energy.

This proposal was based on the idea of using extremely high-power optical radiation accompanying the explosion of a nuclear charge for pumping lasers. However, the emission temperature of a shock wave in air produced by a nuclear explosion does not differ substantially from the emission temperature of a shock wave in noble gases excited by a standard explosive. This simpler and real pumping method was proposed for joint investigations by researchers at the Lebedev Physical Institute, Russian Academy of Sciences (LPI or FIAN in *Russ. abbr.*) and ARIEP.

In December 1965, the first explosion experiment on lasing in ozone was performed, and in December 1966, lasing was obtained in CF_3I. In 1970, an important stage in the study of explosion photodissociation lasers (EPDLs) was completed, when a megajoule laser emitting ~ 100 μs pulses was built in cooperation with LPI and the State Optical Institute (GOI in *Russ. abbr.*).

The successful development of work in this area gave an impetus to the construction of laser facilities at the Russian Federal Nuclear Center in Sarov (RFNC–ARIEP) for studying high energy density physics, including investigations in the field of laser fusion. The natural question arises: Why did this area begin to develop so rapidly at the nuclear center, where the main field of research was nuclear weapons development?

Physical processes proceeding during the explosion of a thermonuclear charge occur at high energy densities. And although such high energy densities cannot yet be achieved under laboratory conditions, it is possible to improve the understanding of the physics of these processes by refining theoretical models for simulations and testing them in laboratory experiments. An advantage of laser studies is the possibility of performing repeated experiments by using the developing precision diagnostics. This allows one to study individual phenomena proceeding in plasmas at thermonuclear temperatures.

S G Garanin Federal State Unitary Enterprise 'Russian Federal Nuclear Center — All-Russian Research Institute of Experimental Physics', Sarov, Nizhny Novgorod region, Russian Federation
E-mail: garanin@vniief.ru

Uspekhi Fizicheskikh Nauk **181** (4) 434–441 (2011)
DOI: 10.3367/UFNr.0181.201104m.0434
Translated by M Sapozhnikov; edited by A Radzig

The use of a laser to ignite a thermonuclear fuel was first proposed by Basov and Krokhin [1]. More recently, paper [2] by American scientists was published. The first successful experiments with spherical targets were performed at the Kal'mar facility at LPI [3]. These investigations initiated the development of laser facilities for studying the physics of inertial thermonuclear fusion.

At present, two basic schemes for compressing thermonuclear targets are considered, which take advantage of either direct or indirect irradiation. In both, the external surface of a spherical shell filled with a thermonuclear fuel [for example, a deuterium–tritium (DT) mixture] is exposed to laser radiation producing the evaporation of the shell, thereby building up the ablation pressure. Under the action of this pressure, an unevaporated spherical piston compresses the fuel up to the required density ρ and heats it up to the needed temperature T.

In the direct irradiation scheme, the shell is evaporated directly upon laser irradiation of the target. In the indirect method, the thermonuclear fuel is compressed by X-rays produced by the laser radiation heating of a special spherical or cylindrical capsule surrounding the thermonuclear target.

In fact, the principle of inertial plasma confinement is realized in such targets, including the existence of a compressed fuel for the time τ required for compressed plasma unloading. During this time, it is necessary to create conditions for igniting the target, i.e., conditions under which the thermonuclear energy release exceeds the energy deposited on the target. Taking into account that $\tau \approx R/c_s$, where R is the radius of a compressed core, and c_s is the speed of sound, we can arrive at the ignition condition in the form $\rho R \geqslant 0.3$ g cm^{-2} for $T \geqslant 10$ keV.

Work on developing single-pulse lasers for studying various aspects of laser fusion was started in 1972 on the initiative of Yu B Khariton, S B Kormer, and G A Kirillov at the RFNC–ARIEP, where high-power Iskra-4 [4], Iskra-5 [5], Luch [6], and Femto [7] laser facilities were built.

2. High-power photodissociation iodine lasers for laser fusion studies

Interest in a photodissociation iodine laser as a driver for laser fusion appeared after the publication of paper [8] in 1971. The possibilities of applications of iodine lasers for these purposes were also studied by Russian [9–11] and foreign [12–14] scientists.

In 1979, a high-power Iskra-4 single-channel iodine laser facility was built at ARIEP, which emitted 2000-J, 0.1–0.3-ns pulses. The facility was equipped with a system dividing the laser beam into four beams for irradiating thermonuclear targets in the tetrahedral symmetry. In the mid-1980s, this facility was the world's highest-power (10 TW) single-channel laser.

The successful solution to the problem of developing and starting the Iskra-4 facility made it possible to begin the development of a considerably larger and higher-power Iskra-5 photodissociation iodine facility, which was started at the end of 1989 and still operates. This facility consists of 12 laser channels emitting ≈ 0.25-ns pulses with a total output energy of up to 30–40 kJ. Pump flashlamps and electric-discharge sources were powered by a specially built system of capacitive energy storage providing a total energy storage of up to ≈ 65 MJ [15].

The target camera of the Iskra-5 facility is equipped with 12 unique three-component mirror–lens focusing systems [16]. The main experiments in the 12-channel irradiation regime were performed with 0.3–0.4-ns pulses with the output energy of 9–10 kJ. At present, this facility provides the coupling of 0.5–0.6-ns, 2.4–3-kJ second-harmonic pulses into the interaction chamber [17].

3. Investigations at the Iskra-4 laser facility

Investigations performed at the Iskra-4 facility were mainly devoted to the direct drive targets in the exploding-shell mode (see also, for example, Ref. [18]). This mode is characterized by a low volume compression degree ($\delta \approx 100$) and a weak sensitivity to the shell converging asymmetry [19]. In this case, the neutron yield N is sufficient for the reliable detection of neutrons, which makes it possible to analyze a complete set of experimental data.

To reach such a compression regime, the laser pulse duration should be $\tau_L \leqslant 0.3$ ns, and the laser power density on the target surface should be $I_L \approx 10^{15}$W cm^{-2}. These irradiation parameters were attained in experiments.

For this laser power density at a wavelength of 1.315 μm, the pressure produced by laser radiation (the ponderomotive pressure) is comparable to the thermal pressure of plasma, which leads to the formation of a density jump at the point corresponding to the critical plasma density (see, for example, [20–22]). Under these conditions, the classical inverse bremsstrahlung absorption of laser radiation decreases, and the role of nonlinear mechanisms resulting in the generation of 'hot' electrons and fast ions in a laser corona becomes dominant.

In experiments [23, 24], spherical glass targets 120–240 μm in diameter, with the aspect ratio $A_s = R_0/\Delta R$ (the ratio of the initial radius to the shell thickness) ranging from 30 to 100, and the initial pressure $P_{DT} = 10-30$ atm of the DT mixture were utilized. Figure 1 shows the absorption coefficient k_a and the fraction k_f of absorbed energy transferred to fast ions as functions of the laser radiation intensity.

These experiments were analyzed by constructing the models of radiation absorption and generation of fast particles, which took into account the above-mentioned effects in the SNDP one-dimensional radiation gas dynamics code [25, 26] and gain satisfactory agreement between experimental and calculated coefficients k_a and k_f (see Fig. 1). The density ρ_f of the compressed DT gas, determined both from the size of a compressed core measured with a pinhole camera and from the line emission of neon added to the DT mixture, was also consistent with the calculated value. In this case, the maximum value of ρ_f was about 1 g cm^{-3} [23].

Although measurements of the target energy input and volume compression were consistent with calculations, the experimental neutron yield, amounting to 10^4-10^6, was 10–100 times lower than the yield predicted by the development of calculations. This discrepancy is mainly explained by the development of hydrodynamic instabilities and turbulent mixing caused by the nonuniform irradiation of a target.

After modernization of the Iskra-4 facility to generate the second-harmonic radiation, a series of experiments on compressing high-aspect-ratio shells with $A_s > 200$ was performed. The stable generation of thermonuclear neutrons was obtained in a strongly converging shock wave with the record high yield of 6×10^7 neutrons per pulse.

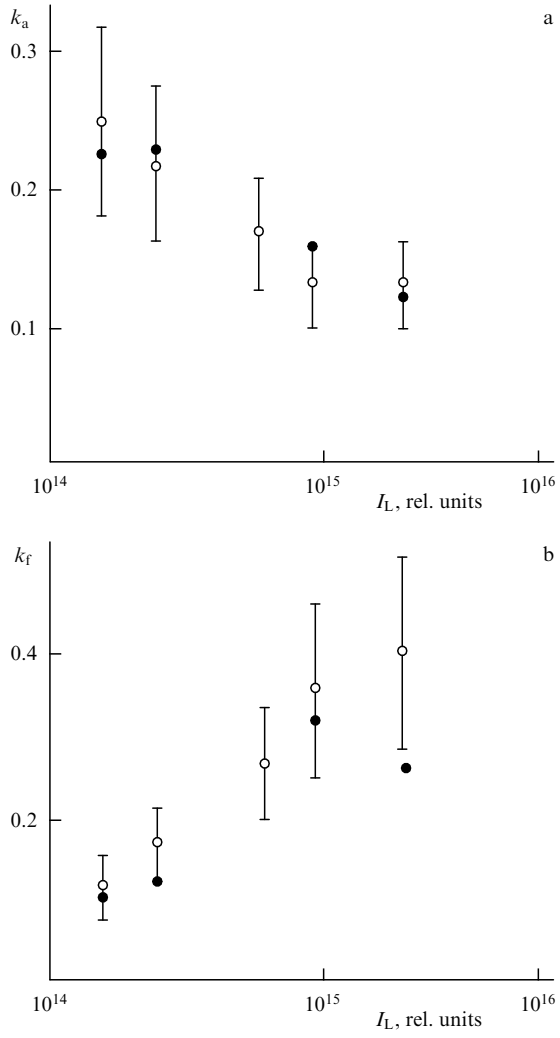

Figure 1. Dependences of the absorption coefficient k_a (a) and the fraction k_f of absorbed energy in fast ions (b) on the laser radiation intensity (○ — experiment at the Iskra-4 facility, and ● — calculations).

4. Investigations at the Iskra-5 laser facility

Experimental investigations at the Iskra-5 facility [27–41] were mainly concerned with the indirect drive targets consisting of a spherical copper box 1.3–4 mm in diameter with a glass capsule, containing the DT gas, located at the center of the box. The efficiency of coupling laser radiation into the box was verified in a series of experiments on targets with a reversed corona [29]. In these experiments, a hot plasma with a record high ion temperature of about 12 keV was obtained. The neutron yield reached $\approx 10^{10}$ DD neutrons per pulse.

An important stage of investigations covered the X-ray field characteristics inside the box, the field spectrum, the effective temperature, and the symmetry properties of irradiation of the central target. For this purpose, the parameters of the central capsule were varied: its diameter was changed from 270 μm to 0.9 mm, the thickness was changed from 1 to 40 μm, and the initial pressure of the DT gas was changed from 3 to 50 atm. Experiments and calculations revealed that the inhomogeneity of the X-ray flux on the capsule surface did not exceed 2–3% for the ratio of the box radius to the central capsule radius in the range from 5 to 10.

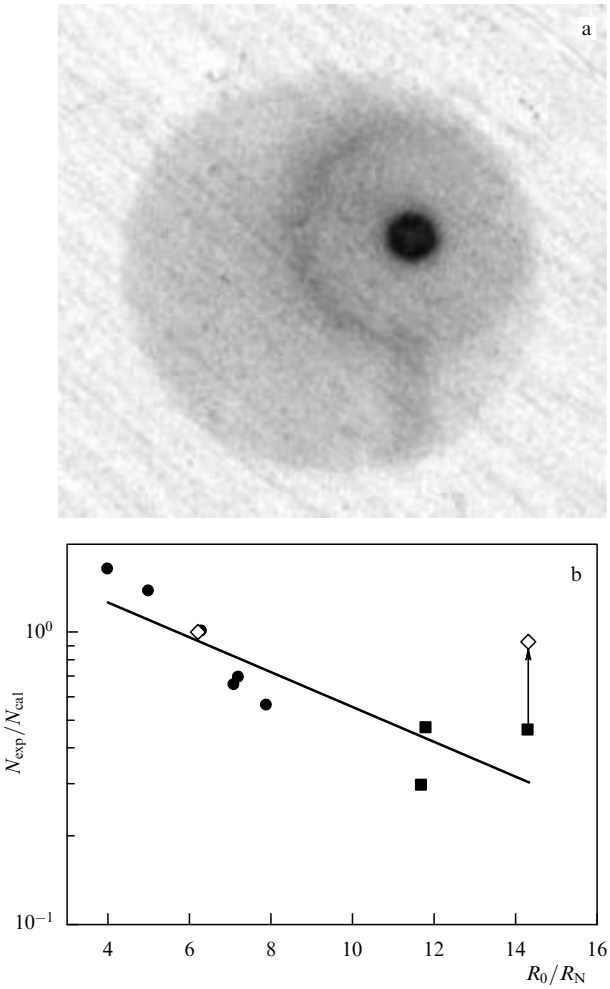

Figure 2. (a) Camera-obscura photograph of a central target obtained in a typical experiment with X-ray targets. (b) Dependences of the ratio of experimental and calculated neutron yields on the calculated degree of the radial convergence of the central capsule at the instant of neutron generation: (●) shell without a coating; (■) shell with a polyparaxylilene coating; (◇) calculations taking turbulent mixing into account.

The recording of the spectrum of X-ray radiation generated by the box walls [37–39] showed that the spectrum is nonequilibrium. According to the absolute measurements of the X-ray energy, the X-ray flux irradiating the glass capsule surface corresponds to the effective temperature of 160–170 eV.

To analyze the experiments, it was necessary to develop one-dimensional and two-dimensional radiation gas dynamics codes. Methods were developed for calculating the generation and transfer of X-rays in a laser plasma by using the spectral-diffusion approximation and the kinetic equation method. The validity and accuracy of both the physical models and developed algorithms and calculation programs were verified in experiments.

Figure 2a presents a camera-obscure photograph of the X-ray emission of the central target, which demonstrates the high degree of symmetry of the compressed region, thus confirming calculated estimates. The high degree of symmetry made it possible to detect the density of the compressed DT gas in experiments at the level from 0.8 to 1.1 g cm^{-3} [31, 33]. Measurements of the shell convergence time $\tau_{\gamma\gamma}$ performed with an X-ray streak camera gave the estimate of the

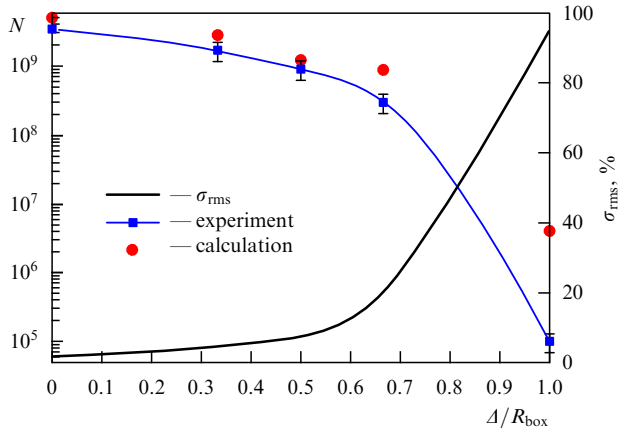

Figure 3. Dependences of the neutron yield N and the inhomogeneity degree σ_{rms} of the X-ray field on the capsule surface on the displacement Δ of the target with respect to the center of the box.

typical shell removal velocity, which was about 3×10^7 cm s^{-1} for a shell thickness of 5–7 μm.

The neutron yield changed from 10^7 to 10^{10}, depending on the shell parameters and experimental conditions. For a target 280 μm in diameter with a shell 5 μm in thickness, the neutron yield was at a level of about 3×10^9, which corresponds to the DT gas temperature of 2.5 keV measured by the time-of-flight method.

A comparison of experimental data with calculations based on the one-dimensional SNDP code showed that the neutron yield was well described within the framework of spherically symmetric calculations (Fig. 2b) for the degrees of a gas volume compression up to 10^3. At higher compression ratios, the neutron yield was lower than that predicted by spherically symmetric calculations, which can be explained by the influence of turbulent mixing.

The high symmetry of the X-ray field made it possible to perform the world's first experimental studies on the influence of a radiation asymmetry on the dynamics of thermonuclear targets and the generation of neutrons in them. The influence of asymmetry in the initial geometry of targets [36, 40, 41] and in the X-ray flux on the target surface was investigated.

The asymmetry of the X-ray field was varied by using an additional hole in the box and displacing the spherical capsule in its direction.

A comparison of experimental results with gas dynamic calculations of the compression of central capsules with the help of the Mimoza-ND program [42, 43], with the target and X-ray parameters corresponding to experiments (Fig. 3), demonstrates the qualitative and quantitative agreement between experiments and calculations in a wide range of varying X-ray field asymmetry [36, 44].

5. Ignition of a thermonuclear target

The key issue of laser fusion is the question about the minimum laser energy E_L required to ignite a laser thermonuclear target. It was shown in Ref. [45] that the optimistic estimate of E_L points to 500 kJ for a nanosecond laser pulse. More detailed information can be obtained with the help of gas dynamic calculations making allowance for combined physical processes determining the target compression dynamics.

Calculations were performed using the SNDP code taking into account the following physical processes [46]: gas

dynamic processes, inverse bremsstrahlung absorption of laser radiation, electron and ion heat conductions, electron–ion relaxation, X-ray radiation transfer in the nonequilibrium spectral diffusion approximation, plasma ionization kinetics in the average ion approximation [47], and the kinetics of thermonuclear reactions with due regard for the transfer of α particles in the multigroup, restricted-flow diffusion approximation [48]. In calculations, the equation of state in the average ion approximation taking cold pressure into account was used [49]. The physical models constructed in this program were confirmed in experiments at the Iskra-4 and Iskra-5 facilities, as shown in Sections 3 and 4.

The calculated optimization of the target design demonstrates that a 500-kJ laser pulse can ignite a thermonuclear target representing a plastic spherical shell ~ 1.5 mm in diameter with ~ 30-μm-thick walls. A 25-μm-thick DT ice layer was frozen on the internal surface of the shell. To provide the isentropic compression, the laser pulse is profiled:

$$P(t) = \begin{cases} P_0 \left(\dfrac{t}{t_0}\right)^{2.8} & \text{for} \quad t < t_0\,, \\ P_0 & \text{for} \quad t_0 < t < t_0 + \Delta t\,, \end{cases}$$

where $P(t)$ is the laser radiation power conveyed to the target, $t_0 = 8.6$ ns, $\Delta t = 1.48$ ns, and $P_0 = 1.34 \times 10^{14}$ W (these values were selected in accordance with the shell radius and mass). Calculations show that in this case the gain coefficient of the target (the excess of the thermonuclear energy over the deposited laser energy) is about 10. The yield of thermonuclear neutrons reaches 2×10^{18} neutrons per pulse, the volume compression of the thermonuclear fuel is about 10^4, and the density of the DT mixture at the instant of maximum compression is about 100 g cm^{-3}.

The nonuniform irradiation of the target, the deviation of the shell symmetry from spherical, and the different thickness of the DT ice layer cause the violation of the one-dimensionality of compression, thereby increasing the energy required for a target ignition. These factors can be conditionally divided into two groups according to the spatial scale. Large-scale inhomogeneities include perturbations with a wavelength of $(0.1-1)R_0$, where R_0 is the initial radius of the target, while small-scale inhomogeneities correspond to perturbations with a wavelength shorter than $0.1R_0$.

The influence of large-scale inhomogeneities has been studied in many laboratories in Russia and abroad (see, for example, preprint [50]). We will analyze this influence based on two-dimensional Mimoza-ND calculations comprising the same thermonuclear target for which the results of one-dimensional calculations were presented above. The variation of the laser radiation intensity along the target surface can be written out in the form

$$I = I_0\left[1 + a_l P_l(\cos\Theta)\right],$$

where I_0 is the laser radiation intensity averaged over the target surface, $P_l(\cos\Theta)$ is the Legendre polynomial, and a_l is the perturbation amplitude. The influence of the inhomogeneity on the target ignition is characterized best of all by the ratio of the thermonuclear energy released during laser fusion and obtained in two-dimensional calculations to the energy produced in one-dimensional calculations. The dependence of this parameter on the perturbation amplitude a_l for two harmonics with $l = 2$ and 10 testifies that the close perturbation levels for both harmonics cause an approximately equal decrease in the released energy (Fig. 4). Note that the energy

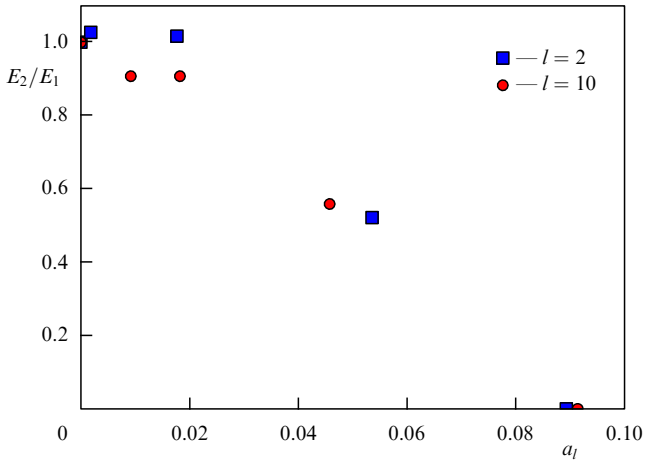

Figure 4. Ratio of thermonuclear energy releases obtained in two-dimensional (E_2) and one-dimensional (E_1) calculations as a function of the amplitude of large-scale perturbations.

release decreases by half when the irradiation inhomogeneity amplitude reaches 5%, and the neutron yield is virtually absent when the inhomogeneity amounts to 9%. These investigations suggest that, when the volume compressibility factor reaches 10^4, large-scale inhomogeneities with the amplitude on the order of 3% do not affect the compressibility and combustion dynamics of a thermonuclear fuel.

The presence of small-scale inhomogeneities leads to the efficient development of gas dynamic instabilities and turbulent mixing. Unfortunately, it is impossible at present to perform direct simulations of the influence of these effects on the compression dynamics of the target and its ignition. Although many experimental and theoretical studies are now underway, it is not clear so far how much the laser energy should be increased to compensate for energy losses caused by instabilities.

6. Megajoule laser facility

Experiments at the Iskra-5 facility revealed its restricted possibilities. In particular, the neutron yield for a laser energy of about 30 kJ is insufficient for studying all the regimes of thermonuclear target compression. In 1996, RFNC–ARIEP proposed building a megajoule laser facility [51] for experiments on the ignition of a nuclear fusion target. In addition, this facility would be used for studying the problems like the X-ray energy transfer in closed volumes, the spectroscopy of hot dense plasmas, the spectral measurements of the X-ray absorption coefficients in equilibrium plasma, the radiative gas dynamics of asymmetric flows, the determination of the equations of state of matter in the pressure region from 10 to 100 million atm, and the development of hydrodynamic instabilities and turbulent mixing on contact boundaries.

Analysis of different possible designs of such a facility showed that the technology of neodymium lasers, which was considerably developed in the 1970s–1980s, provided the best opportunities for increasing the efficiency of the facility and, therefore, for reducing its dimensions. A characteristic feature of such facilities was a multipass (four-pass) power cascade with a sectioned aperture and active rectangular phosphate glass elements (so-called slabs). This design provides a significant increase in the amplifier efficiency and reduces the number of intermediate amplification cascades.

At the first stage, a four-channel Luch neodymium facility was built at RFNC–ARIEP for testing and working out basic scientific and technical solutions [52]. The optical scheme of the Luch facility channel is mainly similar to those of the NIF (National Ignition Facility) [53] and LMJ (Laser Mégajoule) facility [54]. The laser efficiency is increased by utilizing an amplification scheme in which a laser pulse passes four times through active laser elements (neodymium slabs), thereby increasing the extraction of energy stored in them. In addition, laser channels are combined in blocks pumped by a common pumping system containing xenon flashlamps, which also increases the laser efficiency. The amplifying stage of the Luch facility includes two power amplifiers, each of them containing nine neodymium slabs. The laser beam cross section is a 20×20-cm square. To suppress self-excitation in the laser channel, the second and third amplification passages are separated by a Pockels cell, and the laser beam quality is improved by means of a special adaptive system.

It was shown in Ref. [55] that the radiation resistance of domestic optical elements in the facility channel, specifically, Nd-phosphate glass slabs [56], provides an operation with mean output energy densities of up to $\varepsilon \approx 10$ J cm^{-2}. Calculations of the laser pulse amplification showed that, to achieve such a level of ε, the gain should be $g \approx 0.04$–0.05 cm^{-1}; in this case, the output energy of one channel should be 3–3.5 kJ. Experiments [57] demonstrated that amplifiers of the selected design provide the required value of g. These results and the required operation regimes obtained in all systems of the facility made it possible to achieve in experiments the expected output energy of 3.3 kJ per channel (Fig. 5) [58].

A specific feature of the capacitor bank of the Luch facility with the 4.7-MJ energy storage at a voltage of 24 kV is that reversely switched semiconductor dynistors [59] with very high commutation parameters were utilized for the first time in world practice in a high-power laser.

The experimental results demonstrated the validity of the chosen scientific and technical solutions. Further studies aimed at improving the main systems of the facility, including the development of a large-aperture Pockels cell with plasma electrodes [60], the development of manufacturing technology for Nd slabs with enlarged apertures [61], and the application of new operation algorithms for an adaptive system [62], made it possible to formulate the concept for building a laser facility emitting ~ 2.8 MJ, 3–5-ns pulses at a wavelength of 0.53 μm. The laser beam aperture is 40×40 cm, and the number of amplification channels reaches 192. At present, the technical design of this facility is being developed at RFNC–ARIEP.

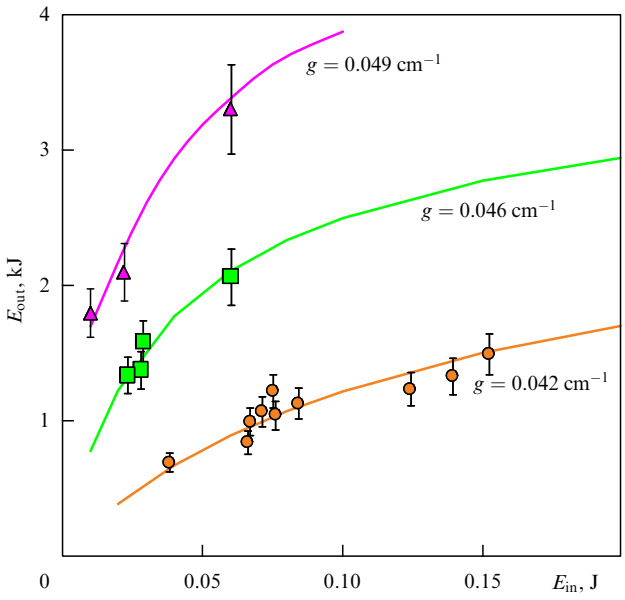

Figure 5. Dependences of the output laser energy E_{out} in one channel of the facility on the input energy E_{in} of power amplifiers for different gains g. Symbols show experimental results, curves correspond to calculations.

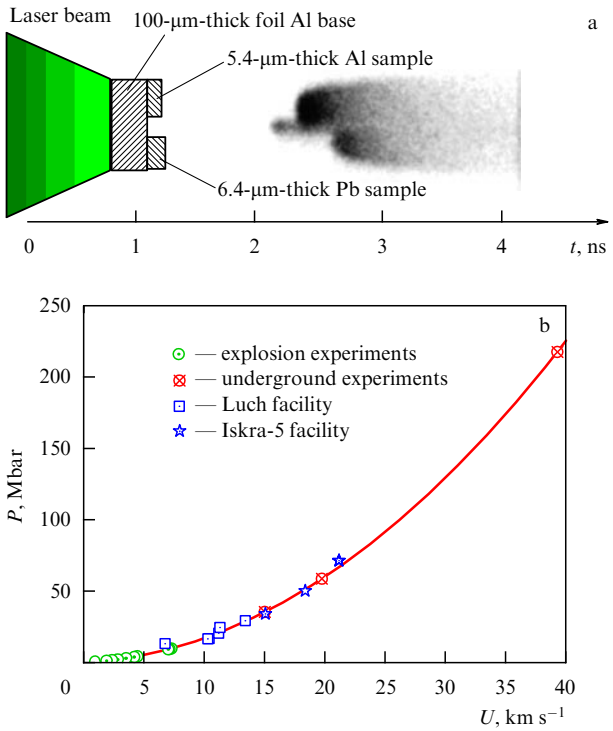

Figure 6. Studies of the shock compressibility of lead at the Luch facility: (a) layout of experiments; (b) the $P-U$ diagram.

Along with studies of laser radiation amplification, the Luch facility is also employed for investigating the behavior of matter under experimental conditions. In particular, an experimental method for studying shock compressibility is being developed. Figure 6a shows the principal experimental layout, and Fig. 6b presents the $P-U$ compressibility diagram obtained for lead. Notice that the pressure reached in laser experiments exceeds 50 Mbar.

7. Petawatt laser complex

Recent years have witnessed considerable progress in the development of solid-state femtosecond lasers. Subpetawatt and petawatt laser facilities emitting 100–500-fs pulses have been started at leading laser laboratories (see, for example, Ref. [63]). Such output power levels in a focused beam provide a power density of up to $10^{18}-10^{22}$ W cm^{-2}.

The appearance of a new tool led to the development of a number of new research avenues, such as the generation of fast electrons and ions, including proton beams, the generation of hard X-rays, and the initiation of nuclear reactions. The possibility of a 'fast' ignition of a thermonuclear target simultaneously irradiated by nanosecond and femtosecond pulses is considered.

At present, two main approaches for achieving petawatt laser powers are being considered. In the first method, a

femtosecond laser pulse with an energy on the order of 1 nJ is stretched up to a few nanoseconds by means of a dispersion optical system (a diffraction grating called a stretcher). Then, the pulse can be amplified by well-known methods. After obtaining the required energy, the pulse is compressed in time with the help of another optical system (a compressor), also consisting of diffraction gratings. If the laser pulse spectrum is not distorted during amplification, the pulse duration can be shortened to its initial value.

However, a neodymium phosphate glass amplifier distorts (narrows) the laser pulse spectrum, and the output pulse of such petawatt laser systems has a 0.5–1-ps duration.

Another system is based on the employment of parametric amplifiers with a considerably broader amplification band. The idea of such a laser system applied to lower radiation power levels was probably first formulated by Soviet researchers more than 25 years ago [64]. However, only at present, after the creation of femtosecond lasers emitting 10-fs pulses and nonlinear crystals with apertures of up to 40 cm, has the realization of this idea for generating record high, multipetawatt powers become possible [65].

Such a system was realized at the Luch facility in collaboration between researchers at RFNC–ARIEP and the Institute of Applied Physics, Russian Academy of Sciences (Nizhny Novgorod). Parametric amplifiers in this system are based on large-aperture DKDP crystals. At present, 1 PW of output power is being achieved [7]. The output energy of the facility is about 50 J for a compressed pulse duration of about 45 fs and a beam diameter of 7.4 cm.

8. Conclusions

The laser stand base built at RFNC–ARIEP is unique. It is the property of the scientific community in Russia and is open for investigations in the field of high-energy-density physics for researchers from different scientific institutes in Russia.

The creation of high-power laser facilities at RFNC–ARIEP for investigations in the field of high-energy-density physics facilitates the development of technologies in the fields of laser science, optics, pulsed power, and measurement techniques.

References

1. Basov N G, Krokhin O N *Zh. Eksp. Teor. Fiz.* **46** 171 (1964) [*Sov. Phys. JETP* **19** 123 (1964)]
2. Nuckolls J et al. *Nature* **239** 139 (1972)
3. Basov N G et al. *Pis'ma Zh. Eksp. Teor. Fiz.* **26** 581 (1977) [*JETP Lett.* **26** 433 (1977)]
4. Kormer S B *Izv. Akad. Nauk SSSR Ser. Fiz.* **44** 2002 (1980)
5. Annenkov V I et al. *Kvantovaya Elektron.* **18** 536 (1991) [*Sov. J. Quantum Electron.* **21** 487 (1991)]
6. Beznasyuk N N et al. *Trudy RFYaTs – VNIIEF* (3) 232 (2002)
7. Andreev N F et al. *Pis'ma Zh. Eksp. Teor. Fiz.* **79** 178 (2004) [*JETP Lett.* **79** 144 (2004)]
8. Gensel P, Hohla K, Kompa K L *Appl. Phys. Lett.* **18** 48 (1971)
9. Basov N G et al. *Kvantovaya Elektron.* **6** (18) 116 (1973) [*Sov. J. Quantum Electron.* **3** 524 (1973)]
10. Gaidash V A et al. *Pis'ma Zh. Eksp. Teor. Fiz.* **20** 243 (1974) [*JETP Lett.* **20** 107 (1974)]
11. Kormer S B *Izv. Akad. Nauk SSSR Ser. Fiz.* **44** 2003 (1980)
12. Aldridge F T *Appl. Phys. Lett.* **22** 180 (1973)
13. Palmer R, Gusinow M *IEEE J. Quantum Electron.* **10** 615 (1974)
14. Baker H J, King T A *J. Phys. D* **8** L31 (1975)
15. Bezuglov V G et al. *Prib. Tekh. Eksp.* (3) 100 (1991)
16. Vasil'ev A S et al. *Izv. Akad. Nauk SSSR Ser. Fiz.* **54** 2027 (1990)
17. Annenkov V I et al. *Kvantovaya Elektron.* **35** 993 (2005) [*Quantum Electron.* **35** 993 (2005)]
18. Storm E K et al. *J. Appl. Phys.* **49** 959 (1978)
19. Bel'kov S A et al. *Vopr. At. Nauki Tekh. Teor. Prikl. Fiz.* (2) 25 (1990)
20. Attwood D T et al. *Phys. Rev. Lett.* **40** 184 (1978)
21. Silin V P *Usp. Fiz. Nauk* **145** 225 (1985) [*Sov. Phys. Usp.* **28** 136 (1985)]
22. Bel'kov S A et al. *Kvantovaya Elektron.* **19** 1187 (1992) [*Sov. J. Quantum Electron.* **22** 1109 (1992)]
23. Bel'kov S A et al. *Zh. Eksp. Teor. Fiz.* **97** 834 (1990) [*Sov. Phys. JETP* **70** 467 (1990)]
24. Bel'kov S A et al. *Zh. Eksp. Teor. Fiz.* **101** 80 (1992) [*JETP* **74** 43 (1992)]
25. Dolgoleva G V *Vopr. At. Nauki Tekh. Algoritmy Metody Chisl. Resh. Zadach Mat. Fiz.* (2) 29 (1983)
26. Bel'kov S A et al. *Vopr. At. Nauki Tekh. Mat. Model. Fiz. Protsessov* (1) 76 (1990)
27. Kochemasov G G, in *Laser Interaction with Matter: Proc. of the 23rd European Conf., Oxford, 19 – 23 September 1994* (Ed. S J Rose) (Bristol: IOP, 1995)
28. Bessarab A V et al. *Zh. Eksp. Teor. Fiz.* **102** 1800 (1992) [*JETP* **75** 970 (1992)]
29. Abzaev F M et al. *Pis'ma Zh. Eksp. Teor. Fiz.* **58** 28 (1993) [*JETP Lett.* **58** 28 (1993)]
30. Abzaev F M et al. *Zh. Eksp. Teor. Fiz.* **114** 155 (1998) [*JETP* **87** 87 (1998)]
31. Bel'kov S A et al. *Zh. Eksp. Teor. Fiz.* **114** 837 (1998) [*JETP* **87** 454 (1998)]
32. Bel'kov S A et al. *Laser Part. Beams* **17** 591 (1999)
33. Bel'kov S A et al. *Laser Part. Beams* **17** 377 (1999)
34. Bel'kov S A et al. *Laser Part. Beams* **17** 385 (1999)
35. Bel'kov S A et al. *Laser Part. Beams* **17** 597 (1999)
36. Bel'kov S A et al. *Pis'ma Zh. Eksp. Teor. Fiz.* **67** 161 (1998) [*JETP Lett.* **67** 171 (1998)]
37. Bessarab A V et al. *Fiz. Plazmy* **20** 90 (1994)
38. Bel'kov S A et al. *Kvantovaya Elektron.* **21** 271 (1994) [*Quantum Electron.* **24** 253 (1994)]
39. Bel'kov S A et al. *Fiz. Plazmy* **24** 154 (1998) [*Plasma Phys. Rep.* **24** 133 (1998)]
40. Mkhitarian L S et al., in *Inertial Fusion Sciences and Applications 99* (Eds C Labaune, W J Hogan, K A Tanaka) (Paris: Elsevier, 2000) p. 142
41. Mkhitar'yan L S et al. *Trudy RFYaTs – VNIIEF* (1) 300 (2001)
42. Afanas'eva E A et al., in *Konstruirovanie Algoritmov i Reshenie Zadach Matematicheskoi Fiziki* (Construction of Algorithms and Solution of Problems in Mathematical Physics) (Eds G P Voskresenskii, A V Zabrodin) (Moscow: IPM AN SSSR, 1989) p. 277
43. Sofronov I D et al. *Vopr. At. Nauki Tekh. Mat. Model. Fiz. Protsessov* (1) 8 (2000)
44. Mkhitarian L S et al. *Laser Part. Beams* **18** 237 (2000)
45. Il'kaev R I, Garanin S G *Vestn. Ross. Akad. Nauk* **76** 503 (2006) [*Herald Russ. Acad. Sci.* **76** 282 (2006)]
46. Bel'kov S A, Dolgoleva G V *Vopr. At. Nauki Tekh. Mat. Model. Fiz. Protsessov* (1) 59 (1992)
47. Bel'kov S A et al. *Zh. Eksp. Teor. Fiz.* **111** 496 (1997) [*JETP* **84** 272 (1997)]
48. Bel'kov S A, Dolgoleva G V, Ermolovich V F *Vopr. At. Nauki Tekh. Mat. Model. Fiz. Protsessov* (1) 51 (2003)
49. Bel'kov S A, Bondarenko S V, Mitrofanov E I *Kvantovaya Elektron.* **30** 963 (2000) [*Quantum Electron.* **30** 963 (2000)]
50. Lindl J, Preprint LLNL, UCRL-JC-119015, L19821-1 (1995)
51. Galakhov I V et al. *Fusion Eng. Design* **44** 51 (1999)
52. Sukharev S A *Proc. SPIE* **3492** 12 (1999)
53. Paisner J A et al. *Proc. SPIE* **2633** 2 (1995)
54. Andre M L *Proc. SPIE* **3047** 38 (1997)
55. Arbuzov V I et al. *Opt. Zh.* **69** (1) 16 (2002) [*J. Opt. Technol.* **69** 13 (2002)]
56. Alexseev V N et al. *Opt. Zh.* **69** (1) 11 (2002) [*J. Opt. Technol.* **69** 9 (2002)]
57. Voronich I N et al. *Kvantovaya Elektron.* **33** 485 (2003) [*Quantum Electron.* **33** 485 (2003)]
58. Garanin S G et al. *Kvantovaya Elektron.* **35** 299 (2005) [*Quantum Electron.* **35** 299 (2005)]

59. Chumakov G D et al., in *Proc. of the Xth IEEE Intern. Pulsed Power Conf., Albuquerque, NM, USA, 1995*
60. Andreev N F et al. *Kvantovaya Elektron.* **34** 381 (2004) [*Quantum Electron.* **34** 381 (2004)]
61. Arbuzov V I et al. *Opt. Zh.* **70** (5) 68 (2003) [*J. Opt. Technol.* **70** 361 (2003)]
62. Voronich I N et al. *Kvantovaya Elektron.* **35** 140 (2005) [*Quantum Electron.* **35** 140 (2005)]
63. Kryukov P G *Kvantovaya Elektron.* **31** 95 (2001) [*Quantum Electron.* **31** 95 (2001)]
64. Piskarskas A, Stabinis A, Yankauskas A *Usp. Fiz. Nauk* **150** 127 (1986) [*Sov. Phys. Usp.* **29** 869 (1986)]
65. Andreev N F et al. *Pis'ma Zh. Eksp. Teor. Fiz.* **79** 178 (2004) [*JETP Lett.* **79** 144 (2004)]

PACS numbers: 07.55.Db, **64.30.–t**, **74.25.–q**
DOI: 10.3367/UFNe.0181.201104n.0441

Research in ultrahigh magnetic field physics

G V Boriskov, A I Bykov, M I Dolotenko, N I Egorov, Yu B Kudasov, V V Platonov, V D Selemir, O M Tatsenko

1. Introduction

The history of the achievements of the All-Russian Research Institute of Experimental Physics (VNIIEF in *Russ. abbr.*) in the field of ultrahigh magnetic field (UHMF) generation and applications in fundamental physical studies begins in 1952, when Andrey D Sakharov put forward the idea of magnetic cumulation as one of the possible methods for achieving a controlled thermonuclear reaction [1]. He also proposed two types of magnetocumulative generators of UHMFs (MC-1) and energy (MC-2) [1, 2]. In the first of them, a special device produces the initial axial magnetic field flux in the cavity of a cylindrical metal shell (liner). A converging detonation wave is initiated in a circular explosive charge surrounding the liner so that it arrives at the external boundary of the liner at the instant of time when the initial magnetic field in the liner achieves a maximum. Under the action of pressure of the detonation products, the liner collapses to the center, compressing the initial magnetic flux. If the compression is rapid enough, the magnetic flux in the cavity is preserved, and the magnetic field strength on the liner axis increases inversely proportionally to the squared radius of the liner, achieving a few megagausses. The chemical energy of the explosive is transformed into the magnetic field energy through the kinetic energy of the liner.

Extensive attempts made in many countries to reproduce UHMFs by the explosive compression of a magnetic flux revealed unexplainable difficulties in obtaining magnetic fields exceeding 3 MG, which resulted in the termination of work in this field.

G V Boriskov, A I Bykov, M I Dolotenko, N I Egorov, Yu B Kudasov, V V Platonov, V D Selemir, O M Tatsenko Federal State Unitary Enterprise 'Russian Federal Nuclear Center — All-Russian Research Institute of Experimental Physics', Sarov, Nizhny Novgorod region, Russian Federation. E-mail: selemir@vniief.ru

Uspekhi Fizicheskikh Nauk **181** (4) 441–447 (2011)
DOI: 10.3367/UFNr.0181.201104n.0441
Translated by M Sapozhnikov; edited by A Radzig

2. MC-1 cascade generator

A group of researchers at VNIIEF headed by A I Pavlovskii proposed and realized a number of concepts supplementing and developing the magnetic cumulation idea and solved the problem of the reproducible generation of UHMFs.

First, it was proposed to make the shells of the MC-1 generator from a material with a controllable electrical conduction. Such a material in the initial state is either completely nonconducting or conducts current only in one direction. At the required instant, a shock wave is passed through the material, making it conducting in all directions. For example, such a material can be produced from closely packed parallel isolated copper wires glued with an epoxy compound.

Second, unique solenoids of the initial magnetic field in the MC-1 generator were constructed in the form of a cylinder made of a composite material with the internal layer containing wires forming a multiple (≈ 500 entry wires), multilayer (7–13 winding layers) solenoid (Fig. 1). This made it possible to reliably obtain high magnetic fluxes and use the solenoid as a liner: after the passage of a shock wave from an explosive charge, the wires are connected up to form a continuous conducting cylinder capturing and compressing the magnetic flux [3].

Third, because the high initial magnetic flux in the wire solenoid provided UHMF generation in large volumes, the X-ray diffraction analysis of the longitudinal cross section of the MC-1 generator showed that the magnetic field strength is mainly restricted by the instability of the matter–field interface during the deceleration of the shell by the pressure of the strengthened magnetic field [4].

Fourth, the cascade principle of magnetic field strengthening was proposed, which removed this restriction, stopped the development of instabilities, and provided the reproducible generation of multimegagauss magnetic fields [5, 6]. One or two cylindrical cascade shells made of the same composite are located coaxially to the shell solenoid. In the initial state, the cascade shells easily transmit the amplified magnetic field flux inside, but each time the internal boundary of the liner can lose its stability, the liner is replaced by a new one, which compresses the magnetic flux when conduction appears in the cascade material after the impact of one cascades with the other.

The MC-1 cascade ten-megagauss magnetic field generator was developed for many years of research work and then produced in batches (see Fig. 1) [7, 8]. The basic

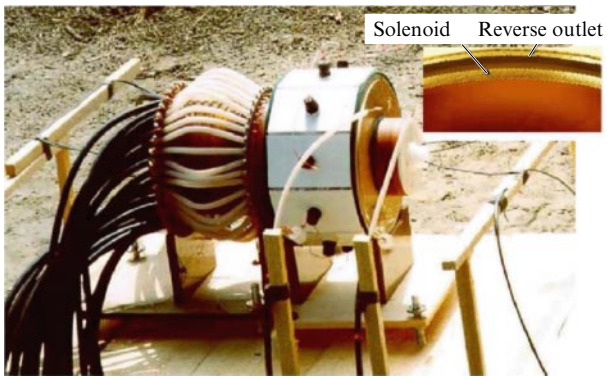

Figure 1. Appearance of the MC-1 cascade generator prepared for an explosion experiment. The inset shows a part of the cross section of the solenoid shell of the MC-1 generator.

parameters of the generator are as follows: the initial internal diameter of the shell is 139 mm, the explosive mass is 16 kg, and the initial magnetic field is up to 250 kG. The second and third cascades of the generator with the internal and external diameters of 28 and 35 mm and 12 and 17 mm, respectively, can be made of a wire composite or a composite based on a finely divided metal powder and a polymer binder [9].

This generator makes up a rather simple and comparatively inexpensive device intended for explosion experiments, which was adjusted to a device made in large numbers (by now a few hundred such generators has been manufactured) with limiting, record parameters. Relatively large UHMF volumes make it possible to study simultaneously several samples even at cryogenic temperatures, while the cylindrical geometry and 'transparency' of the magnetic field allow studying matter under extreme conditions applying various methods, including optical. This generator was used in various investigations, in particular, in the international experiments Dirac in the USA, and Kapitza at the Scientific and Technical Center of High Energy Density Physics of Directed Radiation Fluxes at VNIIEF [10, 11].

In the 'large' MC-1 generator, with approximately doubled explosive charge dimensions (the explosive mass was increased approximately eightfold) and built at VNIIEF, a single-cascade gasdynamic liner-acceleration system with a steel striker is utilized and magnetic field strengths of about 20 MG were detected in several experiments, while in one experiment a record-high magnetic field strength of about 28 MG was achieved (the field energy density was ≈ 3 MJ cm^{-3}!) [12]. Experiments with large generators showed that these experiments are much more complicated and expensive and their cost should be justified by the scientific importance of the studies performed using them.

3. Solid state physics in ultrahigh magnetic fields

Ultrahigh magnetic fields can be efficiently used for solid-state physics studies. Some results obtained by the authors with the help of UHMFs produced by the MC-1 generator were presented in reviews [13, 14].

Ultrahigh magnetic fields attracted considerable interest at once after the discovery of high-temperature superconductivity because high critical temperatures should correspond to high critical magnetic fields B_c, which are the fundamental characteristic of the superconducting state. Of interest are also phase transitions between different states of the superconducting phase itself (for example, the 'vortex glass–vortex lattice' transition). Our first experiments showed that the critical field in $YBa_2Cu_3O_{7-x}$ at 4.2 K exceeds 200 T [15]. The later-developed contactless high-frequency methods for measuring the admittance were applied for precision measurements of the conduction of $YBa_2Cu_3O_{7-x}$ films in UHMFs when the crystallographic c-axis was oriented perpendicular to the magnetic field vector. These measurements were performed in a joint Russian–American series of experiments at VNIIEF and Los Alamos National Laboratory [16]. One can see from Fig. 2 that the imaginary part of the film conduction dominated at low temperatures in weak fields, i.e., vortices were located at the pinning centers. In the field ≈ 75 T (point A), the real part of the conduction began to rapidly increase, while its imaginary part began to decrease. This is caused by lattice melting. In fields above 210 T, only a small part of the pinning vortices remains (the conduction has the imaginary part), and the sample is found

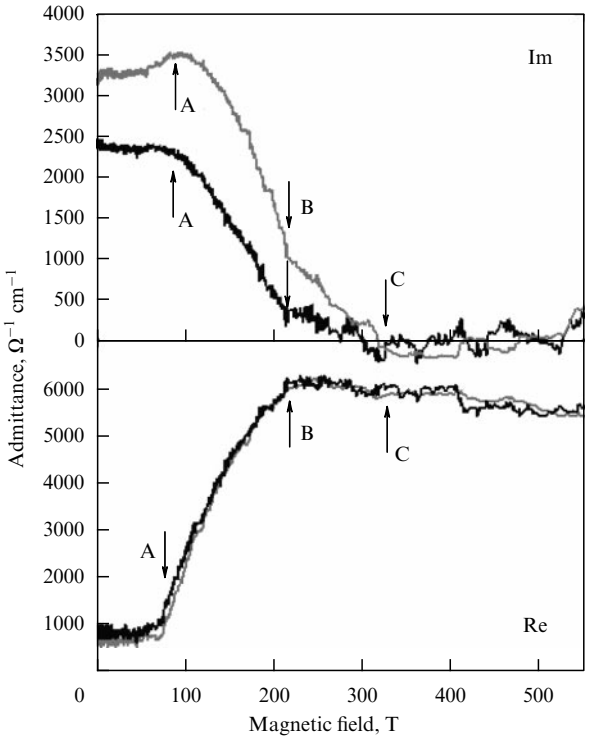

Figure 2. Admittance of $YBa_2Cu_3O_{7-x}$ at a frequency of 94 GHz (the grey and dark curves are measured by the signal transmission and refection methods, respectively).

predominantly in the viscous flow motion regime. The disappearance of the imaginary part of the conduction and flattening out of its real part (point C) correspond to the second critical field $B_{c2}(8 \pm 3\ \mathrm{K}) = 340 \pm 40$ T.

The study of semiconductors in UHMFs makes it possible to determine the energy band diagram in the range from a few dozen to a few hundred meV. Semiconductor samples with low carrier mobility or a high concentration of defects or impurities can also be investigated. As a rule, it has been possible to determine in such experiments the effective electron mass in the conduction band, the Luttinger parameters in the valence band, and g factors for electrons and holes. All these quantities are functions of the electron energy, which can be determined only in UHMFs. (In weak magnetic fields, it is possible to measure the values of these functions corresponding to the band edges because the electron cyclotron energy is much smaller than the band width.)

The cyclotron resonance in a cubic high-energy-gap GaN semiconductor was measured in joint experiments with a group led by M von Ortenberg of Humboldt University of Berlin. This semiconductor is promising for applications in radiation sources. However, its electronic properties in this phase are poorly studied because of the absence of high-purity samples and low carrier mobility. Three resonance peaks were revealed in magnetic fields of 90, 270, and 410 T, which gave the effective masses and dispersion of electronic states [17].

In quantum-well InGaAs/GaAs heterostructures, the fundamental cyclotron resonance of holes and interband magnetoabsorption were studied. These heterostructures were grown at the Institute of Microstructure Physics, Russian Academy of Sciences (Nizhny Novgorod). When transmission is measured at a wavelength of 0.87 μm, which exactly corresponds to the GaAs band gap (quantum energy of 1.425 eV), the sample becomes transparent only in the field

of 50 T. For the same reason, the sample becomes transparent at 0.83 μm in the field of 150 T, although the calculation taking exciton effects into account gives 100 T [18]. In stronger magnetic fields, absorption bands in the range from 230 to 350 T were observed. They are caused by transitions from the two upper (spin-split) Landau levels in the first hole subband to the two lower Landau levels in the first electron subband, and by similar transitions between second subbands (shifted by approximately 50 T to the region of the lower magnetic fields), taking exciton effects into account. The same transitions between the first subbands at $\lambda = 0.87$ μm are responsible for the transmission minimum at 150 T and a singularity observed at 210 T. The cyclotron absorption line observed in these experiments in the magnetic field $B \approx 80$ T can be related to the *intersubband* cyclotron resonance, namely, to the transition from the $3a_1$ upper Landau level of holes in the quantum well in the first hole subband to the $4a_3$ level belonging to the third subband.

Among the family of low-energy-gap semiconductors, iron monosilicide (FeSi) is distinguished by its unusual properties. For example, the sum rule violation in FeSi is broadly discussed in optical spectroscopy: metallization with increasing temperature occurs much earlier than would be expected from band calculations, etc. Because the Zeeman splitting in UHMFs is comparable to the band gap in the spectrum of the s, p, and d electrons in FeSi, equal to 0.11 eV, those fields exceeding 100 T can drastically restructure the electronic spectrum and, therefore, can be used as a powerful tool for studying the electronic structure of low-energy-gap semiconductors.

The induction method with the use of compensation coils proved to be very convenient for studying the magnetization in experiments with the MC-1 [19]. The induced signal is proportional to the differential magnetization multiplied by the magnetic field growth rate, which achieves a record-high value in the MC-1 generator ($\approx 10^6$ T s^{-1}), thus providing the high sensitivity of sensors in the entire measurement range. In pulsed magnetic fields, diamagnetic currents are induced along with magnetization, which allows the conduction to be measured as well. For this purpose, samples of two types are used: in the form of a pure FeSi powder (a single crystal was ground in a porcelain mortar to obtain granules ≈ 100 μm in size), and in the form of a mixture of a single-crystal powder with polymerized polymethyl methacrylate (single-crystal FeSi granules in a dielectric matrix).

A sharp peak (Fig. 3) observed in both samples in the magnetic field of 355 ± 20 T at 4.2 K points to the transition to the conducting phase [19]. The calculated jump in the magnetic moment is $(0.95 \pm 0.2)\,\mu_B$ per Fe atom, which suggests that saturation is achieved due to a single transition rather than due to the two successive phase transitions predicted in some theoretical papers.

The main subjects of studies in magnetics were spin reorientation processes in ultrahigh magnetic fields. Spin-flip and spin-flop transitions in MnF_2, $KMnF_3$, and $FeBO_3$ antiferromagnetics and the step magnetization curve of a multisublattice $Ho_{0.7}Y_{2.3}Fe_5O_{12}$ magnet were studied in Ref. [20]. A magnetic field can distort the electronic structure of the ground state, resulting in induced band magnetism.

The level crossover in the paramagnetic $YbPO_4$, $TmPO_4$, $ErVO_4$, and $PrVO_4$ zircons was studied by the induction method at 4.2 K in magnetic fields of up to 400 T [21, 22]. Figure 4 depicts the experimental and theoretical dependences of the magnetic susceptibility dM/dH for $YbPO_4$ for

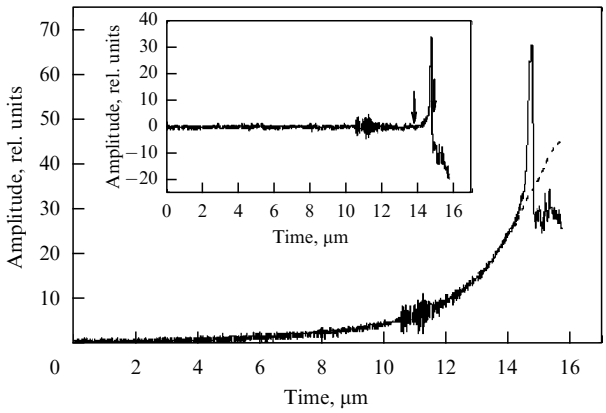

Figure 3. Output signal of an inductive sensor with an FeSi powder at the initial temperature of 4.2 K (solid curve) and the scaled signal of an inductive field sensor (dashed curve). The inset displays a signal purified from the background $\propto \partial B/\partial t$; the arrows show the integration interval for determining the magnetic moment jump.

a magnetic field directed along the tetragonal [001] axis. The broad susceptibility maxima at $B_c \approx 280$ and 50 T are related to the crossover of the energy levels of Yb^{3+} and Pr^{3+} ions. Calculations of the isothermal and adiabatic magnetization of $YbPO_4$ made it possible to determine a change in the sample temperature during experiments. The sample is first heated by approximately 25 K and then is cooled by approximately 20 K in the region of the crossover fields. The sign of the 'elementary' magnetocaloric effect is determined by the sign of the derivative $\partial M/\partial T|_{H=\text{const}}$.

Ultrahigh magnetic fields can induce a change in the valence in some compounds containing Ce, Sm, Eu, Tm, and Yb rare-earth ions. Such a behavior of these compounds is caused by the location of the 4f level near the Fermi level. In particular, the mixed-valence state appears in $EuNi_2Si_2$ and $EuNi_2Ge_2$ solutions. The $4f^6$ Eu^{3+} ion in $EuNi_2Si_2$ is nonmagnetic, whereas the magnetic moment of the $4f^7$ Eu^{2+} ion in $EuNi_2Ge_2$ amounts to $7\,\mu_B$. In $EuNi_2(Si_{1-x}Ge_x)_2$ compounds, the valence transition is induced from the mostly trivalent-ion state to the mostly bivalent-ion state, which is accompanied by a jump in the magnetic moment. The fields of magnetoinduced valence transitions were experimentally determined for these compounds in the range of Ge concentrations up to $x = 0.5$. The critical filed B_c linearly grows with decreasing concentration in the entire concentration range [23].

The study of the Faraday effect in $Tb_3Ga_5O_{12}$ terbium gallate garnet (the energy spectrum of its magnetic subsystem has been thoroughly investigated in static fields) in UHMFs, which increase in the MC-1 generator at a rate of 10^7–10^8 T s^{-1}, was performed to determine the value of the magnetocaloric effect, which is important from the methodical point of view. It was shown that the sample temperature during the adiabatic magnetization in a field of 75 T reached 35 K and no unexpected increase in the temperature occurred in pulsed magnetic fields [23].

4. Isentropic compression of matter by the ultrahigh magnetic field pressure

The investigation of the behavior of materials, first and foremost their equations of state, at ultrahigh pressures is one of the interesting problems of high energy density physics [24, 25]. Of special interest here is the low-temperature region,

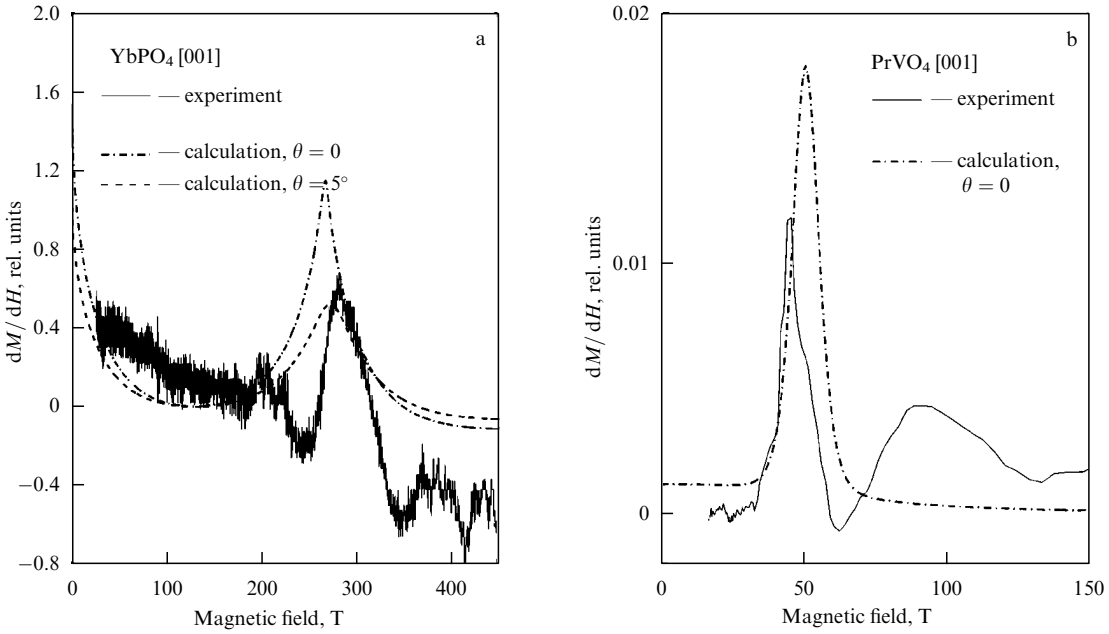

Figure 4. Dependences of the differential susceptibility dM/dH for $YbPO_4$ (a) and $PrVO_4$ (b) for a magnetic field oriented near the tetragonal [001] axis (θ is the reorientation angle).

which is important not only, for example, for understanding the structure and evolution of giant planets, but also for verifying fundamental theoretical concepts.

High and ultrahigh pressures are produced by two basic methods, static and dynamic, which supplement each other. In statics, the regime of isothermal compression is realized, as a rule, at comparatively low temperatures ($T < 1000$ K) [26]; the equations of state are studied at static pressures below 1.5 Mbar to avoid the destruction of samples. (In addition, the growth of pressure is limited by the strength of the anvil material.) On the other hand, the temperature can reach a few dozen thousand degrees in the dynamic shock-wave regime, but in this case the 'cold' pressure does not exceed even 0.5 Mbar (see, for example, Ref. [27]). Another dynamic method is the isentropic compression of matter in a chamber whose external surface is subjected to the action of a uniform, gradually increasing external pressure [28]. The thermal component of the total pressure, unlike that in the shock-wave method, will be considerably smaller as in the static method, than the cold component, and at a low initial temperature of a material under study its isentrope will be close to the zero isotherm. At present, the characteristics of substances in the region of *low temperatures and ultrahigh* (*multimegabar*) *pressures* can be efficiently determined only by the isentropic compression method. The properties of materials in this region are studied at VNIIEF by the method of *isentropic compression by ultrahigh magnetic field pressure* [29, 30]. The experimental results obtained by this method are mainly related to the construction of zero isotherms of the hydrogen isotopes — protium and deuterium. (Notice, by the way, that researchers at VNIIEF were among the first to study hydrogen at ultrahigh pressures [31–33].)

Interest in studying the thermodynamic and kinetic properties of hydrogen is not accidental and is caused by the wide abundance of hydrogen in the Universe and its practical importance as one of the basic elements for future energy production. In addition, a number of unusual, exotic properties of hydrogen have been predicted: the high-temperature superconductivity of its metal phase [34], the temperature maximum in the melting curve [35–37], and the existence of a two-component superfluid and superconducting liquid [38].

The method that we apply is based on a compression device containing an MC-1 magnetocumulative generator [7], a cylindrical compression chamber [39], and a cryogenic device [40] (Fig. 5). The compression chamber is formed by a thick-walled copper compressing tube and massive end caps. The standard sample and sample under study are located coaxially under the compressing tube (at the center). The cryogenic device, containing a liquid helium vessel and an evacuated cryoduct, is destined for preliminary cooling the gas under study to the solid state ($T_0 \approx 5$ K). Under the action of the excess pressure produced in the helium vessel, helium rises upward through the cryoduct and gradually cools the compression chamber together with its content. During the discharge of a high-power capacitor bank to the generator solenoid in its cavity, in the gap between the solenoid and compressing tube, an initial magnetic flux is produced. The magnetic field in the gap is increased up to a few megagausses during the operation of the MC-1 generator and exerts a uniform magnetic pressure $B^2/8\pi$ on the external surface of the compression chamber. As a result, the chamber tube collapses without the generation of shock waves and compresses (for ≈ 15 μs) the materials inside it up to a few megabars.

An important and substantial part of the studies is the numerical simulation of processes proceeding in the compression device with the help of applied program packages developed at VNIIEF [41–43]. One of the main goals of simulations is to determine the compression chamber geometry and initial dimensions and the initial field of the MC-1 generator that would provide minimal pressure gradients in the working region of the compression chamber. The results of calculations were also used in the development of the X-ray diffraction method for measuring the dimensions [44]. Finally, the calculated results are also

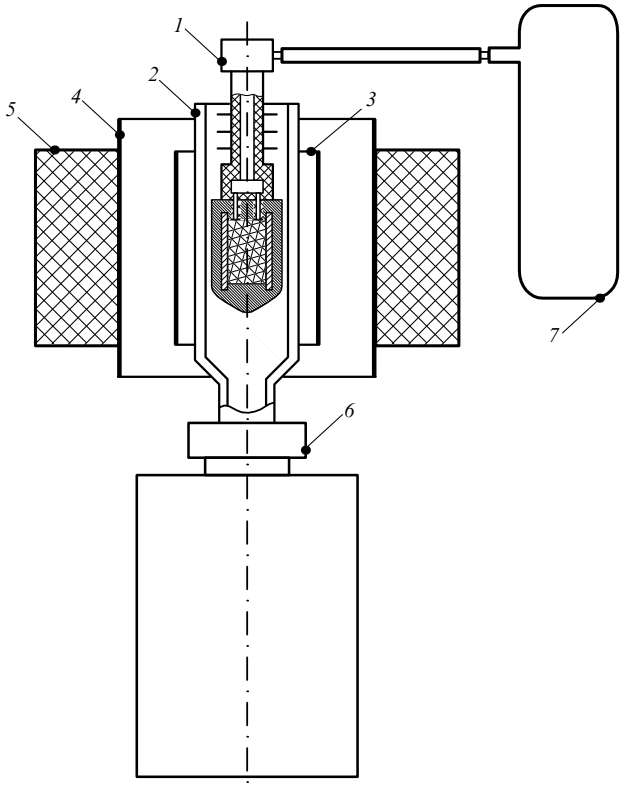

Figure 5. Schematic of the compression device: (*1*) cryogenic vessel with a compression chamber filled with the material under study; (*2*) cryoduct; (*3*) second cascade of the MC-1 generator; (*4*) solenoid of the initial field of the generator (first cascade); (*5*) circular explosive charge; (*6*) liquid helium vessel, and (*7*) container with the gas under study.

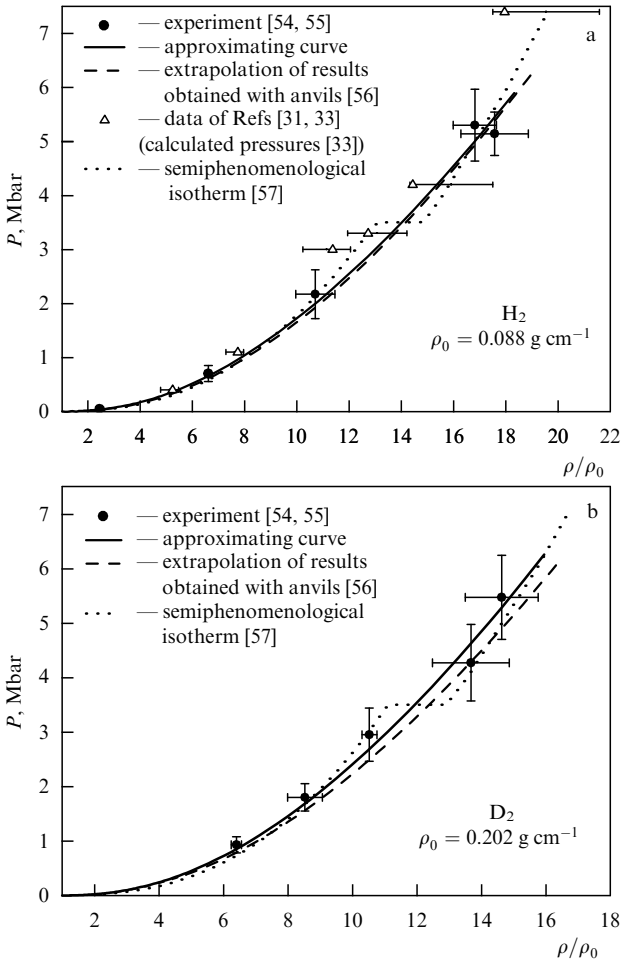

Figure 6. Pressure–compression diagrams for protium (a) and deuterium (b).

employed to analyze experimental data and estimate the gradient correction in measurements of pressure in the sample under study.

The density ρ and pressure P of a compressed material are determined in the following way. The central part of an experimental device is illuminated by a bremsstrahlung pulse from a BIM-234 betatron [45, 46] and the image is recorded on an X-ray film. The X-ray pattern is recorded when pressure in the compression chamber reaches ultrahigh values. The sizes and, hence, compressibilities of the sample under study and standard sample are determined from the processed images in X-ray patterns. The sample density during X-ray pattern recording can be easily obtained from the known compressibility and initial density ρ_0 of the sample. Pressure in the measurement standard can be determined from its density with the aid of its known isentrope. Then, taking into account small calculation corrections, pressure in the sample under study can also be determined. The best material for the standard is aluminium, for which the most comprehensive statistical data covering the required pressure range have been gathered and processed [47–53]. To determine accurately enough the dimensions of compressed samples from an X-ray pattern, a thin layer of a highly dense material should be placed on the boundaries between the samples and between samples and the compressing tube. We utilized an alloy containing 95% tungsten. Thus, we find from the X-ray pattern a point at the $P-\rho$ plane for the material under study. By changing the X-ray recording time from experiment to experiment, we obtain a set of points corresponding to the 'cold' isentrope of the material.

By utilizing the compression devices and measurement methods described above, researchers at VNIIEF performed experiments [54, 55] to obtain the zero isotherms for protium and deuterium in the pressure range from 1 to 5 Mbar. The experimental data obtained for H_2 and D_2 are presented in the $P-\rho/\rho_0$ plane in Fig. 6. The solid curve shows the approximation of experimental data. The zero isotherm obtained in experiments with diamond anvils [56] and extrapolated to the megabar region is illustrated by the dashed curve. The dotted curve was proposed in Ref. [57] for the molecular and atomic phases of protium and deuterium. The data obtained in Refs [54, 55] reveal no dramatic deviations in the behavior of the zero isotherms. Some scatter of points in the diagram at pressures exceeding 4 Mbar may be caused by a polymorphic transformation in the lattice or even by the lattice melting produced by pressure [35]. One can see that the points [54, 55] agree within the measurement error with the zero isotherm [56], although they lie somewhat higher at pressures above 1 Mbar. They are also consistent with the semiphenomenological isotherm [57] based on experiments [31–33] on the quasi-isentropic compression of initially gaseous protium[1] (Fig. 6a). However,

[1] The states of the matter obtained in Refs [31–33] correspond to the calculated temperatures exceeding 2000 K [33]. Recent experiments with diamond anvils [36, 37] demonstrate a turn in the melting curve of protium near $T = 1000$ K, and therefore results [31–33] are related to the dense heated matter rather than to the 'cold' matter.

according to Ref. [57], in the pressure region from 3 to 4 Mbar the crystal should undergo a transition from the molecular to the atomic phase with a considerable density jump ($\approx 14\%$). (According to Ref. [56], the transition pressure exceeds 6 Mbar and the density jump will be a few times smaller.) To determine reliably the run of the zero isotherm in this pressure range, it is necessary to perform additional experiments with the improved accuracy of measuring the sample size. Notice also that the compression curve of the static lattice of protium and deuterium constructed in Ref. [55] based on experimental results is consistent with *ab initio* calculations [58–62].

Finally, it should be emphasized that the investigation method described above can also be used to construct the 'cold' compression curves for many other materials consisting of elements with small atomic numbers, such as helium, lithium, graphite, water, and hydrides of light metals.

5. Conclusion

The idea of the magnetic cumulation of energy proposed by Andrey D Sakharov was developed for many years at VNIIEF to the level of a physical method for obtaining ultrahigh magnetic fields, based on the deep understanding of underlying physical processes. The designs of cascade generators of ultrahigh magnetic fields in the 10- and 20-MG ranges have been worked out. The developed method has been introduced into scientific studies and has been used for systematic fundamental investigations in the fields of solid state physics (optical, magnetic, and transport properties of matter) and the physics of extreme states of matter (isentropic compression by megabar pressures). The results of these studies have been reported at International Megagauss Conferences, two of which, the seventh and ninth, were organized by researchers at VNIIEF [63, 64].

References

1. Sakharov A D et al. *Dokl. Akad. Nauk SSSR* **165** 65 (1965) [*Sov. Phys. Dokl.* **10** 1045 (1966)]
2. Sakharov A D *Usp. Fiz. Nauk* **88** 725 (1966) [*Sov. Phys. Usp.* **9** 294 (1966)]
3. Pavlovskii A I et al. *Prib. Tekh. Eksp.* (5) 195 (1979)
4. Pavlovskii A I et al. *Pis'ma Zh. Tekh. Fiz.* **9** 1360 (1983)
5. Pavlovskii A I et al. *Pis'ma Zh. Eksp. Teor. Fiz.* **38** 437 (1983) [*JETP Lett.* **38** 529 (1983)]
6. Pavlovskii A I et al., in *Sverkhsil'nye Magnitnye Polya. Fizika. Tekhnika. Primenenie* (Ultrahigh Magnetic Fields. Physics. Technique. Application) (Eds V M Titov, G A Shvetsov) (Moscow: Nauka, 1984) p. 14
7. Pavlovskii A I et al., in *Sverkhsil'nye Magnitnye Polya. Fizika. Tekhnika. Primenenie* (Ultrahigh Magnetic Fields. Physics. Technique. Application) (Eds V M Titov, G A Shvetsov) (Moscow: Nauka, 1984) p. 19
8. Bykov A I et al. *Physica B* **216** 215 (1996)
9. Dolotenko M I et al., RF Patent No. 2065247; *Byull. Izobret.* (8) 107 (1996)
10. Tatsenko O M, Selemir V D, in *Megagauss Magnetic Field Generation, its Application to Science and Ultra-High Pulsed-Power Technology*: *Proc. of the VIIIth Intern. Conf. on Megagauss Magnetic Field Generation and Related Topics* (Ed. H J Schneider-Muntau) (Hackensack, NJ: World Scientific, 2004) p. 207
11. Selemir V D, Tatsenko O M, Platonov V V, in *Proc. of the X Intern. Conf. on Megagauss Magnetic Field Generation and Related Topics* (Ed. M von Ortenberg) (Berlin, 2004) p. 219
12. Boyko B A et al., in *12th IEEE Intern. Pulsed Power Conf., Monterey, Calif., USA, 1999, Digest of Technical Papers* (Eds C Stallings, H Kirbie) (New York: IEEE, 1999) p. 746
13. Zvezdin A K et al. *Usp. Fiz. Nauk* **168** 1141 (1998) [*Phys. Usp.* **41** 1037 (1998)]
14. Zvezdin A K et al. *Usp. Fiz. Nauk* **172** 1303 (2002) [*Phys. Usp.* **45** 1183 (2002)]
15. Pavlovskii A I et al. *Physica C* **162 – 164** 1659 (1989)
16. Bykov A I et al. *Sverkhprovodimost Fiz. Khim. Tekh.* **8** (1) 37 (1995)
17. Puhlmann N et al. *Physica B* **294 – 295** 447 (2001)
18. Gavrilenko V I, in *Proc. of the 14th Intern. Symp. "Nanostructures: Physics and Technology", St. Petersburg, Russia, 2006*, p. 166
19. Kudasov Yu B et al. *Pis'ma Zh. Eksp. Teor. Fiz.* **68** 326 (1998) [*JETP Lett.* **68** 350 (1998)]
20. Zvezdin A K et al., in *Itinerant Electron Magnetism*: *Fluctuation Effects* (Eds D Wagner, W Brauneck, A Solontsov) (Dordrecht: Kluwer Acad. Publ., 1998) p. 285
21. Kirste A et al. *Physica B* **336** 335 (2003)
22. Kazei Z A et al. *Physica B* **346 – 347** 241 (2004)
23. Levitin R Z et al. *Fiz. Tverd. Tela* **44** 2013 (2002) [*Phys. Solid State* **44** 2107 (2002)]
24. Zel'dovich Ya B, Raizer Yu P *Fizika Udarnykh Voln i Vysokotemperaturnykh Gidrodinamicheskikh Yavlenii* (Physics of Shock Waves and High-Temperature Hydrodynamic Phenomena) (Moscow: Nauka, 1966) [Translated into English (Mineola, NY: Dover Publ., 2002)]
25. Fortov V E *Ekstremal'nye Sostoyaniya Veshchestva* (Extreme States of Matter) (Moscow: Fizmatlit, 2009); *Extreme States of Matter on Earth and in the Universe* (Berlin: Springer, 2011)
26. Jayaraman A *Rev. Mod. Phys.* **55** 65 (1983)
27. Trunin R F et al. *Zh. Tekh. Fiz.* **76** (7) 90 (2006) [*Tech. Phys.* **51** 907 (2006)]
28. Godwal B K, Sikka S K, Chidambaram R *Phys. Rep.* **102** 121 (1983)
29. Pavlovskii A I et al., in *Megagauss Physics and Technology* (Ed. P J Turchi) (New York: Plenum Press, 1980) p. 627
30. Pavlovskii A I et al., in *Megagauss Technology and Pulsed Power Applications. Proc. of the Fourth Intern. Conf. on Megagauss Magnetic Field Generation and Related Topics* (Eds C M Fowler, R S Caird, D J Erickson) (New York: Plenum Press, 1987) p. 255
31. Grigor'ev F V et al. *Pis'ma Zh. Eksp. Teor. Fiz.* **16** 286 (1972) [*JETP Lett.* **16** 201 (1972)]
32. Grigor'ev F V et al. *Zh. Eksp. Teor. Fiz.* **69** 743 (1975) [*Sov. Phys. JETP* **42** 378 (1975)]
33. Grigor'ev F V et al. *Zh. Eksp. Teor. Fiz.* **75** 1683 (1978) [*Sov. Phys. JETP* **48** 847 (1978)]
34. Ashcroft N W *Phys. Rev. Lett.* **21** 1748 (1968)
35. Bonev S A et al. *Nature* **431** 669 (2004)
36. Deemyad S, Silvera I F *Phys. Rev. Lett.* **100** 155701 (2008)
37. Eremets M I, Troyan I A *Pis'ma Zh. Eksp. Teor. Fiz.* **89** 198 (2009) [*JETP Lett.* **89** 174 (2009)]
38. Babaev E, Sudbø A, Ashcroft N W *Phys. Rev. Lett.* **95** 105301 (2005)
39. Boriskov G V et al., in *"Megagauss-XI", Proc. of the Eleventh Intern. Conf. on Megagauss Magnetic Field Generation and Related Topics* (Eds Ivor Smith, Bucur Novac) (London, 2007) p. 269
40. Boriskov G V et al., in *Proc. of 2006 Intern. Conf. on Megagauss Magnetic Field Generation and Related Topics* (Eds G F Kiuttu, R E Reinovsky, P J Turchi) (Piscataway, NJ: IEEE, 2007) p. 465
41. Boriskov G V, Timareva V I, in *VIII Kharitonovskie Chteniya po Problemam Fiziki Vysokikh Plotnostei Energii* (VIII Khariton Readings on Problems of High Energy Density Physics) (Sarov: FGUP "RFYaTs – VNIIEF", 2006) p. 516
42. Boriskov G V, Timareva V I, in *VIII Kharitonovskie Chteniya po Problemam Fiziki Vysokikh Plotnostei Energii* (VIII Khariton Readings on Problems of High Energy Density Physics) (Sarov: FGUP "RFYaTs – VNIIEF", 2006) p. 509
43. Boriskov G V, Timareva V I, Sokolov S S, in *X Kharitonovskie Chteniya po Problemam Fiziki Vysokikh Plotnostei Energii, Sarov, 11 – 14 Marta, 2008* (X Khariton Readings on Problems of High Energy Density Physics, 11 – 14 March, 2008) (Sarov: FGUP "RFYaTs–VNIIEF", 2008) p. 285

44. Pavlov V N et al., in *XII Intern. Conf. on Megagauss Magnetic Field Generation and Related Topics. Abstracts* (Ed. G A Shvetsov) (Novosibirsk: Lavrentyev Institute of Hydrodynamics, 2008) p. 123
45. Pavlovskii A I et al. *Dokl. Akad. Nauk SSSR* **160** 68 (1965) [*Sov. Phys. Dokl.* **10** 30 (1965)]
46. Kuropatkin Yu P et al., in *11th IEEE Pulsed Power Conf. Digest of Technical Papers* (Eds G Cooperstein, I Vitkovitsky) (Piscataway, NJ: IEEE, 1997) p. 1663
47. Al'tshuler L V et al. *Zh. Eksp. Teor. Fiz.* **38** 790 (1960) [*Sov. Phys. JETP* **11** 573 (1960)]
48. Simonenko V A et al. *Zh. Eksp. Teor. Fiz.* **88** 1452 (1985) [*Sov. Phys. JETP* **61** 869 (1985)]
49. Al'tshuler L V, Brusnikin S E, Kuz'menkov E A *Prikl. Mekh. Tekh. Fiz.* (1) 134 (1987) [*J. Appl. Mech. Tech. Phys.* **28** 129 (1987)]
50. Nellis W J et al. *Phys. Rev. Lett.* **60** 1414 (1988)
51. Greene R G, Luo H, Ruoff A L *Phys. Rev. Lett.* **73** 2075 (1994)
52. Kalitkin N N, Kuz'mina L V, in *Udarnye Volny i Ekstremal'nye Sostoyaniya Veshchestva* (Shock Waves and Extreme States of Matter) (Eds V E Fortov, L V Al'tshuler, R F Trunin, A I Funtikov) (Moscow: Nauka, 2000) p. 107
53. Trunin R F et al., in *Eksperimental'nye Dannye po Udarno-Volnovomu Szhatiyu i Adiabaticheskomu Rasshireniyu Kondensirovannykh Veshchestv* (Experimental Data on Shock Wave Compression and Adiabatic Expansion of Condensed Matter) (Ed. R F Trunin) (Sarov: RFYaTs – VNIIEF, 2006) p. 24
54. Boriskov G V et al. *J. Phys. Conf. Ser.* **121** 072001 (2008)
55. Boriskov G V et al. *Contrib. Plasma Phys.,* DOI 10.1002/ctpp.201010106 (2010)
56. Loubeyre P et al. *Nature* **383** 702 (1996)
57. Kopyshev V P, Urlin V D, in *Udarnye Volny i Ekstremal'nye Sostoyaniya Veshchestva* (Shock Waves and Extreme States of Matter) (Eds V E Fortov, L V Al'tshuler, R F Trunin, A I Funtikov) (Moscow: Nauka, 2000) p. 297
58. Barbee T W (III), Cohen M L, Martins J L *Phys. Rev. Lett.* **62** 1150 (1989)
59. Kaxiras E, Guo Z *Phys. Rev. B* **49** 11822 (1994)
60. Natoli V, Martin R M, Ceperley D M *Phys. Rev. Lett.* **70** 1952 (1993)
61. Natoli V, Martin R M, Ceperley D *Phys. Rev. Lett.* **74** 1601 (1995)
62. Pierleoni C, Ceperley D M, Holzmann M *Phys. Rev. Lett.* **93** 146402 (2004)
63. Chernyshev V K, Selemir V D, Plyashkevich L N (Eds) *Megagauss and Megaampere Pulse Technology and Applications* (Sarov: VNIIEF, 1997)
64. Selemir V D, Plyashkevich L N (Eds) *Megagauss-9* (Sarov: VNIIEF, 2004)